©Copyright 2018
David Williams–Young

Towards Efficient and Scalable Electronic Structure Methods for the Treatment of Relativistic Effects and Molecular Response

David Williams–Young

A dissertation
submitted in partial fulfillment of the
requirements for the degree of

Doctor of Philosophy

University of Washington

2018

Reading Committee:

Xiaosong Li, Chair

Stefan Stoll

David Masiello

Program Authorized to Offer Degree:
Chemistry

University of Washington

Abstract

Towards Efficient and Scalable Electronic
Structure Methods for the Treatment of Relativistic Effects and Molecular Response

David Williams–Young

Chair of the Supervisory Committee:
Professor Xiaosong Li
Chemistry

In the context of electronic structure theory, formal theoretical development must be accompanied by efficient and scalable computer implementation in order to study molecular systems at experimentally relevant scales. Thus, this work outlines several advances in the development of efficient and scalable electronic structure methods for the treatment of relativistic effects and molecular response. As such, the first chapter outlines the theoretical underpinnings from which the rest of the original work is built upon. The second chapter outlines, several contributions to the field of relativistic electronic structure. While relativistic effects are generally considered to only be of consequence only in heavy elements, they can be of profound effect even in light elements. However, implementation of these methods pose several non-trivial complications over their non-relativistic counterparts, and scalable implementation of relativistic electronic structure methods are scarce. The final chapter outlines a contribution to the field of molecular response theory. In electronic structure theory, the problem of molecular response is cast into a large numerical linear algebra problem suitable for modern high–performance computing architectures. This chapter outlines a highly scalable method which allows for rapid evaluation of response functions in a reduced dimension.

TABLE OF CONTENTS

Page

List of Figures iii

List of Tables v

Glossary vi

Chapter 1: Theoretical Preliminaries 1
1.1 The Physical Hilbert Space and The Slater Determinant 1
1.2 Representation of Linear Operators and Expectation Values 6
1.3 Density Matrices 11
1.4 Second Quantization 15
1.5 Time–Independent Solutions of the Wave Equation 20
1.6 Mean–Field Quantum Mechanics and Basis Set Expansions 22
1.7 Non–Relativistic Molecular Hamiltonians 37
1.8 Relativistic Hamiltonians 43

Chapter 2: Two–Component Relativistic Electronic Structure Theory 49
2.1 The Exact Two–Component Hamiltonian 49
2.2 Two–Component Relativistic Mean Field Wave Functions 52
2.3 An Efficient and Scalable Implementation of Non-Collinear Density Functional Theory 55
2.4 The Relativistic Particle–Particle Tamm-Dancoff Approximation 71

Chapter 3: Molecular Response Properties Through Model Order Reduction . . . 81
3.1 Motivation 81
3.2 Linear response and absorption spectrum 84
3.3 Interpolatory Model Order Reduction of Linear Dynamical Systems 87

3.4 Estimating absorption spectrum without explicitly computing eigenvalues and eigenvectors 90
3.5 Interpolation–based algorithms 92
3.6 Computational results 97
3.7 Conclusions 106

Bibliography 108

Appendix A: Pauli Algebra on Even Rank Spinors 127

Appendix B: Proof of Zero Torque Theorem Using Generalized Density Variables . . 130

LIST OF FIGURES

Figure Number Page

2.1 Pictorial representation of the integrand macrobatching scheme for the xc potential integration. Each of the colored regions represent a set of Lebedev spheres over several radial quadrature points, with the solid black dot representing the atomic nucleus. In the batching scheme, the scalar and matrix integrands are evaluated over the entire batch simultaneously to improving caching and μ-op behavior. 64

2.2 Pictorial representation of the screening and updating scheme for each batch in the numerical integration of the xc potential. A list of significant basis functions in the batch (colored patterns in the figure) is selected and then partitioned out for integration of that batch. The accumulation of the matrix integrand over the batch is evaluated by SYR2K and then the final, unscreened result is updated as shown. This scheme allows for only sequential memory access in the performance critical section of the integration and is responsible for drastic performance increases. 65

2.3 X2C-B3LYP 6-311+g(D,P) spin ($|\boldsymbol{m}(\boldsymbol{r})|$, left) and scalar ($\rho^{1,0}(\boldsymbol{r})$, right) densities for a series of hydrogen rings. Blue and Red represent regions of greater density magnitude respectively. 68

2.4 X2C-B3LYP 6-311+G(2D,P) spin densities ($|\boldsymbol{m}(\boldsymbol{r})|$) for phenoxy radicals with an increasing number of fused benzene rings (n=1-10, where n represents the number of fused benzene rings on each side). 68

2.5 Relative scaling with respect to system size on a set of phenoxy radicals for the UKS and proposed X2C-KS methods. Times are presented logarithmically to demonstrate identical scaling with differing prefactors for the two methods. Times presented are the average wall times for the numerical integration of E^{GGA} and $V_{\mu\nu}^{GGA,K}$ over 5 SCF steps. 70

2.6 Wall times for the distributed memory parallel performance of the proposed implementation of X2C-KS on a large phenoxy radical. Times are presented logarithmically to demonstrate the linear (-1.01) scaling of the proposed method. Times presented are the average wall times for the numerical integration of E^{GGA} and $V_{\mu\nu}^{GGA,K}$ over 5 SCF steps. 70

3.1 Adaptive refinement strategy for selecting the interpolation frequencies. . . . 96
3.2 Numerical experiments for the evaluation of the XAS spectrum of 5 H_2O clusters by the proposed MOR algorithms using a fixed model order ($k = 32$). The MOR results are compared to the Lorentzian broadened poles of the propagator, labelled Eigensystem. A damping parameter of 1 eV was chosen both for the MOR calculations and the broadening factor of the Lorentzians for the reference. It can be seen that the use of complex interpolation frequencies for the construction of the model basis is important in spectrally dense regions. 99
3.3 Numerical experiments for the evaluation of the XAS spectrum of variably sized H_2O clusters via Algorithm 2 with adaptively chosen complex interpolation frequencies. The MOR results are compared to the Lorentzian broadened poles of the propagator, labelled Eigensystem. A damping parameter of 1 eV was chosen both for the MOR calculations and the broadening factor of the Lorentzians for the reference. 102
3.4 Cluster of H_2O molecules: MOR results for the absorption spectra computed via Algorithm 2 with adaptively chosen complex interpolation frequencies. The comparisons are made for GMRES convergence tolerances of 10^{-4}, 10^{-5}, and 10^{-6}. 104
3.5 Numerical experiments for the evaluation of the XAS spectrum of 5 H_2O clusters by Algorithm 2 using different damping factors η. (a)–(c) The MOR results are compared to the Lorentzian broadened poles of the propagator, labelled Eigensystem. (d) Effect of the damping factor η on the reduced model order k. 105

LIST OF TABLES

Table Number Page

2.1 Calculated and reference excited-state fine structure splittings (in meV) for single excitations of some atomic systems. The presence of a superscript "$\circ$" in the term symbol denotes an odd state with respect to space inversion. . . 78

2.2 Excited-state fine structure splittings (in meV) for singly excited triplet and doubly excited singlet electronic states calculated by the X2C-pp-TDA method. 79

3.1 The effect of using real and complex interpolation frequencies τ_j on the MOR evaluation of XAS spectra for 5 H_2O clusters. Computational expense for Algorithms 1 and 2. Here k is the reduced–order, GEMMs is the total number of matrix-matrix products, and the total wall-clock time is given in seconds. 100

3.2 Numerical experiments for the evaluation of the XAS spectrum of variably sized H_2O clusters via Algorithm 2 with adaptively chosen complex interpolation frequencies. Here, $\mathbf{MK}$ is of dimension n with $\#\lambda$ eigenvalues lying within the energy window $[540\,\mathrm{eV}, 600\,\mathrm{eV}]$. The comparisons are made for GMRES convergence tolerances of 10^{-4}, 10^{-5}, and 10^{-6}, with k as the reduced model order, GEMMs as the total number of matrix-matrix products, and the total wall-clock time is given in seconds. 103

GLOSSARY

μ-OP: Microarchitecture specific operations

1PDM: One–particle density matrix

1RDM: One–particle reduced density matrix

2C: Two–component

2RDM: Two–particle reduced density matrix

4C: Four–component

ADC: Algebraic diagrammatic construction

B3LYP: The Becke 3–parameter Lee–Yang–Parr exchange correlation functional

BLAS: Basic linear algebra subroutines

BO: Born–Oppenheimer

CC: Coupled cluster

CPP-CC: Complex polarization propagator coupled cluster

CPP-SCF: Complex polarization propagator self–consistent field

CPP: The complex polarization propagator

CPU: Central processing unit

DC: Dirac–Coulomb

DFT: Density functional theory

EOM: Equation of motion

FMA: Fused multiply–add

FOPPA: The first order polarization propagator

FSS: Fine structure splitting

FW: Foldy–Wouthuysen

GEMM: Matrix–matrix product

GEMV: Matrix–vector product

GGA: The generalized gradient approximation

GHF: Generalized Hartree–Fock

GKS: Generalized Kohn–Sham

GMRES: The generalized minimum residual method

GSCF: Generalized self–consistent field

HF-MO: Hartree–Fock molecular orbital

HF: Hartree–Fock

HK: Hohenberg–Kohn

KS-DFT: Kohn–Sham density functional theory

KS-MO: Kohn–Sham molecular orbital

KS: Kohn–Sham

MD: The modified Dirac equation

MIMO: Multiple–input multiple–output

MKL: Math kernel library

MOR: Model order reduction

MO: Molecular orbital

MPI: Message passing interface

NC: Non–collinear

NEXAFS: Near edge X–ray absorption fine structure spectroscopy

NI: Non–interacting

NR: Non–relativistic

PH-RPA: The particle–hole random phase approximation

PH-TDA: The particle–hole Tamm–Dancoff approximation

PP-RPA: The particle–particle random phase approximation

PP-TDA: The particle–particle Tamm–Dancoff approximation

QFT: Quantum field theory

RHF: Restricted Hartree–Fock

RKS: Restricted Kohn–Sham

RPA: The random phase approximation

RSCF: Restricted self–consistent field

SCF: Self–consistent field

SIMD: Single–instruction multiple–data

SYR2K: Symmetric rank-2k update

SYR2: Symmetric rank-2 update

TDA: The Tamm–Dancoff approximation

TDDFT: Time–dependent density functional theory

TDHF: Time–dependent Hartree–Fock

UHF: Unrestricted Hartree–Fock

UKS: Unrestricted Kohn–Sham

USCF: Unrestricted self–consistent field

X2C-HF: Exact two–component Hartree–Fock

X2C-KS: Exact two–component Kohn–Sham

X2C-PH-TDA: The exact two–component particle–hole Tamm–Dancoff approximation

X2C-PP-TDA: The exact two–component particle–particle Tamm–Dancoff approximation

X2C: Exact two–component

XAS: X–Ray absorption spectroscopy.

XC: Exchange–correlation

ACKNOWLEDGMENTS

I express my sincere appreciation to University of Washington (UW), where I have had the opportunity to pursue meaningful research in the field of electronic structure theory. Further, I would like to thank Professor Xiaosong Li, my research adviser, for his invaluable guidance and mentorship over the past five years. The encouragement and criticism I have received from Xiaosong during my time in his group has shaped the scientist that I am and will guide my development in my future scientific endeavors. Xiaosong, thank you for allowing me to pursue my own research directions and make mistakes and realizations in my own time; it's been great working with you.

I would further like to thank my undergraduate adviser, Professor Jaeju Ko, for encouraging my interest in chemical physics and computer science at an early point in my career. I would have likely not pursued higher education were it not for my research experience in her group.

At UW, I've had the pleasure to work with, or adjacent to a number of outstanding faculty who have helped shape my views of science and its interplay with theory. In particular, Professor David Masiello and Professor Stefan Stoll have played an integral part in my development as a scientist. Your opinions are among those which I hold in highest regard. Thank you for keeping me grounded and for never allowing me to forget that theory must always exist parallel to physics.

The Li research group has also played an important role in my research career. In particular, Dr. Alessio Petrone, Dr. Joshua Goings, Dr. Patrick Lestrange, Dr. Feizhi Ding, Dr. Franco Egidi, Dr. Greta Donati, and Dr. David Lingerfelt have been invaluable assets in all of my research projects in one way or another. Their expertise has complemented mine

in fantastic ways as to produce the best possible science that we could. The next academic generation of students in the Li group has kept me honest and has aided my ability to convey scientific ideas to further the knowledge to others (although it may not always seem like it). Thanks to Joseph Kasper, Joseph Radler, Shichao Sun, Hongbin Liu, Ryan Beck, Torin Stetina, Andrew Wildman and Lauren Koulias.

I'd like to thank my friends and family, without whose support I would not be where I am today. My parents Kristen and Thomas were always supportive of what ever crazy ideas I had growing up, and encouraged me to pursue my passions wherever they may lead me.

Finally, I'd like to thank my wonderful wife, Gemma. By far you bore the brunt of all my of successes and failures as a graduate student and have been a never ending source of love and support for as long as I've known you. Thank you for moving all the way across the country and uprooting your life just to come be with me while I pursued my Ph.D. It's hard to express my gratitude in full, but thank you.

DEDICATION

to my dear wife, Gemma

PREFACE

The pursuit of scientific endeavors can not be done in a vacuum: it is largely a collaborative effort in the context of the scientific body as a whole. As such, it would be prudent to outline my contributions and the contributions of others to the research presented in the following chapters.

Chapter 1 presents a reasonably in-depth overview of the theoretical preliminaries which provide a basis for the research in the chapters which follow. While a major part of my graduate research career has been the pursuit of a deep understanding of these theories both from a mathematical and physical perspective, I would be remiss to attribute any of the fundamental theoretical developments outlined in Chapter 1 solely to myself. Chapter 1 depends heavily on the body of scientific literature relating to electronic structure theory and quantum mechanics in general: both contemporary and historical texts. The novel aspect of Chapter 1 is in the presentation of these methods in a cohesive and consistent manner such that the treatments of relativistic and non–relativistic theory are in a sense equivalent. Much of the formal development of the manipulations of these operators in terms of the Pauli matrices was done in collaboration with Dr. Franco Egidi (FE).

Chapter 2 outlines my primary contributions to the field of relativistic electronic structure theory. The first project discussed presents a scalable implementation of non–collinear Kohn–Sham density functional theory in a Gaussian basis set. The general protocol for the generalized density variables utilized in this work were developed by Peralta *et al* (*Phys. Rev. B.* **2007**, 75, pp 196405) and Egidi, *et al* (*J. Chem. Theory Comput.* **2017**, 13, pp 2591), though no implementation details were divulged in either of those papers. My primary contribution to this work was the implementation of the proposed algorithm and

in the formal development of the efficient intermediates used for the assembly of the Fock matrix. This work was done in collaboration with Dr. Alessio Petrone (AP), where much of the code development was written through iterations between him and myself. The proof for the adherence of these generalized density variables to the zero-torque theorem was done in collaboration with Shichao Sun and Professor Xiaosong Li. The distributed memory implementation of the numerical integration was written by myself. The efficient intermediates were originally derived by myself, then further refined through discussions with AP. Further, the framework within which this algorithm was developed (ChronusQ) has been primarily development by myself to this point. The majority of the tests were performed by AP and were selected by the two of us.

The second project discussed in Chapter 2 presents an extension of the particle-particle Tamm-Dancoff approximation to two-component relativistic Hamiltonians. This project was originally inspired through email discussions with Professor Weitao Yang and his student Dr. Yang Yang at Duke University. They provided me with non-relativistic test cases which accelerated the development of this algorithm in Gaussian. The development of this algorithm in Gaussian was written by myself, but much of the development would have been stalled had it not been for thorough discussion with FE at the time. The test cases for this algorithm were chosen by FE and ran by myself. Analysis of the results in the context of the two-component time-dependent Hartree-Fock algorithm was done in equal parts by myself and FE.

Chapter 3 presents a novel algorithm for the estimation of the linear absorption spectrum by model order reduction. This work was done in extensive collaboration with Dr. Chao Yang and his student Roel van Beeuman (RB) at Lawrence Berkeley National Lab. The initial idea for applying model order reduction to the absorption spectrum is due to RB. The formal development of the final algorithm was due to extensive discussion between RB and myself. RB provided a proof-of-concept MATLAB implementation of the algorithm using

data provided by myself. The MATLAB implementation provided the primary reference from which I wrote the production implementation in ChronusQ using small test systems. The validation of the algorithm for larger test cases was done by myself. The full eigendecomposition reference values were obtained by RB on the Cori supercomputer using matrices provided by myself.

Chapter 1

THEORETICAL PRELIMINARIES

In this chapter, I will outline the theoretical preliminaries which will serve as the basis for the subsequent development of relativistic electronic structure theory. Further, this chapter will serve as the primary source of notation which will be used throughout the remainder of this work.

1.1 The Physical Hilbert Space and The Slater Determinant

Perhaps the most fundamental axiom of quantum mechanics is in that for every physical system, there is associated a separable complex Hilbert space, $\mathcal{H}$, such that the vectors of said Hilbert space represent the quantum states of the system [1]. Such vectors are referred to as wave functions and the inner product on $\mathcal{H}$ is referred to as an expectation value. The formal structure of $\mathcal{H}$ is dictated by the Hamiltonian for the physical system, $\hat{H}$, through the wave equation

$$\hat{H}(t)\left|\Psi(t)\right\rangle = \mathrm{i}\partial_t \left|\Psi(t)\right\rangle, \qquad \left|\Psi(t)\right\rangle \in \mathcal{H}. \tag{1.1}$$

Here, t is the proper time of the quantum system and ∂_t is the partial derivative of the wave function with respect to time. The explicit dependence on t will be dropped for brevity in much of the following, except for when its presence is required to avoid ambiguity. The nature of $\hat{H}$ for various physical situations and approximations relevant to this work will be discussed in detail in later sections (see Secs. 1.7 and 1.8 for instance), however the mere existence of such an operator at this stage is sufficient for the subsequent developments. As the primary focus of this work will be the treatment of the many–body electronic problem in molecular quantum mechanics, one might remark that the physical system in question is

a *composite* system consisting of many, indistinguishable particles (electrons). Denoting the Hilbert space of a composite system consisting of N particles as $\mathcal{H}^N$, we know that as $\mathcal{H}^N$ is separable, it must admit a countable, dense basis [2]. The direct product space consisting of the Hilbert spaces which describe its constituent parts, namely those spaces which describe a single particle system: $\mathcal{H}^1$, provides a convenient basis for $\mathcal{H}^N$ such that

$$\mathcal{H}^N = \text{span}\left[\bigotimes_{i=1}^{N} \mathcal{H}^1\right]. \tag{1.2}$$

The separability condition of Eq. (1.2) is crucial to the following developments as it allows one to construct a simple basis for vectors in $\mathcal{H}^N$ as N–fold tensor products of single–particle wave functions which form a countable basis for $\mathcal{H}^1$, i.e. $\mathcal{C} = \{|\phi_p\rangle\} \subset \mathcal{H}^1$ such that $\mathcal{H}^1 = \text{span}\,[\mathcal{C}]$. In the following, vectors in $\mathcal{H}^1$, in particular elements of $\mathcal{C}$, will be referred to as orbitals.

As the electron is the moiety of interest in this work, vectors in $\mathcal{H}^N$ must adhere to certain additional criteria in order for them to represent physically realizable wave functions. As electrons are fermions, physically relevant elements of $\mathcal{H}^N$, which we will denote $\mathcal{H}^N_- \subset \mathcal{H}^N$, must adhere to Fermi–Dirac statistics, namely that they must exhibit anti-symmetric behavior under particle permutation [3, 4], i.e.

$$\mathcal{P}_{ij}\left|\Phi^N\right\rangle = -\left|\Phi^N\right\rangle, \qquad \left|\Phi^N\right\rangle \in \mathcal{H}^N_-, \tag{1.3}$$

where $\mathcal{P}_{ij}$ is the particle permutation operator which interchanges particle i and j (for a more thorough discussion on linear operators acting on $\mathcal{H}^N$, see Sec. 1.2). Remark that this notion of particle interchange is intimately related to Eq. (1.2). With this additional constraint, we may construct a basis for $\mathcal{H}^N_-$ with elements [5]

$$\left|\Phi^N_I\right\rangle = \frac{1}{\sqrt{N!}} \sum_{\xi \in S_N(\mathcal{K}^N_I)} \text{sign}\,(\xi) \bigotimes_{i=1}^{N} \left|\phi_{\xi(i)}\right\rangle, \tag{1.4}$$

where $\mathcal{K}^N_I$ is an N–element subset of $\mathcal{C}$ and $S_N(\mathcal{K}^N_I)$ is the symmetric group of $\mathcal{K}^N_I$ which consists of all permutations of its elements; denoted here as permutation functions ξ. $\text{sign}\,(\xi) \in$

$\{\pm 1\}$ denotes the sign of the permutation and ensures the anti–symmetry of the overall wave function. Equation (1.4) introduces a number of concepts with are typically jargonized in the quantum chemistry community. In this work, $\mathcal{K}_I^N$ will be referred to as an N–particle configuration (or simply a configuration when N is to be understood from the context), and $\left|\Phi_I^N\right\rangle$ will be referred to as a Slater determinant. It is important to note that $\left|\Phi_I^N\right\rangle$ is completely determined by $\mathcal{K}_I^N$ but is only unique up to a unitary transformation [5], i.e. for a unitary matrix $\boldsymbol{U} \in \mathbb{C}^{N\times N}$,

$$\left|\Phi_I^N\right\rangle = \left|\Phi_J^N\right\rangle \quad \text{iff} \quad |\psi_j\rangle = \sum_{i=1}^{N} U_{ji} \, |\phi_i\rangle \quad \forall \, |\psi_j\rangle \in \mathcal{K}_J^N, |\phi_i\rangle \in \mathcal{K}_I^N. \tag{1.5}$$

The N–fold tensor product on the right hand side of Eq. (1.4) if referred to as a Hartree product, and while not a valid fermionic wave function in and of itself, it provides an important building block for constructing such wave functions and will be the primary moiety with which we will develop the arithmetic of many–body quantum theory. As such, we reserve a shorthand for the Hartree product constructed for a general set $\{|\psi_p\rangle\} \subset \mathcal{H}^1$ as $|\psi_1, \psi_2 \cdots\rangle \equiv |\psi_1\rangle \otimes |\psi_2\rangle \otimes \cdots$.

As a basis for $\mathcal{H}_-^N$, any vector $\left|\Psi_n^N\right\rangle \in \mathcal{H}_-^N$ may be written as [5]

$$\left|\Psi_n^N\right\rangle = \sum_I D_I^n \left|\Phi_I^N\right\rangle, \tag{1.6}$$

where $D_I^n = \left\langle \Phi_I^N \mid \Psi_n^N \right\rangle \in \mathbb{C}$ is the complex expansion coefficient of the I-th configuration in the overall wave function, and I runs over all unique N–particle Slater determinants which may be constructed from $\mathcal{C}$. The fact that the set of all Slater determinants forms a basis for $\mathcal{H}_-^N$ serves as the primary foundation for the majority of approximate quantum mechanical methods regarding molecular systems. In the following, we will assume both $\left|\Phi_I^N\right\rangle$ and the elements of $\mathcal{C}$ are orthonormal with respect to the metric on their respective Hilbert spaces.

While the Hilbert space representation of the wave function is the most illuminating description for the development of general quantum mechanical theory, it is often advantageous from the perspective of practical calculations that one projects the vectors of the Hilbert space onto a convenient basis. To this end, we consider a specific single–particle basis,

$\{|\boldsymbol{r},\sigma\rangle = |\boldsymbol{r}\rangle \otimes |\sigma\rangle\}$, which consists of the simultaneous eigenfunctions of both the position and z–spin operators, denoted $\hat{\boldsymbol{r}}$ and $\hat{S}_z$, such that [6]

$$\hat{\boldsymbol{r}}\,|\boldsymbol{r},\sigma\rangle = |\boldsymbol{r},\sigma\rangle\,\boldsymbol{r}, \qquad \boldsymbol{r}\in\mathbb{R}^3, \tag{1.7a}$$

$$\hat{S}_z\,|\boldsymbol{r},\sigma\rangle = |\boldsymbol{r},\sigma\rangle\,\sigma, \qquad \sigma\in\left\{\pm\frac{1}{2}\right\}. \tag{1.7b}$$

Here, we have denoted the particle's position and z–axis spin projection as $\boldsymbol{r}$ and σ, respectively. Namely, if $\mathcal{H}^1$ represents a non-relativistic spin–1/2 fermion, $\{|\boldsymbol{r},\sigma\rangle\}$ forms a complete basis for $\mathcal{H}^1$ and admits the following orthonormality condition on the $\mathcal{H}^1$ inner product,

$$\langle \boldsymbol{r}',\sigma' \mid \boldsymbol{r},\sigma\rangle = \delta^3(\boldsymbol{r}-\boldsymbol{r}')\delta_{\sigma\sigma'}, \tag{1.8}$$

where δ^3 and $\delta_{\sigma\sigma'}$ are the Dirac delta function and Kronecker delta tensor, respectively. As $\{|\boldsymbol{r},\sigma\rangle\}$ is continuous, i.e. its spectrum is continuous, its cardinality is uncountable. Thus, its utility does not manifest as it does in the context of countable bases, such as is required by Eq. (1.4), but rather in the fact that it allows for the casting of inner products on $\mathcal{H}^1$ as integrals through the resolution of the identity on $\mathcal{H}^1$ via

$$\hat{1}_1 = \sum_{\sigma}\int_{\mathbb{R}^3} |\boldsymbol{r},\sigma\rangle\,\langle\boldsymbol{r},\sigma|\;\mathrm{d}^3\boldsymbol{r}. \tag{1.9}$$

As such, for arbitrary $|\phi\rangle, |\phi'\rangle \in \mathcal{H}^1$ we may cast the inner product as

$$\langle\phi \mid \phi'\rangle = \sum_{\sigma}\int_{\mathbb{R}^3} \phi^*(\boldsymbol{r},\sigma)\phi'(\boldsymbol{r},\sigma)\,\mathrm{d}^3\boldsymbol{r}, \tag{1.10}$$

where we have defined

$$\langle\boldsymbol{r},\sigma \mid \phi\rangle \equiv \phi(\boldsymbol{r},\sigma), \quad \text{s.t.} \quad \phi:\mathbb{F}\mapsto\mathbb{C}, \tag{1.11}$$

and $\mathbb{F} = \mathbb{R}^3\times\{\pm 1/2\}$. Equation (1.11), as a projection onto an element of a product space, may be further separated onto the spin basis, $\{\alpha,\beta\}$,

$$\phi(\boldsymbol{r},\sigma) = \phi^{\alpha}(\boldsymbol{r})\alpha(\sigma) + \phi^{\beta}(\boldsymbol{r})\beta(\sigma), \tag{1.12}$$

such that

$$\alpha(\sigma) = \begin{cases} 1 & \sigma = +\frac{1}{2} \\ 0 & \sigma = -\frac{1}{2} \end{cases}, \tag{1.13}$$

$$\beta(\sigma) = \begin{cases} 0 & \sigma = +\frac{1}{2} \\ 1 & \sigma = -\frac{1}{2} \end{cases}. \tag{1.14}$$

In general, single–particle wave functions of the form Eq. (1.11) will be referred to as spinor orbitals, or simply spinors. Noting the two spin components, it is also canonical to refer to these types of wave functions as "two–component" (2C) wave functions. For brevity in the following, we will denote $|\boldsymbol{x}\rangle \equiv |\boldsymbol{r}, \sigma\rangle$ such that

$$\int_{\mathbb{F}} f(\boldsymbol{x}) \, \mathrm{d}^4\boldsymbol{x} \equiv \sum_{\sigma} \int_{\mathrm{R}^3} f(\boldsymbol{r}, \sigma) \, \mathrm{d}^3\boldsymbol{r}, \tag{1.15a}$$

$$\delta^4(\boldsymbol{x} - \boldsymbol{x}') \equiv \delta^3(\boldsymbol{r} - \boldsymbol{r}')\delta_{\sigma\sigma'} \tag{1.15b}$$

As a basis for $\mathcal{H}^1$, we may construct a basis for $\mathcal{H}^N$ through N–fold tensor products of the elements of $\{|\boldsymbol{x}\rangle\}$ via Eq. (1.2). Denoting $|\boldsymbol{x}_i\rangle$ as a specific element of $\{|\boldsymbol{x}\rangle\}$, the vectors

$$|\boldsymbol{x}_1, \boldsymbol{x}_2, \ldots, \boldsymbol{x}_N\rangle = \bigotimes_{i=1}^{N} |\boldsymbol{x}_i\rangle \tag{1.16}$$

form a basis form a basis for $\mathcal{H}^N$. Extending Eqs. (1.8) and (1.9) in a similar manner, we may state

$$\langle \boldsymbol{x}'_1, \boldsymbol{x}'_2, \ldots, \boldsymbol{x}'_N \mid \boldsymbol{x}_1, \boldsymbol{x}_2, \ldots, \boldsymbol{x}_N \rangle = \prod_{i=1}^{N} \delta^4(\boldsymbol{x}'_i - \boldsymbol{x}_i), \tag{1.17}$$

$$\hat{1}_N = \int \cdots \int_{\mathbb{F}} \bigotimes_{i=1}^{N} |\boldsymbol{x}_i\rangle \langle \boldsymbol{x}_i| \, \mathrm{d}^4\boldsymbol{x}_i, \tag{1.18}$$

such that for $\left|\Phi^N\right\rangle, \left|\Psi^N\right\rangle \in \mathcal{H}^N$,

$$\left\langle \Phi^N \mid \Psi^N \right\rangle = \int \cdots \int_{\mathbb{F}} \Phi^{N*}(\boldsymbol{x}_1, \boldsymbol{x}_2, \ldots, \boldsymbol{x}_N) \Psi^N(\boldsymbol{x}_1, \boldsymbol{x}_2, \ldots, \boldsymbol{x}_N) \, \mathrm{d}^4\boldsymbol{x}_1 \cdots \mathrm{d}^4\boldsymbol{x}_N, \tag{1.19}$$

where we have denoted

$$\left\langle \boldsymbol{x}_1, \boldsymbol{x}_2, \ldots, \boldsymbol{x}_N \mid \Phi^N \right\rangle \equiv \Phi^N(\boldsymbol{x}_1, \boldsymbol{x}_2, \ldots, \boldsymbol{x}_N). \tag{1.20}$$

In this work, many–body wave functions of the form Eq. (1.20) will be referred to as spinor wave functions. The utility of such as basis expansion manifests in the context of Slater determinants in that as a direct consequence of Eqs. (1.4), (1.11) and (1.16), we may express

$$\Phi_I^N(\boldsymbol{x}_1, \boldsymbol{x}_2, \ldots, \boldsymbol{x}_N) = \frac{1}{\sqrt{N!}} \sum_{\xi \in S_N(\mathcal{K}_I^N)} \text{sign}\,(\xi) \prod_{i=1}^{N} \phi_{\xi(i)}(\boldsymbol{x}_i). \tag{1.21}$$

Unlike the tensor product definition of Eq. (1.4), the expression of the Slater determinant in will prove to be of much of practical utility due to the fact that the spinor orbital basis, as a set of complex valued functions, is commutative.

1.2 Representation of Linear Operators and Expectation Values

Fundamental to the formulation of any quantum mechanical theory is the identification of linear operators on $\mathcal{H}^N$ which represent the physical observables of the system. In this work we will refer to such observables as properties. A more precise identification of the operators relevant to this work will be presented later (see Secs. 1.7 and 1.8 for instance), however in this section we will focus on the general presentation of these operators and how they will typically manifest in the context of Eq. (1.2).

In this work, linear operators which act on $\mathcal{H}^N$, $\hat{O}^N : \mathcal{H}^N \mapsto \mathcal{H}^N$, will be referred to as N–particle operators. As was the case for the state vectors of $\mathcal{H}^N$, the general description of $\hat{O}^N$ as an operator on a Hilbert space is indeed the most illuminating treatment for general manipulations of quantum mechanical operators which is independent of coordinate projection. However, it will often be the case that we must examine the projection of these operators onto a coordinate space in order to perform practical calculations. To demonstrate this, we examine the action of an operator $\hat{O}^1$ on the spinor basis $\{|\boldsymbol{x}\rangle\}$ from Sec. 1.1 through

the identity resolvent in Eq. (1.9),

$$\hat{O}^1 = \hat{1}_1 \hat{O}^1 \hat{1}_1 = \iint_{\mathbb{F}} |\boldsymbol{x}\rangle \, \hat{O}^1(\boldsymbol{x};\boldsymbol{x}') \, \langle \boldsymbol{x}'| \, \mathrm{d}^4\boldsymbol{x} \, \mathrm{d}^4\boldsymbol{x}', \tag{1.22}$$

where

$$\hat{O}^1(\boldsymbol{x};\boldsymbol{x}') = \left\langle \boldsymbol{x} \left| \hat{O}^1 \right| \boldsymbol{x}' \right\rangle. \tag{1.23}$$

For $|\psi\rangle, |\chi\rangle \in \mathcal{H}^1$ we have

$$\begin{aligned} \left\langle \psi \left| \hat{O}^1 \right| \chi \right\rangle &= \iint_{\mathbb{F}} \psi^*(\boldsymbol{x}) \hat{O}^1(\boldsymbol{x};\boldsymbol{x}') \chi(\boldsymbol{x}') \, \mathrm{d}^4\boldsymbol{x} \, \mathrm{d}^4\boldsymbol{x}' \\ &= \int_{\mathbb{R}^3} \begin{bmatrix} \psi^\alpha(\boldsymbol{r}) \\ \psi^\beta(\boldsymbol{r}) \end{bmatrix}^\dagger \begin{bmatrix} \hat{O}^{1,\alpha\alpha}(\boldsymbol{r}) & \hat{O}^{1,\alpha\beta}(\boldsymbol{r}) \\ \hat{O}^{1,\beta\alpha}(\boldsymbol{r}) & \hat{O}^{1,\beta\beta}(\boldsymbol{r}) \end{bmatrix} \begin{bmatrix} \chi^\alpha(\boldsymbol{r}) \\ \chi^\beta(\boldsymbol{r}) \end{bmatrix} \mathrm{d}^3\boldsymbol{r}, \end{aligned} \tag{1.24}$$

Here we have made an assumption which is crucial to the following developments, namely that the operators that we will work with are *spatially local*, i.e.

$$\hat{O}^1(\boldsymbol{x};\boldsymbol{x}') = \delta^3(\boldsymbol{r} - \boldsymbol{r}') \hat{O}^{1,\sigma\sigma'}(\boldsymbol{r}'). \tag{1.25}$$

However, it will be the case that the linear operators which correspond to observables of the physical system will typically be spatially local, and instances where this is not the case will be treated explicitly.

This notion of operator representation may be generalized to N–particle operators in a similar manner through resolution of $\hat{1}_N$,

$$\begin{aligned} \hat{O}^N = \hat{1}_N \hat{O}^N \hat{1}_N = \int \cdots \int_{\mathbb{F}} \mathrm{d}^4\boldsymbol{x}_1 \cdots \mathrm{d}^4\boldsymbol{x}_N \int \cdots \int_{\mathbb{F}} \mathrm{d}^4\boldsymbol{x}'_1 \cdots \mathrm{d}^4\boldsymbol{x}'_N \times \\ |\boldsymbol{x}_1, \ldots, \boldsymbol{x}_N\rangle \, \hat{O}^N(\boldsymbol{x}_1, \ldots, \boldsymbol{x}_N; \boldsymbol{x}'_1, \ldots, \boldsymbol{x}'_N) \, \langle \boldsymbol{x}'_1, \ldots, \boldsymbol{x}'_N| \end{aligned} \tag{1.26}$$

such that for arbitrary N–body Hartree products constructed from $\{|\psi_p\rangle\}, \{|\chi_p\rangle\} \subset \mathcal{H}^N$

$$\begin{aligned} \left\langle \psi_1, \psi_2, \ldots, \psi_N \left| \hat{O}^N \right| \chi_1, \chi_2, \ldots, \chi_N \right\rangle = \sum_{\sigma_1 \cdots \sigma_N} \sum_{\tau_1 \cdots \tau_N} \int \cdots \int_{\mathbb{R}^3} \mathrm{d}^3\boldsymbol{r}_1 \cdots \mathrm{d}^3\boldsymbol{r}_N \times \\ \psi_1^{\sigma_1 *}(\boldsymbol{r}_1) \cdots \psi_N^{\sigma_N *}(\boldsymbol{r}_N) \; \hat{O}^{N,\sigma_1\tau_1\cdots\sigma_N\tau_N}(\boldsymbol{r}_1, \ldots, \boldsymbol{r}_N) \; \chi_1^{\tau_1}(\boldsymbol{r}_1) \cdots \chi_N^{\tau_N}(\boldsymbol{r}_N). \end{aligned} \tag{1.27}$$

where we have again assumed operator spatial locality,

$$\hat{O}^N(\boldsymbol{x}_1,\ldots,\boldsymbol{x}_N;\boldsymbol{x}'_1,\ldots,\boldsymbol{x}'_N) = \left(\prod_{i=1}^{N}\delta^3(\boldsymbol{r}_i-\boldsymbol{r}'_i)\right)\hat{O}^{1,\sigma_1\sigma'_1\cdots\sigma_N\sigma'_N}(\boldsymbol{r}'_1,\ldots,\boldsymbol{r}'_N). \tag{1.28}$$

For brevity, this representation of N–particle operators will often be interpreted as rank–$2N$ tensors in the basis of spin eigenfunctions,

$$\underline{\hat{O}}^N(\boldsymbol{r}_1,\ldots,\boldsymbol{r}_N) \equiv \sum_{\sigma_1\cdots\sigma_N}\sum_{\sigma'_1\cdots\sigma'_N}\hat{O}^{N,\sigma_1\sigma'_1\cdots\sigma_N\sigma'_N}(\boldsymbol{r}_1,\ldots,\boldsymbol{r}_N)\otimes\bigotimes_{i=1}^{N}\boldsymbol{e}_{\sigma_i}\otimes\boldsymbol{e}_{\sigma'_i}, \tag{1.29}$$

where

$$\boldsymbol{e}_\alpha = \begin{bmatrix}1\\0\end{bmatrix}, \qquad \boldsymbol{e}_\beta = \begin{bmatrix}0\\1\end{bmatrix}. \tag{1.30}$$

The product operation of operators denoted $\underline{\hat{O}}^N(\boldsymbol{r}_1,\ldots,\boldsymbol{r}_N)$ and their action onto spinor wave functions (or more specifically, Hartree products) will be a rank-N tensor contraction over spin indices as depicted in Eq. (1.24) and more generally in Eq. (1.27). For the remainder of this work, we will refer to the projections $\underline{\hat{O}}^N(\boldsymbol{r}_1,\ldots,\boldsymbol{r}_N)$ as spinor representations of $\hat{O}^N$, or simply spinor operators when appropriate. The super-scripted moieties $\hat{O}^{N,\sigma_1\sigma'_1\cdots}$ will be referred to as the spinor operator coefficients relative to the spin basis. It is important to note that spinor representations of N–particle operators are still *operators*, i.e. they still continue to act to the right to complete their operation. The utility of Eqs. (1.25) and (1.28) is in that it allows one to form operators compatible with spinor representations of the wave function as opposed to the general, abstract Hilbert space definition. In the following developments, it will be useful to examine Eq. (1.29) under a change of basis from the Kronecker products of $\boldsymbol{e}_\alpha$ and $\boldsymbol{e}_\beta$ to that of the Pauli matrices,

$$\underline{\hat{O}}^N(\boldsymbol{r}_1,\ldots,\boldsymbol{r}_N) = \sum_{K_1\cdots K_N}\hat{O}^{N,K_1\cdots K_N}(\boldsymbol{r}_1,\ldots,\boldsymbol{r}_N)\otimes\bigotimes_{i=1}^{N}\boldsymbol{\sigma}_{K_i} \tag{1.31}$$

where

$$\boldsymbol{\sigma}_0 = \begin{bmatrix}1&0\\0&1\end{bmatrix}, \quad \boldsymbol{\sigma}_1 = \begin{bmatrix}0&1\\1&0\end{bmatrix}, \quad \boldsymbol{\sigma}_2 = \begin{bmatrix}0&-\mathrm{i}\\\mathrm{i}&0\end{bmatrix}, \quad \boldsymbol{\sigma}_3 = \begin{bmatrix}1&0\\0&-1\end{bmatrix}. \tag{1.32}$$

An explicit derivation for the form of the general rank–$2N$ transformation is given in Appendix A. Here we state the special case of one–particle spinor operators as it will provide the basis for many of the manipulations in subsequent developments,

$$\hat{O}^{1,0}(\boldsymbol{r}) = \frac{1}{2}\left(\hat{O}^{1,\alpha\alpha}(\boldsymbol{r}) + \hat{O}^{1,\beta\beta}(\boldsymbol{r})\right), \tag{1.33a}$$

$$\hat{O}^{1,1}(\boldsymbol{r}) = \frac{1}{2}\left(\hat{O}^{1,\alpha\beta}(\boldsymbol{r}) + \hat{O}^{1,\beta\alpha}(\boldsymbol{r})\right), \tag{1.33b}$$

$$\hat{O}^{1,2}(\boldsymbol{r}) = \frac{\mathrm{i}}{2}\left(\hat{O}^{1,\alpha\beta}(\boldsymbol{r}) - \hat{O}^{1,\beta\alpha}(\boldsymbol{r})\right), \tag{1.33c}$$

$$\hat{O}^{1,3}(\boldsymbol{r}) = \frac{1}{2}\left(\hat{O}^{1,\alpha\alpha}(\boldsymbol{r}) - \hat{O}^{1,\beta\beta}(\boldsymbol{r})\right). \tag{1.33d}$$

The coefficients labeled $\hat{O}^{N,K_1K_2,\cdots}$ will be referred to as the spinor operator coefficients relative to the Pauli matrices, or simply the Pauli coefficients for brevity. This representation is especially convenient when the operator in question is hermitian, i.e. $\hat{O}^N = \hat{O}^{N\dagger}$. In Eq. (1.29), hermiticity of $\hat{O}^N$ simply implies that the *product* of the operator coefficients and basis vectors must be invariant under the hermitian adjoint and states nothing about the hermiticity of the coefficients themselves. Due to the fact that the Pauli matrices are self–adjoint, Eq. (1.31) implies that $\hat{O}^N$ is hermitian if and only if the Pauli coefficients are hermitian. Working with hermitian operators carries a number of benefits, most notably that the spectrum of such operators is strictly real.

Despite the fact that $\mathcal{H}^N$ admits a basis of a direct product space consisting of N single–particle Hilbert spaces, N–particle operators need not carry the same structure, i.e. in general, these operators need not exist solely as direct products of operators on $\mathcal{H}^1$. This is not to say that N–particle operators *cannot* adopt a product structure, just that it is not a requirement, and indeed if often not the case. However, the notion that some N–particle operators *can* adopt a product structure indicates the need to describe the action of M–particle operators on $\mathcal{H}^N$ (with $N \geq M$) while leaving $N - M$ particles unchanged. To demonstrate this state of affairs, it is convenient to examine the action of such an operator,

$\hat{O}^M(i,j,\ldots)$, on a spinor wave function of the form Eq. (1.21),

$$\underline{\hat{O}}^M(\boldsymbol{r}_i,\boldsymbol{r}_j,\ldots)\Phi_I^N(\boldsymbol{x}_1,\boldsymbol{x}_2,\ldots,\boldsymbol{x}_N) = \frac{1}{\sqrt{N!}}\sum_{\xi\in S_N(\mathcal{K}_I^N)}\operatorname{sign}(\xi)\ \left(\underline{\hat{O}}^M(\boldsymbol{r}_i,\boldsymbol{r}_j,\ldots)\phi_{\xi(i)}(\boldsymbol{x}_i)\phi_{\xi(j)}(\boldsymbol{x}_j)\cdots\right)\prod_{k\neq(i,j,\ldots)}^{N-M}\phi_{\xi(k)}(\boldsymbol{x}_k), \tag{1.34}$$

where $(i,j,\ldots)$ is an M–element tuple specifying the subset of particles upon which it acts. In this work, we will typically be concerned with operators which act on no more than two particles at a time.

It will be often the case that N–particle operators may be expressed as sums over one– and two–particle operators. In this context, the realization of Eq. (1.34) is of exceptional utility in that, for an expectation value involving a particular Slater determinant described by configuration $\mathcal{K}_I^N$ [5],

$$\left\langle \Phi_I^N \middle| \sum_i \hat{O}^1(i) \middle| \Phi_I^N \right\rangle = \sum_{i\in\mathcal{K}_I^N} O^1_{ii}, \tag{1.35a}$$

$$\left\langle \Phi_I^N \middle| \sum_{i\neq j} \hat{O}^2(i,j) \middle| \Phi_I^N \right\rangle = \sum_{i\neq j\in\mathcal{K}_I^N} O^2_{ijij} - O^2_{ijji}, \tag{1.35b}$$

where for the $\mathcal{H}^1$ basis $\mathcal{C} = \{|\phi_p\rangle\}$ from the previous section,

$$O^1_{pq} \equiv \left\langle \phi_p \middle| \hat{O}^1(1) \middle| \phi_q \right\rangle = \int_{\mathbb{F}} \phi_p^*(\boldsymbol{x}_1)\underline{\hat{O}}^1(\boldsymbol{x}_1)\phi_q(\boldsymbol{x}_1)\,\mathrm{d}^4\boldsymbol{x}_1, \tag{1.36a}$$

$$O^2_{pqrs} \equiv \left\langle \phi_p,\phi_q \middle| \hat{O}(1,2) \middle| \phi_r,\phi_s \right\rangle = \iint_{\mathbb{F}} \phi_p^*(\boldsymbol{x}_1)\phi_q^*(\boldsymbol{x}_2)\underline{\hat{O}}^2(\boldsymbol{x}_1,\boldsymbol{x}_2)\phi_r(\boldsymbol{x}_1)\phi_s(\boldsymbol{x}_2)\,\mathrm{d}^4\boldsymbol{x}_1\,\mathrm{d}^4\boldsymbol{x}_2. \tag{1.36b}$$

Namely, M–particle on operators on $\mathcal{H}^N$ may be represented as rank–$2M$ tensors on $\mathcal{H}^1$; a fact which will be used extensively in the following developments.

1.3 Density Matrices

In the following, it will be useful to define the N–particle density matrix, $\hat{\gamma}^N$, associated with a particular state vector $\left|\Psi^N\right\rangle \in \mathcal{H}^N$ [6],

$$\hat{\gamma}^N = \left|\Psi^N\right\rangle \left\langle\Psi^N\right| . \tag{1.37}$$

Clearly, $\hat{\gamma}^N$ is an hermitian N–particle operator on $\mathcal{H}^N$ which projects its elements onto $\left|\Psi^N\right\rangle$. The density matrix plays a very central role in the development of quantum mechanical theory in that, in the case of a pure quantum state, it contains the same information as the state vector while its nature as an operator allows for a number of useful manipulations which simplify many expressions, such as inner products. In the spinor coordinate basis, $\hat{\gamma}^N$ takes the form

$$\begin{aligned}\left\langle \boldsymbol{x}_1, \boldsymbol{x}_2, \ldots, \boldsymbol{x}_N \left|\hat{\gamma}^N\right| \boldsymbol{x}'_1, \boldsymbol{x}'_2, \ldots, \boldsymbol{x}'_N \right\rangle &\equiv \gamma^N(\boldsymbol{x}_1, \boldsymbol{x}_2, \ldots, \boldsymbol{x}_N; \boldsymbol{x}'_1, \boldsymbol{x}'_2, \ldots, \boldsymbol{x}'_N) \\ &= \Psi^N(\boldsymbol{x}_1, \boldsymbol{x}_2, \ldots, \boldsymbol{x}_N)\Psi^{N*}(\boldsymbol{x}'_1, \boldsymbol{x}'_2, \ldots, \boldsymbol{x}'_N).\end{aligned} \tag{1.38}$$

From the N–particle density matrix, it is possible to define P–particle reduced density matrices ($P < N$) via contractions over single–particle indices,

$$\begin{aligned}\gamma^P(\boldsymbol{x}_1, \boldsymbol{x}_2, \ldots, \boldsymbol{x}_P; \boldsymbol{x}'_1, \boldsymbol{x}'_2, \ldots, \boldsymbol{x}'_P) = \frac{N!}{P!(N-P)!} \int \cdots \int_{\mathbb{F}} \mathrm{d}^4\boldsymbol{x}_{P+1} \cdots \mathrm{d}^4\boldsymbol{x}_N \times \\ \gamma^N(\boldsymbol{x}_1, \boldsymbol{x}_2, \ldots, \boldsymbol{x}_P, \boldsymbol{x}_{P+1}, \ldots, \boldsymbol{x}_N; \boldsymbol{x}'_1, \boldsymbol{x}'_2, \ldots, \boldsymbol{x}'_P, \boldsymbol{x}_{P+1}, \ldots, \boldsymbol{x}_N),\end{aligned} \tag{1.39}$$

which are hermitian projectors onto the P–particle subspaces of $\mathcal{H}^N$ which construct $\left|\Psi^N\right\rangle$. Of particular interest to this work are the one– and two–particle reduced density matrices,

$$\gamma^1(\boldsymbol{x}_1; \boldsymbol{x}'_1) = N \int \cdots \int_{\mathbb{F}} \gamma^N(\boldsymbol{x}_1, \boldsymbol{x}_2, \ldots, \boldsymbol{x}_N; \boldsymbol{x}'_1, \boldsymbol{x}_2, \ldots, \boldsymbol{x}_N)\, \mathrm{d}^4\boldsymbol{x}_2 \cdots \mathrm{d}^4\boldsymbol{x}_N, \tag{1.40}$$

$$\begin{aligned}&\gamma^2(\boldsymbol{x}_1, \boldsymbol{x}_2; \boldsymbol{x}'_1, \boldsymbol{x}'_2) = \\ &\qquad \frac{N(N-1)}{2} \int \cdots \int_{\mathbb{F}} \gamma^N(\boldsymbol{x}_1, \boldsymbol{x}_2, \boldsymbol{x}_3, \ldots, \boldsymbol{x}_N; \boldsymbol{x}'_1, \boldsymbol{x}'_2, \boldsymbol{x}_3, \ldots, \boldsymbol{x}_N)\, \mathrm{d}^4\boldsymbol{x}_3 \cdots \mathrm{d}^4\boldsymbol{x}_N,\end{aligned} \tag{1.41}$$

which play in important role in the description of one– and two–body interactions in the electronic Hamiltonian. For brevity, we will refer to the one– and two–particle reduced

density matrices for a particular state vector as the 1RDM and 2RDM, respectively. In the case of a single Slater determinant, $\left|\Psi^N\right\rangle = \left|\Phi_I^N\right\rangle$, the 1RDM and 2RDM take on an especially simple form due to Eq. (1.4) [6],

$$\gamma^1(\boldsymbol{x}_1;\boldsymbol{x}_1') = \sum_{i\in\mathcal{K}_I^N} \phi_i(\boldsymbol{x}_1)\phi_i^*(\boldsymbol{x}_1'), \tag{1.42}$$

$$\gamma^2(\boldsymbol{x}_1,\boldsymbol{x}_2;\boldsymbol{x}_1',\boldsymbol{x}_2') = \frac{1}{2}\left(\gamma^1(\boldsymbol{x}_1;\boldsymbol{x}_1')\gamma^1(\boldsymbol{x}_2;\boldsymbol{x}_2') - \gamma^1(\boldsymbol{x}_1;\boldsymbol{x}_2')\gamma^1(\boldsymbol{x}_2;\boldsymbol{x}_1')\right). \tag{1.43}$$

In other words, all P–particle RDMs corresponding to a single Slater determinant are simply P–fold Grassman products of the 1RDM, and thus the state is completely determined by the 1RDM. This is not the case for general many–body wave functions written as Eq. (1.6) and will prove to be of great utility in the manipulation of Slater determinants.

In direct analogy to Eq. (1.35), we may cast the expectation values of 1– and 2–body operators of a general state vector in terms of the 1RDM and 2RDM which correspond to that vector [6],

$$\left\langle \Psi^N \left| \sum_i \hat{O}^1(i) \right| \Psi^N \right\rangle = \sum_{\sigma_1\sigma_1'} \int_{\mathbb{R}^3} \left(\hat{O}^{1,\sigma_1\sigma_1'}(\boldsymbol{r}_1)\gamma^1(\boldsymbol{r}_1,\sigma_1';\boldsymbol{r}_1',\sigma_1)\right)\Big|_{\boldsymbol{r}_1'=\boldsymbol{r}_1} \mathrm{d}^3\boldsymbol{r}_1, \tag{1.44a}$$

$$\begin{aligned}\left\langle \Psi^N \left| \sum_{i\neq j} \hat{O}^2(i,j) \right| \Psi^N \right\rangle = \sum_{\sigma_1\sigma_1'\sigma_2\sigma_2'} \iint_{\mathbb{R}^3} \mathrm{d}^3\boldsymbol{r}_1\,\mathrm{d}^3\boldsymbol{r}_2 \times \\ \left(\hat{O}^{2,\sigma_1\sigma_1'\sigma_2\sigma_2'}(\boldsymbol{r}_1,\boldsymbol{r}_2)\gamma^2(\boldsymbol{r}_1,\sigma_1',\boldsymbol{r}_2,\sigma_2';\boldsymbol{r}_1',\sigma_1,\boldsymbol{r}_2',\sigma_2)\right)\Big|_{\boldsymbol{r}_1'=\boldsymbol{r}_1,\boldsymbol{r}_2'=\boldsymbol{r}_2}.\end{aligned} \tag{1.44b}$$

It is to be understood from the context that the restriction of the spatial indices is to be performed *after* action of the spinor operator on the RDM. This allows for generality even in the case where the spinor operator contains differential character. Substituting in the expressions for the Slater determinant RDMs in Eq. (1.42) yields Eq. (1.35) exactly. However, the expressions in Eq. (1.44) are much more general than that of Eq. (1.35) as they treat an arbitrary many–body wave function. Thus Eq. (1.44) will be the primary focus in the following.

Motivated by the spin sums in Eq. (1.44), it is useful to cast the RDMs as rank–$2P$

tensors on the spin basis in the spirit of Eqs. (1.25) and (1.28) such that

$$\underline{\gamma}^{P}(\boldsymbol{r}_1,\boldsymbol{r}_2,\ldots;\boldsymbol{r}'_1,\boldsymbol{r}'_2,\ldots)\equiv\gamma^{P,\sigma_1\sigma'_1\sigma_2\sigma'_2\cdots}(\boldsymbol{r}_1,\boldsymbol{r}_2,\ldots;\boldsymbol{r}'_1,\boldsymbol{r}'_2,\ldots)\otimes\bigotimes_{i=1}^{P}\boldsymbol{e}_{\sigma_i}\otimes\boldsymbol{e}_{\sigma'_i}. \tag{1.45}$$

In this work, we will refer to this representation as the spinor representation of the RDM and the super scripted moieties $\gamma^{P,\sigma_1\sigma'_1\cdots}$ as the spinor coefficients relative to the spin basis. As was the case for spinor operators in Sec. 1.2, hermiticity of the density matrix does not place any specific restrictions on the hermiticity on the spinor coefficients. In analogy to Eq. (1.31), we may construct hermitian coefficients via

$$\underline{\gamma}^{P}(\boldsymbol{r}_1,\boldsymbol{r}_2,\ldots;\boldsymbol{r}'_1,\boldsymbol{r}'_2,\ldots)\equiv\gamma^{P,K_1K_2\cdots}(\boldsymbol{r}_1,\boldsymbol{r}_2,\ldots;\boldsymbol{r}'_1,\boldsymbol{r}'_2,\ldots)\otimes\bigotimes_{i=1}^{P}\boldsymbol{\sigma}_{K_i}. \tag{1.46}$$

This realization allows for a simplification of Eq. (1.44), such that (see Appendix A)

$$\left\langle\Psi^N\left|\sum_i\hat{O}^1(i)\right|\Psi^N\right\rangle=2\sum_K\int_{\mathbb{R}^3}\left(\hat{O}^{1,K}(\boldsymbol{r}_1)\gamma^{1,K}(\boldsymbol{r}_1;\boldsymbol{r}'_1)\right)\Big|_{\boldsymbol{r}'_1=\boldsymbol{r}_1}\mathrm{d}^3\boldsymbol{r}_1, \tag{1.47a}$$

$$\begin{aligned}\left\langle\Psi^N\left|\sum_{i\neq j}\hat{O}^2(i,j)\right|\Psi^N\right\rangle&=4\sum_{K_1K_2}\iint_{\mathbb{R}^3}\mathrm{d}^3\boldsymbol{r}_1\,\mathrm{d}^3\boldsymbol{r}_2\times\\&\left(\hat{O}^{2,K_1K_2}(\boldsymbol{r}_1,\boldsymbol{r}_2)\gamma^{2,K_1K_2}(\boldsymbol{r}_1,\boldsymbol{r}_2;\boldsymbol{r}'_1,\boldsymbol{r}'_2)\right)\Big|_{\boldsymbol{r}'_1=\boldsymbol{r}_1,\boldsymbol{r}'_2=\boldsymbol{r}_2},\end{aligned} \tag{1.47b}$$

where all of the Pauli components of the spinor operator and RDMs are hermitian. In the case of a single Slater determinant constructed from configuration $\mathcal{K}_I^N$, the Pauli components of the 1RDM are given by

$$\gamma^{1,0}(\boldsymbol{r};\boldsymbol{r}')=\frac{1}{2}\sum_{i\in\mathcal{K}_I^N}\left(\phi_i^{\alpha}(\boldsymbol{r})\phi_i^{\alpha*}(\boldsymbol{r}')+\phi_i^{\beta}(\boldsymbol{r})\phi_i^{\beta*}(\boldsymbol{r}')\right), \tag{1.48a}$$

$$\gamma^{1,1}(\boldsymbol{r};\boldsymbol{r}')=\frac{1}{2}\sum_{i\in\mathcal{K}_I^N}\left(\phi_i^{\alpha}(\boldsymbol{r})\phi_i^{\beta*}(\boldsymbol{r}')+\phi_i^{\beta}(\boldsymbol{r})\phi_i^{\alpha*}(\boldsymbol{r}')\right), \tag{1.48b}$$

$$\gamma^{1,2}(\boldsymbol{r};\boldsymbol{r}')=\frac{\mathrm{i}}{2}\sum_{i\in\mathcal{K}_I^N}\left(\phi_i^{\alpha}(\boldsymbol{r})\phi_i^{\beta*}(\boldsymbol{r}')-\phi_i^{\beta}(\boldsymbol{r})\phi_i^{\alpha*}(\boldsymbol{r}')\right), \tag{1.48c}$$

$$\gamma^{1,3}(\boldsymbol{r};\boldsymbol{r}')=\frac{1}{2}\sum_{i\in\mathcal{K}_I^N}\left(\phi_i^{\alpha}(\boldsymbol{r})\phi_i^{\alpha*}(\boldsymbol{r}')-\phi_i^{\beta}(\boldsymbol{r})\phi_i^{\beta*}(\boldsymbol{r}')\right). \tag{1.48d}$$

The expressions for the 2RDM may be derived from the Grassman product form in Eq. (1.42). It is important to note that Eq. (1.48) is N–representable (i.e. it represents an N–particle Slater determinant) if and only if the orbitals used in its construction are orthonormal [6]. Thus this places a restriction on the possible choices of orbitals which may be used in the construction of Slater determinants for which we would like to utilize the properties of density matrices.

In the case where the operator in equation is scalar multiplicative, i.e. does not contain differential operators, the order in which the coordinate restriction under the integration of Eqs. (1.44) and (1.47) occurs is irrelevant. Thus, Eq. (1.47) reduces to [6]

$$\left\langle \Psi^N \left| \sum_i \hat{O}^1(i) \right| \Psi^N \right\rangle = 2 \sum_K \int_{\mathbb{R}^3} \hat{O}^{1,K}(\boldsymbol{r}_1) \rho^{1,K}(\boldsymbol{r}_1) \, \mathrm{d}^3\boldsymbol{r}_1, \tag{1.49a}$$

$$\left\langle \Psi^N \left| \sum_{i \neq j} \hat{O}^2(i,j) \right| \Psi^N \right\rangle = 4 \sum_{K_1 K_2} \iint_{\mathbb{R}^3} \hat{O}^{2,K_1K_2}(\boldsymbol{r}_1, \boldsymbol{r}_2) \rho^{2,K_1K_2}(\boldsymbol{r}_1, \boldsymbol{r}_2) \, \mathrm{d}^3\boldsymbol{r}_1 \, \mathrm{d}^3\boldsymbol{r}_2 \tag{1.49b}$$

where we have defined

$$\rho^{1,K}(\boldsymbol{r}) = \gamma^{1,K}(\boldsymbol{r}; \boldsymbol{r}), \tag{1.50a}$$

$$\rho^{2,KK'}(\boldsymbol{r}, \boldsymbol{r}') = \gamma^{2,KK'}(\boldsymbol{r}, \boldsymbol{r}'; \boldsymbol{r}, \boldsymbol{r}'), \tag{1.50b}$$

as the diagonal elements of the Pauli components of the 1 and 2RDMs. They may be thought of themselves as Pauli components of moieties satisfying

$$\underline{\rho^1}(\boldsymbol{r}) = \sum_K \rho^{1,K}(\boldsymbol{r}) \otimes \boldsymbol{\sigma}_K \tag{1.51}$$

$$\underline{\rho^2}(\boldsymbol{r}, \boldsymbol{r}') = \sum_{KK'} \rho^{2,KK'}(\boldsymbol{r}, \boldsymbol{r}') \otimes \boldsymbol{\sigma}_K \otimes \boldsymbol{\sigma}_{K'} \tag{1.52}$$

In this work, we will refer to the moieties $\underline{\rho}^1$ and $\underline{\rho}^2$ as the one– and two–particle densities, respectively. With respect the density matrices, manipulating densities directly allows for drastic simplifications in the development of many–body theory as the hermiticity of the density matrix implies that they are strictly real. In regards to the one–particle density, $\rho^{1,0}(\boldsymbol{r})$ will be referred to as the *scalar* density, $\boldsymbol{m}(\boldsymbol{r}) = \{\rho^{1,1}(\boldsymbol{r}), \rho^{1,2}(\boldsymbol{r}), \rho^{1,3}(\boldsymbol{r})\}$ as the magnetization density, and $|\boldsymbol{m}(\boldsymbol{r})|$ as the spin density [7].

1.4 Second Quantization

While Eqs. (1.4) and (1.21) provide the basic structure for the many–body fermionic wave function, its explicit form is a bit unwieldy and thus its use for practical calculation of moieties such as expectation values more complicated than Eq. (1.35) is somewhat limited. To this end we introduce a formalism known as second quantization, or the occupation number formalism [3–5], which aims to greatly simplify the construction and manipulation of anti-symmetric wave functions such as those in Eq. (1.4). The primary hallmark of second quantization is in the representation of a Slater determinant as an array of integers known as *occupation numbers*, denoted $\left\{n_p^I\right\}$, indicate the inclusion (or *occupation*) of elements of $\mathcal{C}$ in the configuration which describes the I-th determinant. As such, the length of said array is $|\mathcal{C}|$ and the sum of its elements is the number of particles in the system for a representation of $\mathcal{H}^N$. Due to the fact that electrons are fermions, there is a further restriction on the possible values of the occupations numbers due to the Pauli exclusion principle, namely that a particle can be occupied ($n_p^I = 1$) or unoccupied ($n_p^I = 0$), i.e. two electrons cannot occupy the same orbital. For the basis $\mathcal{C}$ we may construct a Hilbert space, $\mathcal{F}$, as a product of single particle occupations, denoted $|n_p\rangle$, such that [3]

$$\left|n_1, n_2, \ldots, n_{|\mathcal{C}|}\right\rangle = \bigotimes_{i=1}^{|\mathcal{C}|} |n_i\rangle\,, \quad \left|n_1, n_2, \ldots, n_{|\mathcal{C}|}\right\rangle \in \mathcal{F}, \tag{1.53}$$

where we may define inner and outer products as

$$\left\langle n_1, n_2, \ldots, n_{|\mathcal{C}|} \mid n_1', n_2', \ldots, n_{|\mathcal{C}|}'\right\rangle = \prod_{i=1}^{|\mathcal{C}|} \delta_{n_i n_i'}, \tag{1.54a}$$

$$\sum_{n_1 n_2 \cdots} \left|n_1, n_2, \ldots, n_{|\mathcal{C}|}\right\rangle \left\langle n_1, n_2, \ldots, n_{|\mathcal{C}|}\right| = \hat{1}_{\mathcal{F}}. \tag{1.54b}$$

Here, $\hat{1}_{\mathcal{F}}$ is the identity operator on $\mathcal{F}$. $\mathcal{F}$ is commonly referred to as the Fock space.

One may construct representations of Slater determinants (Eq. (1.4)) in a consistent manner in this formalism through the introduction of two sets of operators, $\left\{c_p^\dagger : \mathcal{F} \to \mathcal{F}\right\}$ and $\{c_p : \mathcal{F} \to \mathcal{F}\}$, which are referred to as creation and annihilation operators respectively,

and the notion of a zero particle occupation vector known as the physical vacuum, $|\text{vac}\rangle \in \mathcal{F}$, such that

$$|\text{vac}\rangle = \left|[0_1, 0_2, \ldots, 0_{|C|}]\right\rangle, \tag{1.55a}$$

$$c_p^\dagger \left|[n_1, n_2, \ldots, n_p, \ldots, n_{|C|}]\right\rangle = \frac{\delta_{n_p 0}}{\sqrt{N+1}} \left|[n_1, n_2, \ldots, 1_p, \ldots, n_{|C|}]\right\rangle, \tag{1.55b}$$

$$c_p \left|[n_1, n_2, \ldots, n_p, \ldots, n_{|C|}]\right\rangle = \delta_{n_p 1}\sqrt{N} \left|[n_1, n_2, \ldots, 0_p, \ldots, n_{|C|}]\right\rangle. \tag{1.55c}$$

Here, N is the number of particles in the occupation vector *before* action. To ensure anti-symmetry in the representation of the wave function, we may specify the following commutation relations

$$[c_p^\dagger, c_q^\dagger]_+ = 0, \tag{1.56a}$$

$$[c_p, c_q]_+ = 0, \tag{1.56b}$$

$$[c_p, c_q^\dagger]_+ = \delta_{pq}, \tag{1.56c}$$

where $[\cdot, \cdot]_+$ is the anti–commutator. The action of products consisting on any number of these operators may be derived inductively from Eqs. (1.55) and (1.56). Such products are often referred to as strings. As such, we may recast Eq. (1.4) as a string of creation operators,

$$\left|\Phi_I^N\right\rangle \mapsto \left|\Phi_I^N\right\rangle_{\mathcal{F}} = \left(\prod_{i \in \mathcal{K}_I^N} c_i^\dagger\right) |\text{vac}\rangle, \tag{1.57}$$

where $\left|\Phi_I^N\right\rangle_{\mathcal{F}} \in \mathcal{F}$ is the occupation vector representation of $\left|\Phi_I^N\right\rangle$.

There are a number of remarkable simplifications that arise from the adoption of second quantization for the practical treatment of many–body quantum theory. The first that we will discuss here relates back to the completeness of the basis of Slater determinants in the construction of many–body fermionic wave functions, i.e. all many–body wave functions may be constructed as a linear combination of all of the unique Slater determinants which may be constructed from $\mathcal{C}$ (Eq. (1.6)), given that $\mathcal{C}$ is a complete basis for $\mathcal{H}^1$. To this end, we introduce the notion of an N–particle reference determinant which will be denoted $\left|0^N\right\rangle$ and

is described by some configuration $\mathcal{K}_0^N$. $\mathcal{K}_0^N$ will be referred to as the *occupied* space (denoted $\mathcal{O} = \mathcal{K}_0^N$), and elements of the occupied space will be denoted with a subscript $i, j, k, \ldots$, i.e. $|\phi_i\rangle \in \mathcal{O}$. Similarly, we will refer the elements of $\mathcal{C}$ which are not in $\mathcal{O}$ as the unoccupied (or *virtual*, denoted $\mathcal{V} = \mathcal{C} \setminus \mathcal{O}$) space and elements of this space will be denoted with a subscript $a, b, c, \ldots$, i.e. $|\phi_a\rangle \in \mathcal{V}$. Subscripts $p, q, r, \ldots$ will remain as the notation for a general element of $\mathcal{C}$ from either $\mathcal{O}$ or $\mathcal{V}$. Clearly, all M–particle Slater determinants (with M not necessarily equal to N) which may be constructed from $\mathcal{C}$ may be constructed by constructing a configuration from N_o elements of $\mathcal{O}$ and N_v elements of $\mathcal{V}$ such that $N_o + N_v = M$. Thus, logically, it follows that all M–particle determinants may be constructed by removing $n_o = \min(N - M, 0) + P$ orbitals from $\mathcal{O}$ (with $P \in [0, \max(N, N - M)]$) and replacing them $n_v = \max(M - N, 0) + P$ orbitals from $\mathcal{V}$. In the language of second quantization, the act of removing and replacing orbitals is made simple through the introduction of so called transition operators

$$\left(\left|0^N\right\rangle_{ijk\cdots}^{abc\cdots}\right)_{\mathcal{F}} = \tau_{ijk\cdots}^{abc\cdots} \left|0^N\right\rangle_{\mathcal{F}}, \tag{1.58}$$

where

$$\tau_{ijk\cdots}^{abc\cdots} = \left(c_a^\dagger c_b^\dagger c_c^\dagger \cdots\right)(c_i c_j c_k \cdots). \tag{1.59}$$

Upon action, $\left|0^N\right\rangle_{ijk\cdots}^{abc\cdots}$ is an $M = N - n_o + n_v$ particle Slater determinant built from removing orbitals $i, j, k, \ldots$ from $\left|0^N\right\rangle$ and replacing them with orbitals $a, b, c, \ldots \in \mathcal{V}$. The set of all τ operators generates all M–particle Slater determinants from the N–particle reference and is complete given any reference [8]. It is worth noting at this point that due to the anti-commutation relations of Eq. (1.56), $\tau_{ijk\cdots}^{abc\cdots}$ is anti symmetric with respect to permutation of adjacent creation and annihilation operators, i.e.

$$\tau_{ijk\cdots}^{abc\cdots} = -\tau_{ijk\cdots}^{acb\cdots} = -\tau_{jik\cdots}^{abc\cdots} = \tau_{jik\cdots}^{acb\cdots}. \tag{1.60}$$

Thus, necessarily, transition operators with repeated indices are zero, $\tau_{ijk\cdots}^{aab\cdots} = \tau_{iij\cdots}^{abc\cdots} = 0$. Within this ansatz for constructing arbitrary Slater determinants from a reference, we may

recast Eq. (1.6) as

$$\left|\Psi_n^N\right\rangle = (t^n)_0 \left|0^N\right\rangle + \sum_{ai} (t^n)_i^a \left|0^N\right\rangle_i^a + \sum_{abij} (t^n)_{ij}^{ab} \left|0^N\right\rangle_{ij}^{ab} + \sum_{abcijk} (t^n)_{ijk}^{abc} \left|0^N\right\rangle_{ijk}^{abc} + \cdots , \quad (1.61)$$

where the transition amplitudes, $\boldsymbol{t}^n$, have taken the place of the D_I^n amplitudes of the original expansion. Based on this construction, the components of $\boldsymbol{t}^n$ must also constitute an anti-symmetric tensor in the same manner as Eq. (1.60). The expansion of Eq. (1.61) may be further cast into a more general, and convenient form in terms of explicit action of the transition operators such that for an arbitrary M–particle Slater determinant,

$$\left|\Psi_n^M\right\rangle_{\mathcal{F}} = \hat{R}_n^{M,N\dagger} \left|0^N\right\rangle_{\mathcal{F}} , \quad (1.62)$$

where $\hat{R}_n^{N,M\dagger}$ is an "excitation" operator which is defined as

$$\hat{R}_n^{M,N\dagger} = \begin{cases} \sum_{abc\cdots} (t^n)^{abc\cdots} \tau^{abc\cdots} + \sum_{abc\cdots di} (t^n)_i^{abc\cdots d} \tau_i^{abc\cdots d} + \sum_{abc\cdots deij} (t^n)_{ij}^{abc\cdots de} \tau_{ij}^{abc\cdots de} + \cdots & M > N \\ (t^n)_0 + \sum_{ai} (t^n)_i^a \tau_i^a + \sum_{abij} (t^n)_{ij}^{ab} \tau_{ij}^{ab} + \sum_{abcijk} (t^n)_{ijk}^{abc} \tau_{ijk}^{abc} + \cdots & M = N \\ \sum_{ijk\cdots} (t^n)_{ijk\cdots} \tau_{ijk\cdots} + \sum_{aijk\cdots l} (t^n)_{ijk\cdots l}^a \tau_{ijk\cdots l}^a + \sum_{abijk\cdots lm} (t^n)_{ijk\cdots lm}^{ab} \tau_{ijk\cdots lm}^{ab} + \cdots & M < N \end{cases} \quad (1.63)$$

Here the extent of extended sums of transition operators involving unbalanced creation and annihilation operators in the cases $M \neq N$ is to be understood from the context, i.e. for the special case that $M = N + 1$, we obtain

$$\hat{R}_n^{N+1,N\dagger} = \sum_a (t^n)^a \tau^a + \sum_{abi} (t^n)_i^{ab} \tau_i^{ab} + \sum_{abcij} (t^n)_{ij}^{abc} \tau_{ij}^{abc} + \cdots \quad (1.64)$$

The remarkable thing about Eq. (1.62) is that all possible many–body wave functions may be constructed (hence the †) from a single Slater determinant (or any other wave function) within an operator formalism. Thus one need only understand the manipulation of $\hat{R}_n^{M,N\dagger}$ in the context of other many–body operators and how their combined action affects the reference determinant to to determine expectation values: the primary moiety which we will manipulate in this work.

To this point, the next property of second quantization which we will exploit in this work, and the one that we will use most often, is the fact that one may cast M–particle operators on $\mathcal{H}^N$ as scalar contractions of $2M$–element operator strings with rank–$2M$ tensors on $\mathcal{H}^1$ [3–5],

$$\sum_i \hat{O}^1(i) \mapsto \hat{O}^1_{\mathcal{F}} = \sum_{pq} O^1_{pq} c^\dagger_p c_q, \tag{1.65a}$$

$$\sum_{i\neq j} \hat{O}^2(i,j) \mapsto \hat{O}^2_{\mathcal{F}} = \sum_{pqrs} O^2_{qprs} c^\dagger_p c^\dagger_q c_r c_s. \tag{1.65b}$$

The tensors O^1_{pq} and O^2_{qprs} are defined as in Eq. (1.36). This is a truly remarkable result from a practical perspective at it allows a simple prescription for the evaluation of inner products for general elements $\left|\Psi^N_n\right\rangle, \left|\Psi^N_m\right\rangle \in \mathcal{H}^N$

$$\left\langle \Psi^N_n \left| \sum_i \hat{O}^1(i) \right| \Psi^N_m \right\rangle = \sum_{pq} O^1_{pq} \left\langle \Psi^N_n \left| c^\dagger_p c_q \right| \Psi^N_m \right\rangle_{\mathcal{F}}, \tag{1.66a}$$

$$\left\langle \Psi^N_n \left| \sum_{i\neq j} \hat{O}^2(i,j) \right| \Psi^N_m \right\rangle = \sum_{pq} O^1_{qprs} \left\langle \Psi^N_n \left| c^\dagger_p c^\dagger_q c_r c_s \right| \Psi^N_m \right\rangle_{\mathcal{F}}. \tag{1.66b}$$

The moieties $\langle \cdot | \cdot | \cdot \rangle_{\mathcal{F}}$ denote that all quantities in that inner product are expressed in second quantization. To demonstrate the utility of this concept, we examine the substitution of the reference excitation ansatz from Eq. (1.62) into the one–body inner product such that

$$\begin{aligned}
\left\langle \Psi^N_n \left| c^\dagger_p c_q \right| \Psi^N_m \right\rangle_{\mathcal{F}} &= \left\langle 0^N \left| \hat{R}^{N,N\dagger}_n c^\dagger_p c_q \hat{R}^{N,N\dagger}_m \right| 0^N \right\rangle_{\mathcal{F}} \\
&= (t^n)^*_0 \left((t^m)_0 \left\langle 0^N \left| c^\dagger_p c_q \right| 0^N \right\rangle_{\mathcal{F}} + \sum_{ai} (t^m)^a_i \left\langle 0^N \left| c^\dagger_p c_q \tau^a_i \right| 0^N \right\rangle_{\mathcal{F}} + \cdots \right) + \\
&\quad \sum_{ai} (t^n)^{a*}_i \left((t^m)_0 \left\langle 0^N \left| \tau^{a\dagger}_i c^\dagger_p c_q \right| 0^N \right\rangle_{\mathcal{F}} + \sum_{bj} (t^m)^b_j \left\langle 0^N \left| \tau^{a\dagger}_i c^\dagger_p c_q \tau^b_j \right| 0^N \right\rangle_{\mathcal{F}} + \cdots \right) + \\
&\quad \cdots
\end{aligned} \tag{1.67}$$

As first glance, it may seems as though casting the inner product into a second quantized form has drastically complicated its evaluation. However, the rather complicated task of evaluating inner productions involving determinants of the form Eq. (1.4) or Eq. (1.21)is

cast into tensor contractions of few–body integrals (Eq. (1.36)) and transition amplitudes ($\boldsymbol{t}^n$), with inner products involving strings of creation and annihilation operators. Given the prior, one may heavily exploit the commutation relationships of Eq. (1.56) to easily evaluate inner products of arbitrary operator strings through various diagrammatic techniques or explicitly by Wick's theorem [3, 4, 9].

In essence, second quantization provides a common language which allows one to factor elements of a particular many–body quantum theory into parts which are dependent and independent of the single–particle basis. Such a state of affairs has been demonstrated in Eqs. (1.66) and (1.67). If one can define an inner product on $\mathcal{H}^1$ and is able to develop an ansatz for the form of Eq. (1.62) for a particular theory, it is immediately compatible with second quantization. In this work, second quantization will play a crucial role in the translation of the results of non–relativistic quantum mechanics to the consistent treatment of relativistic effects.

1.5 Time–Independent Solutions of the Wave Equation

Examination of the time–independent solutions of Eq. (1.1) plays a central role in the development of both time–dependent and time–independent quantum theory. Thus, for the time being, we will restrict ourselves to Hamiltonians which are independent of time. Within this consideration, the electronic Hamiltonians one typically encounters for molecular systems with N electrons, $\hat{H}_{el} : \mathcal{H}^N \to \mathcal{H}^N$ take the general form

$$\hat{H}_{el} = \sum_{i}^{N} \Big(\hat{h}(i) + \hat{v}(i) \Big) + \frac{1}{2} \sum_{i \neq j}^{N} \hat{g}(i,j), \tag{1.68}$$

where $\hat{h}$ and $\hat{v}$ are the one–body free particle Hamiltonian and potential operators respectively. $\hat{g}$ is a two–body operator which describes the interaction between two electrons. At this point, the explicit structure of these operators are immaterial to the following developments; simply noting that the presence of $\hat{g}$ renders direct solution of Eq. (1.1) for the many–body wave function impractical. Nevertheless, one may write down a general form for

the solution of Eq. (1.1) with this Hamiltonian as [10]

$$|\Psi(t)\rangle = \exp\left[-i(t-t_0)\hat{H}_{el}\right]|\Psi(t_0)\rangle\,, \tag{1.69}$$

where t_0 is a reference time point for which one may specify an initial condition for the electronic wave function. Without loss of generality, we will typically take $t_0 = 0$. We now consider the eigen spectrum of the electronic Hamiltonian such that there exists a set of wave functions $|\Psi_n\rangle \in \mathcal{H}^N$ which yield

$$\hat{H}_{el}\,|\Psi_n\rangle = E_n\,|\Psi_n\rangle\,, \tag{1.70}$$

where E_n is the energy eigenvalue of $|\Psi_n\rangle$. The pairs $(|\Psi_n\rangle\,, E_n)$ will be referred to as the adiabatic electronic states, and Eq. (1.70) as the time–independent quantum wave equation in the following. As a spectral decomposition of $\hat{H}_{el}$, $\mathcal{H}^N = \text{span}\left[\{|\Psi_n\rangle\}\right]$ such that any arbitrary vector in $\mathcal{H}^N$ may be decomposed as

$$|\Psi(t)\rangle = \sum_n c_n(t)\,|\Psi_n\rangle\,, \qquad c_n(t) = \langle\Psi_n\,|\,\Psi(t)\rangle\,. \tag{1.71}$$

Here, the coefficients are assumed to be unit normal, i.e. $\sum_n |c_n(t)|^2 = 1$. Note that the coefficients $c_n(t)$ are different from those of Eq. (1.6) as the adiabatic states are in general *not* Slater determinants due to the presence of $\hat{g}$.

Suppose that we specify the initial condition of the wave function to be an adiabatic state of the electronic Hamiltonian, $|\Psi(0)\rangle = |\Psi_m\rangle$. Equation (1.70) immediately yields the action of the Hamiltonian on the state such that

$$|\Psi(t)\rangle = \exp\left[-itE_m\right]|\Psi_m\rangle\,. \tag{1.72}$$

Time–dependent solutions such as this comprise a special class of solutions to Eq. (1.1) known as stationary states. As E_m is a real constant (due to the hermiticity of $\hat{H}_{el}$), Eq. (1.72) is referred to as stationary as it trivially rotates through the complex plane such that for operators void of differentiation with respect to time, $\hat{O}^N$

$$\left\langle \Psi(t)\left|\hat{O}^N\right|\Psi(t)\right\rangle = \left\langle \Psi_m\left|\hat{O}^N\right|\Psi_m\right\rangle \quad \forall t, \tag{1.73}$$

i.e. the wave function itself is not, strictly speaking, time independent, but its expectation values are. This is not to be confused with the time–dependence of the physical state itself, which is a moiety independent of mathematical representation. In the case of stationary solutions, it is only the mathematical representation of this state which is time dependent, whereas the physical state represented is in fact time–independent. Of particular interest to this work, at least in the development of a theoretical framework, will be the so called ground electronic state: the electronic adiabat which has the lowest energy, $(E_0, |\Psi_0\rangle)$. In practice, one may determine the ground state by minimizing the energy functional,

$$E[\Psi] = \frac{\left\langle \Psi \left| \hat{H}_{el} \right| \Psi \right\rangle}{\langle \Psi \mid \Psi \rangle}, \tag{1.74}$$

which admits a sole minimum at the ground electronic state due to the variational theorem [5, 10].

1.6 Mean–Field Quantum Mechanics and Basis Set Expansions

1.6.1 The Hartree–Fock Approximation

Up to this point, no approximations in the treatment of the many–body wave function have been introduced. That is to say, given that $\mathcal{C}$ is a complete, countable basis for $\mathcal{H}^1$, all of the developments in this and the previous sections treat the electronic many–body problem *exactly*. However, even a cursory inspection of the nature of $\mathcal{C}$ indicates that it must be countably infinite in order to satisfy completeness on $\mathcal{H}^1$. Thus it must be truncated in some systematic way in order for it to be useful in any practical treatment of the many–body problem. Unfortunately, any truncation of Eq. (1.6) or Eq. (1.61) will make it impossible in general to construct exact many–body states, such as those of Eq. (1.70). In this work, we will be primarily concerned with optimizing a set $\mathcal{C}$ such that we may construct a reference determinant (per Eq. (1.62)) which minimizes the energy functional in Eq. (1.74) over all possible Slater determinants. In effect, such a minimization will construct the best single Slater determinant approximation to the many–body ground electronic state which may

serve as a reference determinant in the context of Eq. (1.62) for better approximations for true many–body wave functions. The approximation which describes the ground state wave function as the minimizing Slater determinant of Eq. (1.74) is known as the Hartree–Fock (HF) approximation [5, 6].

Before delving into the specifics of how one might go about optimizing $\mathcal{C}$ to minimize Eq. (1.74), one might note that in the absence of $\hat{g}$, i.e. many–body operators of the form

$$\hat{f}^N = \sum_i^N \hat{f}^1(i), \qquad \hat{f}^1(i) = \hat{h}(i) + \hat{v}^{\text{eff}}(i), \tag{1.75}$$

admit eigen functions which may be written as single Slater determinants. That is to say that given a set $\mathcal{C}$ whose elements are eigen functions of $\hat{f}^1(1)$,

$$\hat{f}^1(1)\,|\phi_p\rangle = |\phi_p\rangle\,\epsilon_p, \tag{1.76}$$

the Slater determinants which may be constructed from $\mathcal{C}$ are eigen functions of Eq. (1.75) [5]. Here, ϵ_p will be referred to as the orbital eigenenergy corresponding to $|\phi_p\rangle$. Due to the lack of explicit two–body interaction in Eq. (1.75), the determinants which may be constructed from the solutions of Eq. (1.76) will be referred to as a *non–interacting* system, i.e. they particles are treated as independent particles in an effective external potential $\hat{v}^{\text{eff}}$. Given an configuration subset, $\mathcal{K}_I^N \subset \mathcal{C}$, the energy of a non–interacting system is given by

$$E_{\text{NI}} = \sum_{i \in \mathcal{K}_I^N} \epsilon_i. \tag{1.77}$$

If one wishes to minimize E_{NI} over the possible Slater determinants which may be constructed from $\mathcal{C}$, one must select the N orbitals with the lowest eigenenergy to build the determinant. This choice yields an ordering on $\mathcal{C}$ which orders orbitals in increasing orbital eigenenergy. This ordering also happens to correspond identically to the phenomenological ordering dictated by the Aufbauprinzip.

Due to the fact that a single Slater determinant is completely described by its orbital configuration, minimizing Eq. (1.74) over Slater determinants amounts to determining a configuration which minimizes the Hamiltonian expectation value. Thus it is useful to think of

Eq. (1.74) not as a functional of a single parameter, but rather as a functional of several parameters, namely N orbitals which comprise some configuration. However, as was discussed in Sec. 1.3, if we wish to utilize N–representable density matrices in the development of our theories, we must constrain the choice of possible configurations to only include those which contain orthonormal orbitals. To this end we will employ the a constrained energy Lagrangian [5],

$$\mathcal{L}[\mathcal{K}^N] = E^{\mathrm{HF}}[\mathcal{K}^N] - \sum_{i,j\in\mathcal{K}^N} \lambda_{ij} \left(\langle \phi_i \mid \phi_j \rangle - \delta_{ij} \right), \tag{1.78}$$

where $\mathcal{K}^N$ is an arbitrary N–orbital configuration and λ_{ij} is a set of to–be–determined Lagrange multipliers which will constrain our choice of orbitals to be orthonormal. HF has been used to denote the fact that this form is only valid for single Slater determinants. A necessary condition for minimization of Eq. (1.74) in this context is given by

$$\frac{\delta \mathcal{L}[\mathcal{K}^N]}{\delta \phi_i(\boldsymbol{x})} = 0, \quad \forall \phi_i(\boldsymbol{x}) \in \mathcal{K}^N, \tag{1.79}$$

where derivatives set to zero are *functional derivatives*.

The energy functional for a configuration consisting of orthonormal orbitals is often most conveniently written as a functional of the 1RDM which may be constructed from that configuration [6],

$$E^{\mathrm{HF}}[\mathcal{K}^N] = E[\gamma^1] = H^{\mathrm{core}}[\gamma^1] + J[\gamma^1] - K[\gamma^1], \tag{1.80}$$

where we have defined

$$H^{\mathrm{core}}[\gamma^1] = \iint_{\mathbb{F}} \left(\hat{h}(\boldsymbol{x}_1; \boldsymbol{x}_1') + \hat{v}(\boldsymbol{x}_1; \boldsymbol{x}_1') \right) \gamma^1(\boldsymbol{x}_1'; \boldsymbol{x}_1) \, \mathrm{d}^4\boldsymbol{x}_1 \, \mathrm{d}^4\boldsymbol{x}_1' \tag{1.81}$$

$$J[\gamma^1] = \iiiint_{\mathbb{F}} \hat{g}(\boldsymbol{x}_1, \boldsymbol{x}_2; \boldsymbol{x}_1', \boldsymbol{x}_2') \gamma^1(\boldsymbol{x}_1'; \boldsymbol{x}_1) \gamma^1(\boldsymbol{x}_2'; \boldsymbol{x}_2) \, \mathrm{d}^4\boldsymbol{x}_1 \, \mathrm{d}^4\boldsymbol{x}_1' \, \mathrm{d}^4\boldsymbol{x}_2 \, \mathrm{d}^4\boldsymbol{x}_2' \tag{1.82}$$

$$K[\gamma^1] = \iiiint_{\mathbb{F}} \hat{g}(\boldsymbol{x}_1, \boldsymbol{x}_2; \boldsymbol{x}_1', \boldsymbol{x}_2') \gamma^1(\boldsymbol{x}_1'; \boldsymbol{x}_2) \gamma^1(\boldsymbol{x}_2'; \boldsymbol{x}_1) \, \mathrm{d}^4\boldsymbol{x}_1 \, \mathrm{d}^4\boldsymbol{x}_1' \, \mathrm{d}^4\boldsymbol{x}_2 \, \mathrm{d}^4\boldsymbol{x}_2' \tag{1.83}$$

Equation (1.79) then becomes

$$\iint_{\mathbb{F}} \frac{\delta E^{\mathrm{HF}}[\mathcal{K}^N]}{\delta \gamma^1(\boldsymbol{x}_1'; \boldsymbol{x}_1)} \frac{\delta \gamma^1(\boldsymbol{x}_1'; \boldsymbol{x}_1)}{\delta \phi_i(\boldsymbol{x})} \, \mathrm{d}^4\boldsymbol{x}_1' \, \mathrm{d}^4\boldsymbol{x}_1 - \sum_{j,k\in\mathcal{K}^N} \lambda_{jk} \frac{\delta \langle \phi_j \mid \phi_k \rangle}{\delta \phi_i(\boldsymbol{x})} = 0, \quad \forall \phi_i(\boldsymbol{x}) \in \mathcal{K}^N. \tag{1.84}$$

Due to the hermiticity of both γ^1 and the inner products $\langle \phi_p \,|\, \phi_q \rangle$, Eq. (1.84) will factor into two parts which are conjugates of each other, thus requiring both terms to go to zero simultaneously. By rearranging the summation indices, Eq. (1.84) may be written as

$$\sum_{j \in \mathcal{K}^N} \int_{\mathbb{F}} \left(\hat{F}^{\mathrm{HF}}(\boldsymbol{x}_1; \boldsymbol{x}_1') \delta_{ij} - \delta^4(\boldsymbol{x}_1 - \boldsymbol{x}_1') \lambda_{ij} \right) \phi_j(\boldsymbol{x}_1') \, \mathrm{d}^4\boldsymbol{x}_1' = 0, \quad \forall \phi_i(\boldsymbol{x}) \in \mathcal{K}^N, \tag{1.85}$$

where

$$\hat{F}^{\mathrm{HF}}(\boldsymbol{x}; \boldsymbol{x}') = \frac{\delta E^{\mathrm{HF}}[\gamma^1]}{\delta \gamma^1(\boldsymbol{x}'; \boldsymbol{x})} = \hat{H}(\boldsymbol{x}; \boldsymbol{x}') + \hat{J}(\boldsymbol{x}; \boldsymbol{x}') - \hat{K}(\boldsymbol{x}; \boldsymbol{x}'), \tag{1.86}$$

$$\hat{H}^{\mathrm{core}}(\boldsymbol{x}; \boldsymbol{x}') = \frac{\delta H[\gamma^1]}{\delta \gamma^1(\boldsymbol{x}'; \boldsymbol{x})}, \qquad \hat{J}(\boldsymbol{x}; \boldsymbol{x}') = \frac{\delta J[\gamma^1]}{\delta \gamma^1(\boldsymbol{x}'; \boldsymbol{x})}, \qquad \hat{K}(\boldsymbol{x}; \boldsymbol{x}') = \frac{\delta K[\gamma^1]}{\delta \gamma^1(\boldsymbol{x}'; \boldsymbol{x})}. \tag{1.87}$$

Equation (1.85) is the general form of a set of non–linear integrodifferential equations known as the Hartree–Fock equations and $\hat{F}^{\mathrm{HF}}$ is known as the Fock operator corresponding to Eq. (1.68) [5, 6]. The non–linearity of Eq. (1.85) comes in the fact that the functionals J and K are quadratic in the density matrix, thus their functional derivative still maintains a dependence on γ^1. A configuration's satisfaction of Eq. (1.85) is the minimal requirement for the corresponding Slater determinant to minimize Eq. (1.74)

Using the fact that γ^1 (and thus $\hat{F}^{\mathrm{HF}}$) is invariant to unitary transformation of the orbitals which comprise its construction (Eq. (1.5)), we may choose to transform Eq. (1.85) in such a way as to diagonalize the matrix of Lagrange multipliers, $\boldsymbol{U} : \lambda_{ij} \to \tilde{\lambda}_i \delta_{ij}$,

$$\int_{\mathbb{F}} \hat{F}^{\mathrm{HF}}(\boldsymbol{x}_1; \boldsymbol{x}_1') \tilde{\phi}_i(\boldsymbol{x}_1'), \, \mathrm{d}^4\boldsymbol{x}_1' = \tilde{\lambda}_i \tilde{\phi}_i(\boldsymbol{x}_1), \qquad \tilde{\phi}_i = \sum_j U_{ij} \phi_j. \tag{1.88}$$

Equation (1.88) is known as the canonical Hartree–Fock equation and $\tilde{\phi}_i$ is referred to as a canonical Hartree-Fock molecular orbital (HF-MO). Due to Eq. (1.5), the Slater determinant which is formed from $\{\tilde{\phi}_i\}$ is equivalent to the one formed from $\{\phi_i\}$, we will henceforth only consider sets $\mathcal{C}$ such that $\boldsymbol{\lambda}$ is diagonalized. Clearly, Eq. (1.88) has the same form as Eqs. (1.75) and (1.76). Thus within the HF approximation, the effective external potential is given by

$$\hat{v}^{\mathrm{HF}} = \hat{v} + \hat{J} - \hat{K}, \tag{1.89}$$

and we may identify the diagonalized Lagrange multipliers as orbital eigenenergies,

$$\tilde{\lambda}_i \equiv \epsilon_i^{\mathrm{HF}}. \tag{1.90}$$

$\{\epsilon_i^{\mathrm{HF}}\}$ will be referred to as the set of canonical HF eigenenergies. The realization of Eq. (1.89) is rather profound in that it states that the minimizing Slater determinant of Eq. (1.74) is the one constructed from a set of *self–consistent, mean–field* orbitals. That is to say that each of the HF-MOs which make of this configuration in effect "feel" the effect of the other orbitals through action of the Fock operator, i.e. the orbitals themselves are non–interacting, but each orbital "knows" about all of the others through the $\hat{J}$ and $\hat{K}$ operators. Thus the HF wave function (the minimizing Slater determinant) is often referred to as the mean–field solution to Eq. (1.70) and thus Eq. (1.1).

In and of themselves, Eqs. (1.85) and (1.88) represent a challenging class of nonlinear integrodifferential equations. It was in the realization of Roothaan [11] that Eq. (1.88) may instead be cast into a numerical linear algebra problem by expanding the orbitals of $\mathcal{C}$ in a basis set,

$$\phi_p^\sigma(\boldsymbol{r}) = \sum_{\mu=1}^{N_b} C_{\mu p}^{\mathrm{HF},\sigma} \chi_\mu(\boldsymbol{r}), \tag{1.91}$$

where $C_{\mu p}^{\mathrm{HF},\sigma} = \left\langle \chi_\mu \,|\, \phi_p^\sigma \right\rangle$ is a tensor of expansion coefficients which expand each HF-MO as a linear combination of N_b basis functions, $\{\chi_\mu\}$. The tensor $\boldsymbol{C}^{\mathrm{HF}}$ will be referred to as the HF-MO coefficients in the following. Substituting Eq. (1.91) into Eq. (1.88) projecting on the left by χ_ν, we obtain

$$\sum_{\mu=1}^{N_b} \sum_{\sigma'} \iint_{\mathbb{R}^3} \chi_\nu^*(\boldsymbol{r}) \hat{F}^{\mathrm{HF},\sigma\sigma'}(\boldsymbol{r};\boldsymbol{r}') \chi_\mu(\boldsymbol{r}') C_{\mu i}^{\mathrm{HF},\sigma'} \, \mathrm{d}^3\boldsymbol{r} \, \mathrm{d}^3\boldsymbol{r}' = \sum_{\mu=1}^{N_b} \int_{\mathbb{R}^3} \chi_\nu^*(\boldsymbol{r}) \chi_\mu(\boldsymbol{r}) C_{\mu i}^{\mathrm{HF},\sigma} \epsilon_i^{\mathrm{HF}} \, \mathrm{d}^3\boldsymbol{r}, \tag{1.92}$$

or more compactly

$$\underline{\boldsymbol{F}}^{\mathrm{HF}} \, \underline{\boldsymbol{C}}_o^{\mathrm{HF}} = \underline{\boldsymbol{S}} \, \underline{\boldsymbol{C}}_o^{\mathrm{HF}} \, \boldsymbol{\epsilon}_o^{\mathrm{HF}} \tag{1.93}$$

where the Fock matrix, $\underline{\boldsymbol{F}}^{\mathrm{HF}} \in \mathbb{C}^{2N_b \times 2N_b}$ and overlap matrix $\underline{\boldsymbol{S}} \in \mathbb{C}^{2N_b \times 2N_b}$ are given by

$$\underline{\boldsymbol{F}}^{\mathrm{HF}} = \begin{bmatrix} \boldsymbol{F}^{\mathrm{HF},\alpha\alpha} & \boldsymbol{F}^{\mathrm{HF},\alpha\beta} \\ \boldsymbol{F}^{\mathrm{HF},\beta\alpha} & \boldsymbol{F}^{\mathrm{HF},\beta\beta} \end{bmatrix}, \tag{1.94}$$

$$\underline{\boldsymbol{S}} = \begin{bmatrix} \boldsymbol{S} & \boldsymbol{0} \\ \boldsymbol{0} & \boldsymbol{S} \end{bmatrix}, \tag{1.95}$$

with

$$\underline{\boldsymbol{C}}_o^{\mathrm{HF}} = \begin{bmatrix} \boldsymbol{C}_o^{\mathrm{HF},\alpha} \\ \boldsymbol{C}_o^{\mathrm{HF},\beta} \end{bmatrix} \tag{1.96}$$

$$\underline{\boldsymbol{F}}^{\mathrm{HF}} = \underline{\boldsymbol{H}}^{\mathrm{core}} + \underline{\boldsymbol{J}} - \underline{\boldsymbol{K}}, \tag{1.97a}$$

$$X_{\mu\nu}^{\sigma\sigma'} = \iint_{\mathbb{R}^3} \chi_\nu^*(\boldsymbol{r}) \hat{X}^{\sigma\sigma'}(\boldsymbol{r};\boldsymbol{r}') \chi_\mu(\boldsymbol{r}') \, \mathrm{d}^3\boldsymbol{r} \, \mathrm{d}^3\boldsymbol{r}', \quad \boldsymbol{X} \in \{\boldsymbol{H}^{\mathrm{core}}, \boldsymbol{J}, \boldsymbol{K}\}. \tag{1.97b}$$

$$S_{\mu\nu} = \langle \chi_\mu \,|\, \chi_\nu \rangle \,. \tag{1.97c}$$

Here, the rectangular matrices $\boldsymbol{C}_o^{\mathrm{HF},\sigma} \in \mathbb{C}^{N_b \times N}$ are the spin–basis coefficients which expand the occupied HF-MOs (in the sense of second quantization) in the basis set. $\boldsymbol{\epsilon}_o^{\mathrm{HF}} \in \mathbb{R}^{2N_b \times N}$ is the diagonal matrix of occupied HF-MO eigenenergies.

Clearly, Eq. (1.93) represents a partial diagonalization of $\underline{\boldsymbol{F}}^{\mathrm{HF}}$ in the case when $N < 2N_b$ and does not yield coefficients of all of the elements of $\mathcal{C}$. If instead we examine the full diagonalization of $\underline{\boldsymbol{F}}^{\mathrm{HF}}$,

$$\underline{\boldsymbol{F}}^{\mathrm{HF}} \, \underline{\boldsymbol{C}}^{\mathrm{HF}} = \underline{\boldsymbol{S}} \, \underline{\boldsymbol{C}}^{\mathrm{HF}} \, \boldsymbol{\epsilon}^{\mathrm{HF}}, \tag{1.98}$$

where $\underline{\boldsymbol{C}}^{\mathrm{HF}} \in \mathbb{C}^{2N_b \times 2N_b}, \boldsymbol{\epsilon}^{\mathrm{HF}} \in \mathbb{R}^{2N_b \times 2N_b}$ represent a full–rank eigendecomposition of $\underline{\boldsymbol{F}}^{\mathrm{HF}}$. Thus from a set of N_b basis functions, one may construct a set of orbitals which has $|\mathcal{C}| = 2N_b$ such that $\mathrm{span}\,[\mathcal{C}] = \mathrm{span}\,[\{\chi_\mu\}]$. That is to say that if $\{\chi_\mu\}$ is complete on $\mathcal{H}^1$, so is $\mathcal{C}$. Equation (1.98) is known as the Roothaan–Hall equation. To find the minimizing HF wave function, we must minimize Eq. (1.77) by choosing the orbitals with the lowest N eigenenergies from which we will construct the ground state HF configuration. In general, Eq. (1.98) may be solved iteratively to self–consistency by constructing the Fock matrix

from some guess of the ground state configuration and rediagonalizing until the eigenvectors obtained are unchanging up to a unitary transformation. This procedure is known as the self–consistent field (SCF) procedure [5], and Eq. (1.98) is often referred to as an SCF equation.

1.6.2 Density Functional Theory

The Hartree–Fock approximation provides an excellent reference determinant for systematic improvement by way of Eq. (1.62). However, in order to obtain the exact many–body wave function, one must obtain the full expansion of Eq. (1.62); a feat which is computationally intractable for all but the simplest problems. Even at very low orders of truncation, obtaining the coefficients for these types of expansions is often so computationally demanding that only relatively small molecular systems are able to be studied on a routine basis. This poses a rather formidable problem in the field of electronic structure theory in that the Hartree–Fock wave function itself is not a sufficient description of the many–body wave function for relatively trivial problems, and any reasonable improvement of the wave function leads to computationally intractable problems for experimentally relevant molecular systems. Luckily, the deficiencies of the Hartree–Fock approximation are well known: it simply lacks explicit two–body interactions in the effective Hamiltonian, i.e. the non–interacting system is said to lack electron correlation. Thus if one were able to account for electron correlation in an effective one–body Hamiltonian, one would not need to use expensive many–body expansions such as Eq. (1.62). To this end, we will employ density functional theory (DFT) as a means to approximately account for electron correlation effects.

The Hohenberg–Kohn (HK) theorem states that there exists a bijection between an external scalar potential and the scalar one–body density of the many–body wave function [12]. More generally, the HK theorem may be extended to the 1RDM if the external potential has spin structure or is generally non–local in character [13]. Thus the total energy of the

many–body state may be written in terms of functionals of the 1RDM,

$$E[\Psi] = E[\gamma^1] = F^{\mathrm{HK}}[\gamma^1] + \iint_{\mathbb{F}} \hat{v}(\boldsymbol{x};\boldsymbol{x}')\gamma^1(\boldsymbol{x}';\boldsymbol{x})\ \mathrm{d}^4\boldsymbol{x}\,\mathrm{d}^4\boldsymbol{x}' \tag{1.99}$$

where F^{HK} is an energy functional which describes the energetic contributions arising from all one and two–body interactions separate from the external potential. F^{HK} may be broken down into its substituent contributions as follows,

$$F^{\mathrm{HK}}[\gamma^1] = H^{\mathrm{free}}[\gamma^1] + J[\gamma^1] + E^{xc}[\gamma^1] \tag{1.100}$$

where H^{free} is the energy functional pertaining to the free–particle part of the electronic Hamiltonian describing the system arising from $\hat{h}$ in Eq. (1.81), J is the classical Coulomb functional of Eq. (1.82), and E^{xc} is the *exchange–correlation* (xc) functional which describes all purely quantum many–body energetic contributions, including those which enforce the proper spin statistics (i.e. Fermi–Dirac in the case of fermions) for the wave function. Thus given the exact forms of H^{free} and E^{xc}, one would be able to obtain all information pertaining to the physical system.

There are a number of problems implicit in Eqs. (1.99) and (1.100). The most problematic is that the exact form of E^{xc} is unknown, thus rendering the practical treatment of DFT as an exact method impossible. In practice however, the lack of knowledge of an exact E^{xc} is not so egregious that it becomes an impractical tool for chemical inquiry. Due to the vast availability of approximate xc–functionals which have been developed to reproduce certain physical quantities, the cost–to–accuracy ratio over methods which use explicit many–body expansions is within the realm of tolerability for routine inquiry into chemical phenomena. There is another, more subtle problem relating to the form Eq. (1.100) in that the exact form for H^{free} is just as complex as E^{xc} in the case when γ^1 is derived from a truly interacting many–body wave function [6]. While the explicit form of the 1RDM is a simple finite sum in the case of a single Slater determinant (Eq. (1.42)), the form for the true many–body wave function contains an infinite sum over orbital products such that

$$H^{\mathrm{free}}[\gamma^1] = \sum_{i=1}^{\infty} f_i \left\langle \psi_i \middle| \hat{H}^{\mathrm{free}} \middle| \psi_i \right\rangle, \quad \text{s.t.} \quad \int_{\mathbb{F}} \gamma^1(\boldsymbol{x};\boldsymbol{x}')\psi_i(\boldsymbol{x}')\ \mathrm{d}^4\boldsymbol{x}' = f_i\psi_i(\boldsymbol{x}). \tag{1.101}$$

Thus in DFT methods which rely solely on the HK theorems, one must make rather crude approximations to the H^{free} functional, such as the Thomas–Fermi functional [6], for practical calculations.

A solution to the problem of handling H^{free} in a consistent manner comes from Kohn–Sham density functional theory (KS-DFT), where one reintroduces the concept of a fictitious non–interacting (Slater determinant) wave function to represent the true many–body wave function [14]. As such the total energy of the system may be written as,

$$E^{\text{KS}}[\gamma_s^1] = H_s^{\text{free}}[\gamma_s^1] + J[\gamma_s^1] + \tilde{E}^{xc}[\gamma_s^1] + \iint_{\mathbb{F}} \hat{v}(\boldsymbol{x};\boldsymbol{x}')\gamma_s^1(\boldsymbol{x}';\boldsymbol{x})\ \mathrm{d}^4\boldsymbol{x}\,\mathrm{d}^4\boldsymbol{x}', \tag{1.102}$$

where all of the moieties with an s subscript denote that they relate to the fictitious non–interaction system, i.e. a single Slater determinant such that γ_s^1 may be composed as Eq. (1.48). Thus

$$H_s^{\text{free}} = \sum_i \left\langle \phi_i \left| \hat{H}^{\text{free}} \right| \phi_i \right\rangle, \tag{1.103}$$

where $\{\phi_i\}$ is the set of so called *Kohn–Sham molecular orbitals* (KS-MOs) used to construct γ_s^1. $\tilde{E}^{xc}$ is an augmented xc functional which accounts for the difference of H_s^{free} and H^{free},

$$\tilde{E}^{xc}[\gamma_s^1] = H^{\text{free}}[\gamma_s^1] - H_s^{\text{free}}[\gamma_s^1] + E^{xc}[\gamma_s^1]. \tag{1.104}$$

Due to the introduction of the non–interacting system, or equivalently a set of orbitals, we may derive a set of SCF equations in analogy to the HF approximation which minimizes Eq. (1.102). In analogy of Eq. (1.88), we may write

$$\int_{\mathbb{F}} \hat{F}^{\text{KS}}(\boldsymbol{x}_1;\boldsymbol{x}_1')\phi_i(\boldsymbol{x}_1')\ \mathrm{d}^4\boldsymbol{x}_1' = \epsilon_i^{\text{KS}}\phi_i(\boldsymbol{x}_1), \tag{1.105}$$

where

$$\hat{F}^{\text{KS}}(\boldsymbol{x};\boldsymbol{x}') = \hat{H}^{\text{core}}(\boldsymbol{x};\boldsymbol{x}') + \hat{J}(\boldsymbol{x};\boldsymbol{x}') + \hat{V}^{xc}(\boldsymbol{x};\boldsymbol{x}') \tag{1.106}$$

$$\hat{V}^{xc}(\boldsymbol{x};\boldsymbol{x}') = \frac{\delta\tilde{E}^{xc}[\gamma_s^1]}{\delta\gamma_s^1(\boldsymbol{x}';\boldsymbol{x})}, \tag{1.107}$$

and $\hat{V}^{xc}$ is referred to as the *exchange–correlation* (xc) potential. Equation (1.105) is known generally as the Kohn–Sham (KS) equations. In comparison with Eq. (1.76), we may identify Eq. (1.106) as an effective one–body operator by the effective potential for KS-DFT as,

$$\hat{v}^{\mathrm{KS}} = \hat{v} + \hat{J} + \hat{V}^{xc}. \tag{1.108}$$

In further analogy to the treatment of the HF approximation, by examining the similarities between Eq. (1.86) and Eq. (1.106); setting $E^{xc}[\gamma_s^1] = -K[\gamma_s^1]$ yields the canonical HF equations. Knowing that the HF wave function lacks explicit treatment of electron correlation, the HF approximation may be thought of as a special case of KS-DFT where the xc functional only contains enough information to ensure the proper (anti-symmetric) particle exchange symmetry while neglecting any treatment of electron correlation. The attractive aspect on KS-DFT is that for relatively the same computational cost as obtaining a HF wave function one is able to (at least approximately) treat the electron correlation of the many–body problem. Further, unlike the HF approximation, in the limit where the orbital set $\mathcal{C}$ is taken to be complete and one has exact forms for the E^{xc} functional, KS-DFT is *exact*. Neither of these limits are realizable in practice, but nevertheless, electronic structure methods based on KS-DFT have seen enormous success in the prediction of many chemical phenomena which would be computationally inaccessible over explicit many–body methods [15, 16].

Casting Eq. (1.106) onto a finite basis as in Eq. (1.91), we obtain a generalized eigenvalue problem analogous to the Roothaan–Hall equation of Eq. (1.98) [17],

$$\underline{\boldsymbol{F}}^{\mathrm{KS}}\,\underline{\boldsymbol{C}}^{\mathrm{KS}} = \underline{\boldsymbol{S}}\,\boldsymbol{C}^{\mathrm{KS}}\,\boldsymbol{\epsilon}^{\mathrm{KS}}, \tag{1.109}$$

where

$$\underline{\boldsymbol{F}}^{\mathrm{KS}} = \underline{\boldsymbol{H}}^{\mathrm{core}} + \underline{\boldsymbol{J}} + \underline{\boldsymbol{V}}^{xc}, \tag{1.110}$$

$$\underline{\boldsymbol{V}}^{xc} = \begin{bmatrix} \boldsymbol{V}^{xc,\alpha\alpha} & \boldsymbol{V}^{xc,\alpha\beta} \\ \boldsymbol{V}^{xc,\beta\alpha} & \boldsymbol{V}^{xc,\beta\beta} \end{bmatrix}, \tag{1.111}$$

$$V_{\mu\nu}^{xc,\sigma\sigma'} = \iint_{\mathbb{R}^3} \chi_\mu^*(\boldsymbol{r}) \frac{\delta \tilde{E}^{xc}[\gamma_s^1]}{\delta \gamma^{\sigma'\sigma}(\boldsymbol{r}';\boldsymbol{r})} \chi_\nu(\boldsymbol{r}')\ \mathrm{d}^3\boldsymbol{r}\,\mathrm{d}^3\boldsymbol{r}'. \tag{1.112}$$

Here, $\underline{\boldsymbol{C}}^{\mathrm{KS}} \in \mathbb{C}^{2N_b \times 2N_b}$ and $\boldsymbol{\epsilon}^{KS} \in \mathbb{R}^{2N_b \times 2N_b}$ are the KS-MO coefficients and orbital eigenenergies, respectively. In the limit when the external potential is spatially local but has spin structure, Eq. (1.113) may be written as

$$V_{\mu\nu}^{xc,\sigma\sigma'} = \int_{\mathbb{R}^3} \frac{\delta \tilde{E}^{xc}[\gamma_s^1]}{\delta \rho^{\sigma\sigma'}(\boldsymbol{r})} \chi_\mu^*(\boldsymbol{r}) \chi_\nu(\boldsymbol{r}) \, \mathrm{d}^3\boldsymbol{r}, \tag{1.113}$$

where $\rho^{\sigma\sigma'}(\boldsymbol{r})$ are the spin basis coefficients of the one–particle density defined in Eq. (1.51) and we have exploited the fact that $\tilde{E}^{xc}[\gamma_s^1] \in \mathbb{R}$ in the interchange of the spin labels in the functional derivative. The form of Eq. (1.113) will allow for several simplifications in the methods which will be developed in Sec. 2.3.

1.6.3 Density Matrices for Non–Interacting Wave Functions

It is useful to examine the representation of the 1RDM and 2RDM, or more specifically the one– and two–particle densities in the case of spatially local potentials, in the basis which expands the single–particle orbitals for a particular reference. In this section we examine these quantities for a reference determinant $\left|\Phi_0^N\right\rangle$ which represents either a HF or KS-DFT determinant without loss of generality. Expanding Eq. (1.42) in Eq. (1.91), we obtain,

$$\gamma^{1,K}(\boldsymbol{r};\boldsymbol{r}') = \sum_{\mu\nu} P_{\mu\nu}^K \chi_\mu(\boldsymbol{r}) \chi_\nu^*(\boldsymbol{r}'), \quad K \in \{0,1,2,3\}, \tag{1.114}$$

where

$$P_{\mu\nu}^0 = \frac{1}{2} \sum_i C_{\mu i}^\alpha C_{\nu i}^{\alpha *} + C_{\mu i}^\beta C_{\nu i}^{\beta *}, \tag{1.115a}$$

$$P_{\mu\nu}^1 = \frac{1}{2} \sum_i C_{\mu i}^\alpha C_{\nu i}^{\beta *} + C_{\mu i}^\beta C_{\nu i}^{\alpha *}, \tag{1.115b}$$

$$P_{\mu\nu}^2 = \frac{\mathrm{i}}{2} \sum_i C_{\mu i}^\alpha C_{\nu i}^{\beta *} - C_{\mu i}^\beta C_{\nu i}^{\alpha *}, \tag{1.115c}$$

$$P_{\mu\nu}^3 = \frac{1}{2} \sum_i C_{\mu i}^\alpha C_{\nu i}^{\alpha *} - C_{\mu i}^\beta C_{\nu i}^{\beta *}. \tag{1.115d}$$

The matrix $\underline{\boldsymbol{P}}$ is referred to as the one–particle density matrix (1PDM), which is not to be confused with the 1RDM, although they are related through the above expansion. The

utility of the definition of the 1PDM is clearly seen in the evaluation of expectation values of operators expressed in the basis set,

$$\left\langle \Phi_0^N \left| \sum_i \hat{O}^1(i) \right| \Phi_0^N \right\rangle = 2 \sum_K Tr\left[\boldsymbol{P}^K \boldsymbol{O}^{1,K} \right] \tag{1.116}$$

where

$$O_{\mu\nu}^{1,K} = \left\langle \chi_\mu \left| \hat{O}^{1,K}(1) \right| \chi_\nu \right\rangle . \tag{1.117}$$

1.6.4 Spin Symmetries of Non–Interacting Wave Functions

In this section, we consider the spin symmetries of a general Fock matrix, $\underline{\boldsymbol{F}}$, which could be described as either Eq. (1.97a) for Hartree–Fock wave functions, or Eq. (1.110) for Kohn–Sham wave functions. The full treatment of the spin–structure of the Fock matrix is known as the generalized self–consistent field (GSCF) method which takes the form of generalized Hartree–Fock (GHF) and generalized Kohn–Sham (GKS) for the two methods, respectively. In GSCF, no assumptions are made regarding the spin symmetry of the non–interacting wave function, i.e. the resulting lowest–energy GSCF wave function need not be an eigenfunction of $\hat{S}_z$ or $\hat{S}^2$ regardless of the symmetries that are inherent in the electronic Hamiltonian [18, 19]. In general, if the electronic Hamiltonian contains non–trivial spin structure, a GSCF framework must be employed and the Fock matrix may be decomposed in the same manner as the general operators in Eq. (1.31) via ,

$$\underline{\boldsymbol{F}}^{\mathrm{GSCF}} = \boldsymbol{F}^0 \otimes \boldsymbol{\sigma}_0 + \boldsymbol{F}^1 \otimes \boldsymbol{\sigma}_1 + \boldsymbol{F}^2 \otimes \boldsymbol{\sigma}_2 + \boldsymbol{F}^3 \otimes \boldsymbol{\sigma}_3. \tag{1.118}$$

However, if the electronic Hamiltonian admits spin as a symmetry, $[\hat{H}_{el}, \hat{X}] = 0$, $\hat{X} \in \{\hat{S}_z, \hat{S}^2\}$, several simplifications can be made in the treatment of the Fock matrix, and more generally in the structure of the MO coefficients and density matrices.

We examine the different spin symmetries in turn, noting that $\hat{S}^2$ as a symmetry implies $\hat{S}_z$ as a symmetry but not the converse. If we restrict our solutions of the SCF equations to adhere to $\hat{S}_z$ symmetry, but not $\hat{S}^2$, the SCF matrix equations can adopt the block diagonal

form,

$$\begin{bmatrix} \boldsymbol{F}^{\alpha\alpha} & \mathbf{0} \\ \mathbf{0} & \boldsymbol{F}^{\beta\beta} \end{bmatrix} \begin{bmatrix} \boldsymbol{C}^{\alpha} & \mathbf{0} \\ \mathbf{0} & \boldsymbol{C}^{\beta} \end{bmatrix} = \begin{bmatrix} \boldsymbol{S} & \mathbf{0} \\ \mathbf{0} & \boldsymbol{S} \end{bmatrix} \begin{bmatrix} \boldsymbol{C}^{\alpha} & \mathbf{0} \\ \mathbf{0} & \boldsymbol{C}^{\beta} \end{bmatrix} \begin{bmatrix} \boldsymbol{\epsilon}^{\alpha} & \mathbf{0} \\ \mathbf{0} & \boldsymbol{\epsilon}^{\beta} \end{bmatrix}. \tag{1.119}$$

Equation (1.119) is referred to as the Pople–Nebst equation [5], and the restriction on the SCF solution is known as unrestricted SCF (USCF), or analogously UHF (UKS) for Hartree–Fock (Kohn–Sham) wave functions. The block structure of Eq. (1.119) warrants brief discussion as a number of new concepts have been implicitly introduced. Due to the enforced block structure, the eigenvectors of Eq. (1.119) are not generally able to be placed into energetic order. In a sense, USCF separates the spin components of the SCF equations into two coupled (through $\hat{J}$ of Eq. (1.87)) eigenvalue problems which partition $\mathcal{C}$ such that all orbitals are either purely spin–up (α) or spin–down (β) in nature. That is to say $\mathcal{C} = \mathcal{C}^{\alpha} \cup \mathcal{C}^{\beta}$ with $\mathcal{C}^{\alpha} \cap \mathcal{C}^{\beta} = \emptyset$ and $|\mathcal{C}^{\alpha}| = |\mathcal{C}^{\beta}| = N_b$ such that

$$\mathcal{C}^{\alpha} = \{|\phi_p\rangle \in \mathcal{C} \text{ s.t. } \phi_p(\boldsymbol{x}) = \phi_p^{\alpha}(\boldsymbol{r})\alpha(\sigma)\}, \tag{1.120}$$

and similarly for $\mathcal{C}^{\beta}$. As such, the block structure of the MO coefficients in Eq. (1.119) may be interpreted as follows: the USCF equations still generate $2N_b$ orbitals from a basis set consisting of N_b functions; however, due to the partitioning of $\mathcal{C}$ into $\mathcal{C}^{\alpha}$ and $\mathcal{C}^{\beta}$, the MO coefficients have also been partitioned into two sets which expand the α and β orbitals separately. That is to say that both sets of MO coefficients both *technically* expand the α and β components of the spinor orbitals of the form Eq. (1.11), but if a MO coefficient vector pertains to an orbital of a particular spin character, the coefficients of that vector which pertain to the opposite spin function are restricted to be zero. Thus yielding the block structure of the MO coefficients in Eq. (1.119). As such, the the α and β blocks of Eq. (1.119) may be energetically ordered in and of themselves, but no global orbital energetic ordering is implied. To demonstrate the validity of this block diagonalization, we examine the conditions under which Eq. (1.118) commutes with $\hat{S}_z = \frac{1}{2}\hat{1} \otimes \boldsymbol{\sigma}_3$,

$$\left[\underline{\boldsymbol{F}}^{\mathrm{GSCF}}, \underline{\boldsymbol{S}}_z\right] = \frac{1}{2}\left[\boldsymbol{F}^1, \boldsymbol{S}\right] \otimes \left[\boldsymbol{\sigma}_1, \boldsymbol{\sigma}_3\right] + \frac{1}{2}\left[\boldsymbol{F}^2, \boldsymbol{S}\right] \otimes \left[\boldsymbol{\sigma}_2, \boldsymbol{\sigma}_3\right], \qquad \underline{\boldsymbol{S}}_z = \frac{1}{2}\boldsymbol{S} \otimes \boldsymbol{\sigma}_3. \tag{1.121}$$

Here $\boldsymbol{S}_z$ is the basis representation of $\hat{S}_z$. Due to the non–zero commutation relationships of the Pauli matrices, we may state

$$\left[\underline{\boldsymbol{F}}^{\mathrm{GSCF}}, \underline{\boldsymbol{S}}_z\right] = \boldsymbol{0} \quad \text{iff} \quad \left[\boldsymbol{F}^1, \boldsymbol{S}\right] = \left[\boldsymbol{F}^2, \boldsymbol{S}\right] = \boldsymbol{0}, \tag{1.122}$$

which is in general only satisfied if $\boldsymbol{F}^1 = \boldsymbol{F}^2 = \boldsymbol{0}$. Thus we may define a restriction of the GSCF Fock matrix as

$$\underline{\boldsymbol{F}}^{\mathrm{USCF}} = \boldsymbol{F}^0 \otimes \boldsymbol{\sigma}_0 + \boldsymbol{F}^3 \otimes \boldsymbol{\sigma}_3 = \begin{bmatrix} \boldsymbol{F}^0 + \boldsymbol{F}^3 & \boldsymbol{0} \\ \boldsymbol{0} & \boldsymbol{F}^0 - \boldsymbol{F}^3 \end{bmatrix} \quad \text{s.t.} \quad \left[\underline{\boldsymbol{F}}^{\mathrm{USCF}}, \underline{\boldsymbol{S}}_z\right] = \boldsymbol{0}, \tag{1.123}$$

which clearly has the same block structure as Eq. (1.119). Constructing a ground–state configuration from Eq. (1.119) introduces ambiguity in that that projection onto the z–spin axis must be chosen *a priori*. The z–spin projection of a reference determinant may be written in terms of its 1PDM (via Eq. (1.116)) as,

$$\left\langle \Phi_0^N \left| \hat{S}_z \right| \Phi_0^N \right\rangle = Tr\left[\boldsymbol{P}^3 \boldsymbol{S}\right] = \frac{N^\alpha - N^\beta}{2}, \quad N = N^\alpha + N^\beta, \tag{1.124}$$

where we have used the fact that $\underline{\boldsymbol{C}}^\dagger \underline{\boldsymbol{S}} \underline{\boldsymbol{C}} = \boldsymbol{I}$ by convention. Here N^α and N^β are taken to be the number of elements from $\mathcal{C}^\alpha$ and $\mathcal{C}^\beta$ which have been chosen to make up the ground–state determinant, respectively. Thus, in USCF, one may enforce a particular spin configuration by restricting the number of α and β orbitals in the resulting determinant. The ground–state configuration is constructed by choosing the N^α orbitals from $\mathcal{C}^\alpha$ with the lowest α orbital eigenvalues ($\boldsymbol{\epsilon}^\alpha$), and the N^β orbitals from $\mathcal{C}^\beta$ with the lowest β orbital eigenvalues ($\boldsymbol{\epsilon}^\beta$). This restricting does not, however, guarantee a particular spin–multiplicity as the resulting wave function is not guaranteed to be an eigenfunction of $\hat{S}^2$. USCF is typically used in cases where the electronic Hamiltonian is either spin independent and the desired determinant is restricted to have $N^\alpha \neq N^\beta$ (i.e. open–shell systems), or when the electronic Hamiltonian depends only on $\boldsymbol{\sigma}_0$ and $\boldsymbol{\sigma}_3$. In essence, the USCF equations enforce a particular projection onto the z–spin axis while the GSCF equations to not. As such, USCF determinants are referred to as *collinear* solutions (i.e. collinear with the z–spin axis) while GSCF determinants are referred to as *non–collinear* solutions.

The USCF equations may be further restricted to be eigenfunctions of $\hat{S}^2$ in what will be referred to as the restricted SCF equations (RSCF) given by

$$\begin{bmatrix} \boldsymbol{F}^{\alpha\alpha} & \mathbf{0} \\ \mathbf{0} & \boldsymbol{F}^{\alpha\alpha} \end{bmatrix} \begin{bmatrix} \boldsymbol{C}^{\alpha} & \mathbf{0} \\ \mathbf{0} & \boldsymbol{C}^{\alpha} \end{bmatrix} = \begin{bmatrix} \boldsymbol{S} & \mathbf{0} \\ \mathbf{0} & \boldsymbol{S} \end{bmatrix} \begin{bmatrix} \boldsymbol{C}^{\alpha} & \mathbf{0} \\ \mathbf{0} & \boldsymbol{C}^{\alpha} \end{bmatrix} \begin{bmatrix} \boldsymbol{\epsilon}^{\alpha} & \mathbf{0} \\ \mathbf{0} & \boldsymbol{\epsilon}^{\alpha} \end{bmatrix}, \tag{1.125}$$

or more compactly

$$\boldsymbol{F}^{\alpha\alpha}\boldsymbol{C}^{\alpha} = \boldsymbol{S}\boldsymbol{C}^{\alpha}\boldsymbol{\epsilon}^{\alpha}. \tag{1.126}$$

This block structure arises from that fact that $\hat{S}^2$ symmetry implies simultaneous commutation of the Fock matrix with each of $\hat{S}_x, \hat{S}_y, \hat{S}_z$. From the form of Eq. (1.123), this may only be achieved if the Fock matrix takes the form

$$\underline{\boldsymbol{F}}^{\mathrm{RSCF}} = \boldsymbol{F}^{0} \otimes \boldsymbol{\sigma}_0, \tag{1.127}$$

which clearly has the same block structure as Eq. (1.125). By this restriction, $\mathcal{C}$ is again partitioned into two sets of of orbitals which correspond to α and β spin character. However, unlike USCF, the block structure of Eq. (1.125) implies that there exists a single set of purely spatial orbitals, $\mathcal{S} = \{\psi_m(\boldsymbol{r})\}$ with $|\mathcal{S}| = N_b$, such that

$$\mathcal{C}^{\alpha} = \{\phi(\boldsymbol{x}) = \psi_m(\boldsymbol{r})\alpha(\sigma) \quad \forall \psi_m \in \mathcal{S}\}, \tag{1.128}$$

and similarly for β. In a sense, $\mathcal{C}^{\alpha}$ and $\mathcal{C}^{\beta}$ may be considered somewhat equivalent in the fact that there exists an isomorphism between their elements in which the image of each orbital of a particular spin set is the orbital in the other spin set which has the same spatial part and energy eigenvalue (via the degenerate block structure of Eq. (1.125)). As such, there should be no preference in the inclusion of an orbital from one set or its image in the other. Thus the ground–state configuration may be constructed by choosing the $N/2$ equivalent pairs of the two sets with the lowest energy eigenvalues, i.e. inclusion of a particle from $\mathcal{C}^{\alpha}$ implies that the image of that orbital under the isomorphism is also included. Due to this paired nature, RSCF may meaningfully employed only in the cases where the electronic Hamiltonian is spin independent and the system in question may be restricted to be closed shell (i.e. the same number of α and β orbitals in the configuration due to pairing).

As it often the case, it is useful to examine relationship between the the above restrictions on the SCF equations and the structure of the 1PDM which arises from their solution. For a general Fock matrix $\underline{\boldsymbol{F}}$ and corresponding SCF 1PDM $\underline{\boldsymbol{P}}$ (i.e. the 1PDM resulting from the solution of the SCF equations), these relationships are given by

$$\underline{\boldsymbol{F}} = \underline{\boldsymbol{F}}^{\mathrm{GSCF}} \quad \text{iff} \quad \underline{\boldsymbol{P}} = \underline{\boldsymbol{P}}^{\mathrm{GSCF}} = \boldsymbol{P}^0 \otimes \boldsymbol{\sigma}_0 + \boldsymbol{P}^1 \otimes \boldsymbol{\sigma}_1 + \boldsymbol{P}^2 \otimes \boldsymbol{\sigma}_2 + \boldsymbol{P}^3 \otimes \boldsymbol{\sigma}_3, \tag{1.129a}$$

$$\underline{\boldsymbol{F}} = \underline{\boldsymbol{F}}^{\mathrm{USCF}} \quad \text{iff} \quad \underline{\boldsymbol{P}} = \underline{\boldsymbol{P}}^{\mathrm{USCF}} = \boldsymbol{P}^0 \otimes \boldsymbol{\sigma}_0 + \boldsymbol{P}^3 \otimes \boldsymbol{\sigma}_3, \tag{1.129b}$$

$$\underline{\boldsymbol{F}} = \underline{\boldsymbol{F}}^{\mathrm{RSCF}} \quad \text{iff} \quad \underline{\boldsymbol{P}} = \underline{\boldsymbol{P}}^{\mathrm{RSCF}} = \boldsymbol{P}^0 \otimes \boldsymbol{\sigma}_0. \tag{1.129c}$$

The consequences of these relationships will be explored in future sections.

1.7 Non–Relativistic Molecular Hamiltonians

1.7.1 The Molecular Schrödinger Equation

Fundamental to the description of any quantum molecular system, relativistic or non–relativistic, is the non–relativistic molecular Hamiltonian, $\hat{H}^{\mathrm{NR}} : \mathcal{H}^{\mathrm{NR}} \mapsto \mathcal{H}^{\mathrm{NR}}$, where $\mathcal{H}^{\mathrm{NR}}$ describes a quantum system containing N_{el} electrons and N_{nuc} nuclei in the absence of relativistic effects. $\hat{H}^{\mathrm{NR}}$ is so fundamental to the description of quantum molecular systems in that it is the linear operator on $\mathcal{H}^{\mathrm{NR}}$ which represents the non–relativistic total energy of the system. In the absence of external fields, $\hat{H}^{\mathrm{NR}}$ takes the form [5, 10, 20]

$$\hat{H}^{\mathrm{NR}} = \hat{H}^{\mathrm{NR}}_{el} + \hat{H}^{\mathrm{NR}}_{nuc} + \hat{H}^{\mathrm{NR}}_{mix} \tag{1.130}$$

where

$$\hat{H}^{\mathrm{NR}}_{el} = \sum_{i}^{N_{\mathrm{el}}} \hat{T}^{\mathrm{NR}}(i) + \frac{1}{2} \sum_{i \neq j}^{N_{\mathrm{el}}} \hat{g}^{C}(i,j), \tag{1.131a}$$

$$\hat{H}^{\mathrm{NR}}_{nuc} = \sum_{A}^{N_{\mathrm{nuc}}} \hat{T}^{\mathrm{NR}}(A) + \frac{1}{2} \sum_{A \neq B}^{N_{\mathrm{nuc}}} \hat{g}^{C}(A,B), \tag{1.131b}$$

$$\hat{H}^{\mathrm{NR}}_{mix} = \sum_{i}^{N_{\mathrm{el}}} \sum_{A}^{N_{\mathrm{nuc}}} \hat{g}^{C}(i,A). \tag{1.131c}$$

Here we have denoted operator action onto the electronic degrees of freedom as i, j and A, B for the nuclear degrees of freedom. For a general (electronic or nuclear) coordinate, ξ, the non–relativistic kinetic energy operator, $\hat{T}^{\mathrm{NR}}$, is given by

$$\hat{T}^{\mathrm{NR}}(\xi) = \frac{1}{2m_\xi}\hat{\boldsymbol{p}}(\xi)\cdot\hat{\boldsymbol{p}}(\xi), \tag{1.132}$$

where $\hat{\boldsymbol{p}}$ is the linear momentum operator and m_ξ is the mass of the ξ-th particle. $\hat{g}^C$ is the two–body Coulomb operator which describes the electrostatic interaction between charged particles.

In the spinor representation, these operators take the general form (in atomic units)

$$\underline{\hat{\boldsymbol{p}}}(\boldsymbol{r}_\xi) = -\mathrm{i}\nabla_\xi \otimes \hat{I}_S(\xi) \quad \Longrightarrow \quad \underline{\hat{T}}^{\mathrm{NR}}(\boldsymbol{r}_\xi) = -\frac{1}{2m_\xi}\Delta_\xi \otimes \hat{I}_S(\xi), \tag{1.133}$$

$$\underline{\hat{g}}^C(\boldsymbol{r}_\xi, \boldsymbol{r}_\zeta) = \frac{Z_\xi Z_\zeta}{r_{\xi\zeta}} \otimes \hat{I}_S(\xi) \otimes \hat{I}_S(\zeta), \qquad r_{\xi\zeta} = |\boldsymbol{r}_\xi - \boldsymbol{r}_\zeta| \tag{1.134}$$

where ∇_ξ and Δ_ξ are the gradient and Laplacian operators acting on the ξ-th spatial coordinate, respectively. Z_ξ is the charge of the ξ-th particle, which in atomic units is given by -1 for electrons and the number of protons for a particular nucleus, respectively. $\hat{I}_S(\xi)$ is the identity spin operator for particle ξ, which has been introduced to make a careful distinction between the spinor basis of electrons, which are spin–1/2 fermions, and nuclei, which are in general *not* spin–1/2 fermions and thus potentially carry a much more complicated spin structure [21]. For electrons, $\hat{I}_S = \boldsymbol{\sigma}_0$. The presence of $\hat{I}_S$ in Eqs. (1.133) and (1.134) may be interpreted as the action of these operators *do not* manipulate the spin degrees of freedom of the total wave function.

The wave equation governed by Eq. (1.130) as a specialization of Eq. (1.1) is given by

$$\hat{H}^{\mathrm{NR}}\left|\Psi_{tot}(t)\right\rangle = \mathrm{i}\partial_t\left|\Psi_{tot}(t)\right\rangle, \tag{1.135}$$

where $|\Psi_{tot}(t)\rangle$ is the total molecular wave function which describes both the electronic and nuclear degrees of freedom. Equation (1.135) will be referred to as the molecular Schrödinger equation. In this work, all non–relativistic specializations of Eq. (1.1) will be referred to as

Schödinger equations due to the presence of the kinetic energy operator in their Hamiltonian. As such, they are direct quantum analogues of the classical Hamiltonian which was the basis of the original Schrödinger Hamiltonian of the general form [10]

$$\hat{H}(t) = \hat{T}^{\mathrm{NR}} + \hat{V}(t). \tag{1.136}$$

1.7.2 The Born–Oppenheimer Approximation

As has been previously stated on numerous occasions, the primary focus of this work is to treat the many–body electronic problem for molecular systems, not the quantum nature of the nuclei. The combined quantum treatment of Eq. (1.130) obfuscates this point in that the presence of $\hat{H}^{\mathrm{NR}}_{mix}$ intimately couples the electronic and nuclear degrees of freedom. Thus it would be of practical utility to, in some way, decouple the quantum treatment of the electrons and the nuclei such that they may be treated separately. To this end, we will work within the Born–Oppenheimer ansatz for the molecular wave function [20, 22] such that it may be written as a single tensor product of an electronic and nuclear wave function,

$$|\Psi_{tot}\rangle \approx |\Psi_{el}\rangle \otimes |\Theta_{nuc}\rangle \,. \tag{1.137}$$

Due to a large disparity in mass between electrons and nuclei, the energetic regimes which describe their respective dynamics are typically well separated. Namely, from the inertial frame of the electrons, one might approximate the nuclear kinetic energy to be negligible, i.e.

$$\left\langle \Psi_{el} \left| \sum_{A}^{N_{\mathrm{nuc}}} \hat{T}^{\mathrm{NR}}(A) \right| \Psi_{el} \right\rangle \approx 0. \tag{1.138}$$

This assumption is referred to as the Born–Oppenheimer approximation [20] (a concept distinct from from the Born–Oppenheimer ansatz for the molecular wave function). This is typically a safe assumption for reasonably heavy nuclei as the ratio of the electronic and nuclear kinetic energies are of the same order as the ratio of the electronic and proton masses, $\mathcal{O}(10^3)$. Thus, from the electronic perspective, the nuclear configuration is approximately static, and the electrons only "feel" the electrostatic potential of a fixed nuclear wave function

at any given time. This approach is therefore analogous to the mean–field treatment of the Hartree–Fock wave function in Eq. (1.88). Denoting a particular fixed nuclear wave function $\left|\Theta_{nuc}^{fix}\right\rangle$, we may write down a Hamiltonian which acts on the electronic component of the wave function and is valid in the inertial frame of the electrons [20],

$$\hat{H}_{el}^{\mathrm{BO}} = \left\langle \Theta_{nuc}^{fix} \middle| \hat{H}^{\mathrm{NR}} - \sum_{A}^{N_{\mathrm{nuc}}} \hat{T}^{\mathrm{NR}}(A) \middle| \Theta_{nuc}^{fix} \right\rangle = E_{nn} + \sum_{i}^{N_{\mathrm{el}}} \hat{T}^{\mathrm{NR}}(i) + \hat{V}_{ne}(i) + \sum_{i \neq j}^{N_{\mathrm{el}}} \hat{g}^{C}(i,j), \quad (1.139)$$

where

$$\underline{\hat{V}}_{ne}(\boldsymbol{r}_i) = -\sum_{A}^{N_{\mathrm{nuc}}} \left(\int_{\mathbb{R}^3} \frac{Z_A \rho_{\mathrm{nuc,A}}^{1,0}(\boldsymbol{R})}{|\boldsymbol{r}_i - \boldsymbol{R}|} \, \mathrm{d}^3\boldsymbol{R} \right) \otimes \boldsymbol{\sigma}_0, \quad (1.140)$$

$$E_{nn} = \frac{1}{2} \sum_{A \neq B}^{N_{\mathrm{nuc}}} \iint_{\mathbb{R}^3} \frac{Z_A Z_B \rho_{\mathrm{nuc,A}}^{1,0}(\boldsymbol{R}) \rho_{\mathrm{nuc,B}}^{1,0}(\boldsymbol{R}')}{|\boldsymbol{R} - \boldsymbol{R}'|} \, \mathrm{d}^3\boldsymbol{R} \, \mathrm{d}^3\boldsymbol{R}'. \quad (1.141)$$

$\rho_{nuc,A}^{1,0}(\boldsymbol{R})$ is the one–particle scalar density of the A–the nucleus defined through a proper generalization of Eq. (1.50) for non spin–1/2 fermions. The explicit form of $\rho_{nuc,A}^{1,0}(\boldsymbol{R})$ is immaterial to this work except for the property,

$$\sum_{A}^{N_{\mathrm{nuc}}} \int_{\mathbb{R}^3} \rho_{nuc,A}^{1,0}(\boldsymbol{R}) \, \mathrm{d}^3\boldsymbol{R} = N_{\mathrm{nuc}}. \quad (1.142)$$

This criteria is clearly met if $\rho_{nuc,A}^{1,0}(\boldsymbol{R})$ is a normalized function. In this work, we will approximate $\rho_{nuc,A}^{1,0}(\boldsymbol{R})$ as a classical charge distribution described by a single Gaussian function [23, 24],

$$\rho_{nuc,A}^{1,0}(\boldsymbol{R}) = \left(\frac{\upsilon_A}{\pi}\right)^{3/2} e^{-\upsilon_A(\boldsymbol{R}-\boldsymbol{R}_A)^2}, \quad (1.143)$$

where $\boldsymbol{R}_A$ is the classical nuclear position and

$$\upsilon_A = \frac{3}{2\zeta}, \qquad \zeta = 0.836 M_A^{1/3} + 0.570. \quad (1.144)$$

1.7.3 Non–Relativistic Mean–Field Wave Functions

In the case of the non–relativistic Born–Oppenheimer electronic Hamiltonian of Eq. (1.139), the Fock matrix components of Eq. (1.87) take the form [6],

$$\hat{H}^{\text{core}}(\boldsymbol{x};\boldsymbol{x}') = \delta^4(\boldsymbol{x}-\boldsymbol{x}')\left(\hat{T}^{\text{NR}}(\boldsymbol{x}) + \hat{V}_{ne}(\boldsymbol{x})\right) \tag{1.145a}$$

$$\hat{J}(\boldsymbol{x};\boldsymbol{x}') = \delta^4(\boldsymbol{x}-\boldsymbol{x}')\int_{\mathbb{F}} \frac{\gamma^1(\boldsymbol{x}_2;\boldsymbol{x}_2)}{|\boldsymbol{x}-\boldsymbol{x}_2|}\,\mathrm{d}^4\boldsymbol{x}_2 \tag{1.145b}$$

$$\hat{K}(\boldsymbol{x};\boldsymbol{x}') = \frac{\gamma^1(\boldsymbol{x};\boldsymbol{x}')}{|\boldsymbol{x}-\boldsymbol{x}'|} \tag{1.145c}$$

Carrying out the integration in a finite basis set via Eq. (1.97b), we obtain

$$H_{\mu\nu}^{\text{core},\sigma\sigma'} = \delta_{\sigma\sigma'}\left(T_{\mu\nu}^{\text{NR}} + V_{\mu\nu}^{ne}\right), \tag{1.146a}$$

$$J_{\mu\nu}^{\sigma\sigma'} = 2\delta_{\sigma\sigma'}\sum_{\lambda\kappa}\left\langle\mu\lambda\left|r_{12}^{-1}\right|\nu\kappa\right\rangle P_{\kappa\lambda}^{0}, \tag{1.146b}$$

$$K_{\mu\nu}^{\sigma\sigma'} = \sum_{\lambda\kappa}\left\langle\mu\lambda\left|r_{12}^{-1}\right|\kappa\nu\right\rangle P_{\kappa\lambda}^{\sigma\sigma'}, \tag{1.146c}$$

where we have substituted in the basis expansions of the density matrix from Eq. (1.115) and introduced

$$T_{\mu\nu}^{\text{NR}} = -\frac{1}{2}\int_{\mathbb{R}^3}\chi_\mu^*(\boldsymbol{r})\Delta\chi_\nu(\boldsymbol{r})\,\mathrm{d}^3\boldsymbol{r}, \tag{1.147}$$

$$V_{\mu\nu}^{ne} = -\iint_{\mathbb{R}^3}\frac{\chi_\mu^*(\boldsymbol{r})\chi_\nu(\boldsymbol{r})\rho_{nuc}^{1,0}(\boldsymbol{R})}{|\boldsymbol{r}-\boldsymbol{R}|},\,\mathrm{d}^3\boldsymbol{r}\,\mathrm{d}^3\boldsymbol{R} \tag{1.148}$$

$$\left\langle\mu\nu\left|r_{12}^{-1}\right|\lambda\kappa\right\rangle = \iint_{\mathbb{R}^3}\frac{1}{r_{12}}\chi_\mu^*(\boldsymbol{r}_1)\chi_\nu^*(\boldsymbol{r}_2)\chi_\lambda(\boldsymbol{r}_1)\chi_\kappa(\boldsymbol{r}_2)\,\mathrm{d}^3\boldsymbol{r}_1\,\mathrm{d}^3\boldsymbol{r}_2. \tag{1.149}$$

Recognizing that the definitions of $\underline{\boldsymbol{H}}^{\text{core}}$ and $\underline{\boldsymbol{J}}$ in Eq. (1.146) are spin diagonal, we may define the Pauli components of the HF Fock matrix corresponding to Eq. (1.139) (see Eq. (1.94)) as,

$$\boldsymbol{F}^0 = \boldsymbol{H}^{\text{core},0} + \boldsymbol{J}^0 + \boldsymbol{X}^0, \tag{1.150}$$

$$\boldsymbol{F}^k = \boldsymbol{X}^k, \quad k \in \{1,2,3\}, \tag{1.151}$$

where $\underline{\boldsymbol{F}} \in \{\underline{\boldsymbol{F}}^{\mathrm{HF}}, \underline{\boldsymbol{F}}^{\mathrm{KS}}\}$ and $\underline{\boldsymbol{X}}$ is $-\underline{\boldsymbol{K}}$ for HF wave functions and $\underline{\boldsymbol{V}}^{xc}$ for KS wave functions, and

$$H_{\mu\nu}^{\mathrm{core},0} = \left(T_{\mu\nu}^{\mathrm{NR}} + V_{\mu\nu}^{ne}\right), \tag{1.152a}$$

$$J_{\mu\nu}^{0} = 2\sum_{\lambda\kappa} \left\langle \mu\lambda \left| r_{12}^{-1} \right| \nu\kappa \right\rangle P_{\kappa\lambda}^{0}, \tag{1.152b}$$

$$K_{\mu\nu}^{L} = \sum_{\lambda\kappa} \left\langle \mu\lambda \left| r_{12}^{-1} \right| \kappa\nu \right\rangle P_{\kappa\lambda}^{L}, \qquad L \in \{0,1,2,3\}, \tag{1.152c}$$

$$V_{\mu\nu}^{xc,L} = \int_{\mathbb{R}^3} \frac{\delta \tilde{E}^{xc}[\gamma_s^1]}{\delta \rho^L(\boldsymbol{r})} \chi_\mu^*(\boldsymbol{r}) \chi_\nu(\boldsymbol{r}) \, \mathrm{d}^3\boldsymbol{r}, \quad L \in \{0,1,2,3\}, \tag{1.152d}$$

Note that the spin dependence of the Fock matrix components comes solely through the mean–field dependence of the Fock operators on the 1RDM, thus restriction of the spin components of the 1RDM implies restriction of the spin components of the Fock matrix (i.e. Eq. (1.129)). This is a direct consequence of Eq. (1.139) being spin diagonal. This introduces a strange concept which is manifest in mean–field theory but not in exact treatments of the electronic problem: the spin symmetry of the density and Fock matrices need not exhibit the same spin structure as the Hamiltoninan which they represent. This phenomena is known an symmetry breaking, and is a well studied problem in electronic structure theory [18, 19]. The simplest example of this is the treatment of open–shell systems via Eq. (1.139): the treatment of unpaired spins necessarily introduces an explicit treatment of spin through $\boldsymbol{F}^3/\boldsymbol{P}^3$ despite the fact that Eq. (1.139) has no explicit treatment thereof. It is typically the case that in non–relativistic electronic structure that one chooses to obtain the ground–state wave function under the RSCF or USCF restrictions of the Fock and density matrices for closed– and open–shell systems, respectively. However, there are well documented cases in which one must utilize GSCF methods even for non–relativistic theory, such as those discussed in Sec. 2.3.4.

1.8 Relativistic Hamiltonians

1.8.1 Deficiencies of the Non–Relativistic Schrödinger Equation

There are a number of problems inherent in the form of Eqs. (1.130), (1.136) and (1.139). The first problem that is of interest to this work, and perhaps the most glaring in the context of molecular calculations involving the quantum treatment of electrons, is that in the limit of electrostatics in the absence of external fields there is only trivial action of the Hamiltonian onto the spin components of the electronic wave function. To be clear, electronic spin is inherent in any quantum treatment of electrons as it manifests naturally through the irreducible representations of the Galilean group which governs non–relativistic mechanics [25]. Phenomenologically, one may introduce non–trivial spin manipulation into the non–relativistic Hamiltonian through the interaction with an external magnetic field, $\boldsymbol{B}$, via the spin–Zeeman term,

$$\hat{H}_{el}^{\mathrm{BO}} \mapsto \hat{H}_{el}^{\mathrm{BO}} + \hat{H}^{\mathrm{Zeeman}}, \qquad \hat{H}^{\mathrm{Zeeman}} = \frac{1}{2}\sum_{i=1}^{N_{\mathrm{el}}}\sum_{k=1}^{3} B^{k}\left(\boldsymbol{\sigma}_{k}(i) + \hat{L}_{k}(i)\right), \tag{1.153}$$

due to observation of the linear relationship between the magnetic field strength and energy level splittings in the Stern–Gerlach experiment [10]. Here, $\hat{\boldsymbol{L}}$ is the one–body orbital angular momentum operator. It is well known, however, that $\hat{H}^{\mathrm{Zeeman}}$ only yields a proper physical description of the electronic spin degrees of freedom in the strong–field limit [21], whereas in the weak–field limit, intrinsic magnetic effects which arise from special relativity, such as spin–orbit coupling, become energetically competitive.

The second, perhaps more subtle problem relating specifically to the form of Eq. (1.136) is that it is manifestly incapable of adhering to the laws of special relatively, i.e. it is impossible to write down a Hamiltonian of the form in Eq. (1.136) which is Lorentz covariant. This problem is easily identified through recognizing that the Schrödinger equation is quadratic in spatial coordinates through $\hat{T}^{\mathrm{NR}}$ and linear in time, and thus incapable of being compatible with Lorentz boosts. At first glance, one might be tempted to think in terms of a classical analogue for the quantum picture, where for velocities much lower than the speed of light, the

dynamics of classical bodies is approximately governed by Newtonian mechanics: the classical analogue of the Schrödinger equation. Within such a mindset, one might consider relativistic effects as only being important for heavy elements, such as Gold or Uranium, due to the fact that their core electrons move at velocities which are a considerable fraction of the speed of light. However, as is often the case with the quantization of classical mechanics, such a simplistic assumption yields qualitatively incorrect model physics even for light elements such as Carbon and Oxygen [26]. The realization of relativistic effects in light elements typically manifests in context of the *ab initio* introduction of spin couplings into the Hamiltonian, which not surprisingly also solves the aforementioned problem with treating electronic spin non–relativistically. The following sections provide a brief overview of the treatment of relativistic effects in molecular quantum mechanics.

1.8.2 The Dirac Equation

Fundamental to the treatment of relativistic effects in the electronic problem is the Dirac equation [27, 28],

$$\hat{h}^D \left|\psi(t)\right\rangle = \mathrm{i}\partial_t \left|\psi(t)\right\rangle, \tag{1.154}$$

where $|\psi(t)\rangle$ is the wave function for a spin–1/2 fermion, and the Dirac Hamiltonian, $\hat{h}^D : \mathcal{H}^{4\mathrm{C}} \to \mathcal{H}^{4\mathrm{C}}$, is given in atomic units by

$$\hat{h}^D = \hat{v} \otimes \boldsymbol{I}_2 + c\hat{\boldsymbol{p}} \cdot \boldsymbol{a} + (\boldsymbol{b} - \boldsymbol{I}_4)c^2. \tag{1.155}$$

Here, c is the speed of light, $\hat{v}$ is an external scalar potential, and $\boldsymbol{I}_2$ and $\boldsymbol{I}_4$ are the 2-by-2 and 4-by-4 identity matrices, respectively. We have defined the Dirac matrices as

$$\boldsymbol{a}_k = \boldsymbol{\sigma}_k \otimes \begin{bmatrix} 0 & 1 \\ 1 & 0 \end{bmatrix}, \quad k \in \{1, 2, 3\}, \tag{1.156a}$$

$$\boldsymbol{b} = \begin{bmatrix} \boldsymbol{I}_2 & \boldsymbol{0}_2 \\ \boldsymbol{0}_2 & -\boldsymbol{I}_2 \end{bmatrix}, \tag{1.156b}$$

and have used short hand notation

$$\hat{\boldsymbol{p}} \cdot \boldsymbol{a} \equiv (\hat{p}_x \boldsymbol{\sigma}_1 + p_y \boldsymbol{\sigma}_2 + p_z \boldsymbol{\sigma}_3) \otimes \begin{bmatrix} 0 & 1 \\ 1 & 0 \end{bmatrix}, \tag{1.157}$$

where $\hat{\boldsymbol{p}}$ is the linear momentum operator of Eq. (1.133). Equation (1.154) governs the quantum mechanical behavior of a spin–1/2 fermion in full adherence to the principles of special relativity, i.e. it is fully covariant under Lorentz transformations [27, 28].

Examining the form of Eq. (1.155), it is clear that the coordinate space spanned by $\mathbb{F}$ which is defined in Eq. (1.11) is no longer sufficient in the description of relativistic electrons. By block structure of Eq. (1.156a) indicates the need for an extra dimension in the description of the electronic such that,

$$|\psi\rangle = \begin{bmatrix} |\phi^L\rangle \\ |\phi^S\rangle \end{bmatrix}, \tag{1.158}$$

where $|\phi^L\rangle$ and $|\phi^S\rangle$ are referred to as the "large" and "small" component of the electronic wave function, respectively, and are both representable as spinors in the sense of Eq. (1.11). Represented as a vector of two spinors, the wave functions relating to the Dirac equation are often referred to as bispinors [27] as they are constructed from four complex components (hence $|\psi\rangle \in \mathcal{H}^{4\mathrm{C}}$).

The formal treatment of relativistic theory in the context of the consequences of adhering to Lorentz covariance is outside the scope of this work. One should be referred to more comprehensive texts on the subject for a more thorough treatment of these matters [27, 28]. There are, however, several aspects of Eq. (1.154) which will play an important role in the following developments. Perhaps the largest departure from non–relativistic quantum mechanics is in the spectrum of Eq. (1.155). Unlike the single–particle Schrödinger equation, the spectrum of Eq. (1.155) is partitioned into three regions relative to the rest mass of the electron: a strictly positive energy continuum $E > 0$, a strictly negative energy continuum $E < -2c^2$, and a set of discrete states with $E \in (-c^2, 0)$ which arise due to the presence of the external potential. The solutions of the Dirac equation with $E > -c^2$ may be interpreted as an analogue to the non–relativistic electrons, while the solutions with $E < -c^2$ have no

non–relativistic analogue. They are typically interpreted as the positronic solutions to the Dirac equation [29]. As this work is to treat the electronic problem in molecular physics, we will be interested in treating the electronic solutions to the Dirac equation, not the positronic solutions. However, this does not negate the presence of these positronic states, and their presence is crucial to a rigorous treatment of relativistic effects in molecular physics.

If Eq. (1.154) is interpreted as a mean–field Hamiltonian where $\hat{v}$ somehow encompasses the effects of a "sea" of other electrons in the system, the presence of the positronic solutions causes a number of practical problems in obtaining mean–field electronic solutions of the form Eq. (1.76). This is due to the fact that in our presentation of mean–field quantum mechanics, the premise was built on *minimization* of the energy functional in Eq. (1.74) over Slater determinants. The analogous problem of determining a mean–field electronic solution to the Dirac equation is a constrained minimization over only *electronic* solutions, as there are an infinite number of continuum positronic solutions. Minimization of Eq. (1.74) over purely electronic Slater determinants in generally impractical using standard optimization techniques and requires rather opaque projection schemes to avoid variational collapse into the positronic regime [27]. However, as we know *a priori* that the electronic solutions are the ones of interest, we may transform Eq. (1.155) such that we may solve for only the electronic states in an approximate manner. In Sec. 2.1, we will briefly discuss this procedure in the context of the exact two–component Hamiltonian.

1.8.3 The Dirac–Coulomb Molecular Hamiltonian

Although it is rarely outright stated in the context of the electronic structure theory literature, there is no *truly* relativistically covariant formulation of many–body quantum mechanics. This is due to the fact that the Coulomb interaction only treats the instantaneous interactions of charged particles and is thus manifestly incapable of adhering to the principles of special relativity. One must venture into the realm of quantum field theory (QFT) in order to develop truly covariant quantized descriptions of the electromagnetic force; however, QFT has proven to be rather difficult to exploit in the context of practical calculations on

molecular systems [30, 31]. Here, we will work with *approximate* relativistic descriptions of molecular quantum mechanics within a Hamiltonian formulation, which have been shown to have good agreement with experiment [27, 28, 32, 33]. For simplicity in the subsequent developments, we will posit *a priori* the validity of the Born–Oppenheimer ansatz and approximations of the previous section in the context of relativistic theory [27]. Further, while no approximation of the quantum nature of the nuclei was required in the context of the Schödinger equation, in the context of relativistic theory we will approximate nuclei to be classical charge distributions, i.e. no intrinsic angular momentum (spin) which yields an absence of magnetic interactions into the Hamiltonian within the fixed–nuclei approximation. This approximation is justified because energetic corrections due to the interaction between the magnetic moments of electrons and nuclei are $\mathcal{O}(10^3)$ smaller than the internal magnetic interactions between electrons due to the disparity in magnetic moment between electrons and nuclei [27]. This approximation will drastically simplify the resulting quantum mechanical treatment.

Within the context of the electronic problem, relativistic quantum mechanics is approximately governed by the Dirac–Coulomb equation in cases where retardation effects may be considered negligible,

$$\hat{H}^{\mathrm{DC}} \left|\Psi_{el}(t)\right\rangle = \mathrm{i}\partial_t \left|\Psi_{el}(t)\right\rangle , \tag{1.159}$$

where $\hat{H}^{\mathrm{DC}} : \mathcal{H}^{\mathrm{REL}} \rightarrow \mathcal{H}^{\mathrm{REL}}$ is the Dirac–Coulomb (DC) Hamiltonian. In the absence of external fields , the DC Hamiltonian for N electrons is given in atomic units by [27, 28]

$$\hat{H}^{\mathrm{DC}} = \sum_{i}^{N} \hat{h}^{D}(i) + \frac{1}{2} \sum_{i \neq j} \hat{g}^{C}(i,j) \otimes \boldsymbol{I}_2 \tag{1.160}$$

where $\hat{h}^D$ and $\hat{g}^C$ are the one–body Dirac Hamiltonian and two–body classical Coulomb interactions of Eq. (1.155) and Eq. (1.134), respectively. It is to be understood from the context of the Born–Oppenheimer approximation that the scalar potential of Eq. (1.155) is taken to be the nuclear scalar potential of Eq. (1.140). In analogy to the single–particle case in Eq. (1.158), the relativistic many–body electronic wave function may be written as

bispinors,

$$|\Psi_{el}\rangle = \begin{bmatrix} \left|\Psi_{el}^{\mathrm{L}}\right\rangle \\ \left|\Psi_{el}^{\mathrm{S}}\right\rangle \end{bmatrix}, \quad |\Psi_{el}\rangle \in \mathcal{H}^{\mathrm{REL}}, \tag{1.161}$$

where the superscripts L and S again refer to the large and small components of the electronic wave function, and may be treated as spinor wave functions in analogy to the non–relativistic case. Just like in the case of non–relativistic spinor wave functions, many–body bispinor wave functions may be written as the anti-symmetric tensor product of single–particle bispinors which span $\mathcal{H}^{4\mathrm{C}}$ (i.e. in the sense of Eqs. (1.4) and (1.6)).

Due to the increased dimensionality of the wave functions in Eqs. (1.154) and (1.159), the RDM must now represent a higher–dimensional tensors field as the restriction of an outer product in Eq. (1.37). As such we will introduce a new notation for e.g. the 1RDM,

$$\begin{aligned} \overline{\gamma}^1(\boldsymbol{x};\boldsymbol{x}') = N \int \cdots \int_{\mathbb{F}} \mathrm{d}^4\boldsymbol{x}_2 \cdots \mathrm{d}^4\boldsymbol{x}_N \times \\ \begin{bmatrix} \Psi^L(\boldsymbol{x},\boldsymbol{x}_2,\cdots)\Psi^{L*}(\boldsymbol{x}',\boldsymbol{x}_2,\cdots) & \Psi^L(\boldsymbol{x},\boldsymbol{x}_2,\cdots)\Psi^{S*}(\boldsymbol{x}',\boldsymbol{x}_2,\cdots) \\ \Psi^S(\boldsymbol{x},\boldsymbol{x}_2,\cdots)\Psi^{L*}(\boldsymbol{x}',\boldsymbol{x}_2,\cdots) & \Psi^S(\boldsymbol{x},\boldsymbol{x}_2,\cdots)\Psi^{S*}(\boldsymbol{x}',\boldsymbol{x}_2,\cdots) \end{bmatrix}. \end{aligned} \tag{1.162}$$

For the case of a Slater determinant constructed from from a set $\mathcal{K}_I^N = \{|\psi_i\rangle\}$ of eigen functions of Eq. (1.155), this becomes

$$\overline{\gamma}^1(\boldsymbol{x};\boldsymbol{x}') = \sum_{i\in\mathcal{K}_I^N} \psi_i(\boldsymbol{x})\psi_i^\dagger(\boldsymbol{x}') = \sum_{i\in\mathcal{K}_I^N} \begin{bmatrix} \phi_i^L(\boldsymbol{x})\phi_i^{L*}(\boldsymbol{x}') & \phi_i^L(\boldsymbol{x})\phi_i^{S*}(\boldsymbol{x}') \\ \phi_i^S(\boldsymbol{x})\phi_i^{L*}(\boldsymbol{x}') & \phi_i^S(\boldsymbol{x})\phi_i^{S*}(\boldsymbol{x}') \end{bmatrix}. \tag{1.163}$$

It is possible to develop a consistent treatment of $\overline{\gamma}^1$ in relativistic theory and and γ^1 in non–relativistic theory through the understanding that integral contractions over the indices of the 1RDM also imply a matrix operation over the dimension added as a result of the bispinor nature of the wave function. However, as we will be solely manipulating effective 2C relativistic Hamiltonians, the explicit development of this consistent treatment is beyond the scope of this work (see Sec. 2.2 Eqs. (2.23) and (2.24)).

Chapter 2

TWO–COMPONENT RELATIVISTIC ELECTRONIC STRUCTURE THEORY

2.1 The Exact Two–Component Hamiltonian

The problem of the dichotomy between the electronic and positronic states of the Dirac equation may be attributed to the $c\hat{\boldsymbol{p}}\cdot\boldsymbol{a}$ terms which couple the large and small components of the bispinor in Eq. (1.155). In an attempt to decouple these equations, we may perform a similarity transformation under an operator $\hat{U}$, such that [27, 28, 34, 35]

$$\hat{h}^D \mapsto \hat{h}^{2\mathrm{C}} = \hat{U}\hat{h}^D\hat{U}^{-1} = \begin{bmatrix} \hat{h}^+ & 0 \\ 0 & \hat{h}^- \end{bmatrix}. \tag{2.1}$$

where both $\hat{h}^+$ and $\hat{h}^-$ are effective 2C operators (i.e. they act on spinors). In general, $\hat{U}$ is referred to as a Foldy-Wouthuysen (FW) transformation [35]. In essence, the FW transformation convolves the information contained in the large and small component of the bispinor such that solution of Eq. (1.154) amounts to solving two decoupled differential equations,

$$\hat{h}^\pm \left|\phi^\pm(t)\right\rangle = \mathrm{i}\partial_t \left|\phi^\pm(t)\right\rangle, \qquad \hat{U}\left|\psi\right\rangle = \begin{bmatrix} \left|\phi^+\right\rangle \\ \left|\phi^-\right\rangle \end{bmatrix}. \tag{2.2}$$

As such, the spectrum of $\hat{h}^+$ and $\hat{h}^-$ are given by

$$\mathrm{spec}(\hat{h}^+) = (-c^2, \infty), \quad \mathrm{spec}(\hat{h}^-) = (-\infty, -2c^2). \tag{2.3}$$

In the case of a free electron, we obtain

$$\hat{v} = 0 \quad \Longrightarrow \quad \hat{h}^{2\mathrm{C}} = \boldsymbol{b}\sqrt{1+\hat{p}^2}, \tag{2.4}$$

which is known as the Newton–Wigner representation of the Dirac equation [36]. Even in the case when $\hat{v} \neq 0$, the FW transformation is possible, only one is not able to write down a closed–form expression such as Eq. (2.4), and power series approximations must be made in order to make use of them in practical calculations [1] [27]. This series expansion may be avoided in the case of basis set calculations in that the problem of block–diagonalizing an operator in a basis representation is a well defined numerical linear algebra problem.

To this end, we will account for relativistic effects using the exact two–component (X2C) method [37–42]. The name X2C is a misnomer due to the fact that it is only "exact" in the one–electron case. There exist many basis set methods to obtain effective 2C Hamiltonians such as Eq. (2.1) [27,43–48], but the X2C method is an especially attractive method in that it is a one–step transformation, rather than an iterative procedure such as those involved in the Douglass–Kroll–Hess method and its variants [43]. The X2C method operates under the assumption that there exists a linear, energy–independent transformation which links the large and small component of the electronic wave function. Expanding out the action of Eq. (1.155) on a bispinor of the form Eq. (1.158), we obtain the following relationship between the large and small components for positive–energy solutions

$$\left|\phi^S\right\rangle = \frac{c\hat{\boldsymbol{p}}\cdot\boldsymbol{\sigma}}{(E-v+2c^2)}\left|\phi^L\right\rangle \approx \left|\phi^{PL}\right\rangle = \frac{\hat{\boldsymbol{p}}\cdot\boldsymbol{\sigma}}{2c}\left|\phi^L\right\rangle, \tag{2.5}$$

where E and v are the expectation values of the Dirac Hamiltonian and the potential operator in the bispinor, respectively. The approximation on the right of Eq. (2.5), where we have defined the so–called pseudo large component, $\left|\phi^{PL}\right\rangle$, holds in the non–relativistic limit ($E \approx v$, i.e. small momentum) and is known as the kinetic balance condition for the small component of the electronic wave function [27]. Thus the action of the Dirac Hamiltonian

[1] It is actually in the FW transformation in the presence of the scalar nuclear potential that we are able to define terms like "spin–orbit" coupling and the mass–velocity correction. The Dirac Equation need not know explicitly about these effects and accounts for them implicitly through the coupling of the large and small components of the electronic wave function. These terms which we typically associate with relativistic effects are in fact terms in a series expansion which is only good in the non–relativistic limit.

on the bispinor may now be written as

$$\begin{bmatrix} \hat{v} & \hat{T}^{\mathrm{NR}} \\ \hat{T}^{\mathrm{NR}} & \frac{1}{4c^2}\hat{W} - \hat{T}^{\mathrm{NR}} \end{bmatrix} \begin{bmatrix} \left|\phi^{L}\right\rangle \\ \left|\phi^{PL}\right\rangle \end{bmatrix} \tag{2.6}$$

where $\hat{T}^{\mathrm{NR}}$ is the non–relativistic kinetic energy operator of Eq. (1.133). $\hat{W}$ is a transformed potential operator given by

$$\hat{W} = (\hat{\boldsymbol{p}} \cdot \boldsymbol{\sigma})\hat{v}(\hat{\boldsymbol{p}} \cdot \boldsymbol{\sigma}). \tag{2.7}$$

Equation (2.6) is known as the modified Dirac Hamiltonian [27].

In a finite basis $\{\chi_\mu\}$ with $|\{\chi_\mu\}| = N_b$, we may develop a Roothaan–Hall–like equation from Eq. (2.6) such that

$$\boldsymbol{H}^{\mathrm{MD}}\boldsymbol{C}^{\mathrm{MD}} = \boldsymbol{S}^{\mathrm{MD}}\boldsymbol{C}^{\mathrm{MD}}\boldsymbol{\epsilon}^{\mathrm{MD}}, \tag{2.8}$$

where

$$\boldsymbol{H}^{\mathrm{MD}} = \begin{bmatrix} \boldsymbol{v} & \boldsymbol{T}^{\mathrm{NR}} \\ \boldsymbol{T}^{\mathrm{NR}} & \frac{1}{4c^2}\boldsymbol{W} - \boldsymbol{T}^{\mathrm{NR}} \end{bmatrix}, \tag{2.9}$$

$$\boldsymbol{S}^{\mathrm{MD}} = \begin{bmatrix} \boldsymbol{S} & \boldsymbol{0} \\ \boldsymbol{0} & \frac{1}{2c^2}\boldsymbol{T}^{\mathrm{NR}} \end{bmatrix}, \tag{2.10}$$

$$\boldsymbol{\epsilon}^{\mathrm{MD}} = \begin{bmatrix} \boldsymbol{\epsilon}^{+} & \boldsymbol{0} \\ \boldsymbol{0} & \boldsymbol{\epsilon}^{-} \end{bmatrix}, \tag{2.11}$$

and the basis representations of these operators are given as in Eq. (1.97b). The superscripts $+$ and $-$ on the orbital eigenvalues denote electronic and positronic eigenvalues, respectively. $\boldsymbol{C}^{\mathrm{MD}}$ takes the block form

$$\boldsymbol{C}^{\mathrm{MD}} = \begin{bmatrix} \boldsymbol{C}^{L+} & \boldsymbol{C}^{L-} \\ \boldsymbol{C}^{PL+} & \boldsymbol{C}^{PL-} \end{bmatrix}, \tag{2.12}$$

such that we may construct a basis $\mathcal{C} = \mathcal{C}^{+} \cup \mathcal{C}^{-}$ which approximately spans $\mathcal{H}^{4\mathrm{C}}$ with

$\mathcal{C}^+ \cap \mathcal{C}^- = \emptyset$ and $|\mathcal{C}^+| = |\mathcal{C}^-| = 2N_b$ via

$$\mathcal{C}^+ = \left\{ |\psi_p\rangle \in \mathcal{C} \text{ s.t. } \psi_p(\boldsymbol{x}) = \begin{bmatrix} \phi_p^{L+}(\boldsymbol{x}) \\ \phi_p^{PL+}(\boldsymbol{x}) \end{bmatrix} \right\}, \tag{2.13}$$

$$\mathcal{C}^- = \left\{ |\psi_p\rangle \in \mathcal{C} \text{ s.t. } \psi_p(\boldsymbol{x}) = \begin{bmatrix} \phi_p^{L-}(\boldsymbol{x}) \\ \phi_p^{PL-}(\boldsymbol{x}) \end{bmatrix} \right\}, \tag{2.14}$$

$$\phi_p^{L\pm,\sigma}(\boldsymbol{r}) = \sum_\mu C_{\mu p}^{L\pm,\sigma} \chi_\mu(\boldsymbol{r}), \tag{2.15}$$

$$\phi_p^{PL\pm,\sigma}(\boldsymbol{r}) = \sum_\mu C_{\mu p}^{PL\pm,\sigma} \chi_\mu(\boldsymbol{r}). \tag{2.16}$$

To decouple Eq. (2.8), the X2C method employs the use of a unitary operator in the basis representation [41, 42],

$$\boldsymbol{U}^{\text{X2C}} = \begin{bmatrix} \boldsymbol{Y}_1 & -\boldsymbol{X}^\dagger \boldsymbol{Y}_2 \\ \boldsymbol{X}\boldsymbol{Y}_1 & \boldsymbol{Y}_2 \end{bmatrix}, \quad \boldsymbol{Y}_1 \left(\boldsymbol{I} + \boldsymbol{X}^\dagger \boldsymbol{X}\right)^{-\frac{1}{2}}, \quad \boldsymbol{Y}_2 \left(\boldsymbol{I} + \boldsymbol{X}\boldsymbol{X}^\dagger\right)^{-\frac{1}{2}}. \tag{2.17}$$

such that $\boldsymbol{X}$ is constructed from the eigenvectors of Eq. (2.8) by

$$\boldsymbol{X} = \boldsymbol{C}^{PL+} \left(\boldsymbol{C}^{L+}\right)^{-1}. \tag{2.18}$$

An account on how to efficiently assemble $\boldsymbol{X}$ is given in Ref [41]. Given $\boldsymbol{X}$, Eq. (2.17) may be constructed and in the limit that $\hat{v}$ only contains one–body operators, Eq. (2.6) is block diagonalized exactly,

$$\boldsymbol{U}^{\text{X2C}} \boldsymbol{H}^{\text{MD}} \boldsymbol{U}^{\text{X2C}\dagger} = \begin{bmatrix} \boldsymbol{h}^{\text{X2C}} & \boldsymbol{0} \\ \boldsymbol{0} & \boldsymbol{h}^- \end{bmatrix}. \tag{2.19}$$

Here we have labeled $\boldsymbol{h}^{\text{X2C}}$ as the positive energy block diagonal of the transformed Hamiltonian. $\boldsymbol{h}^{\text{X2C}}$ will serve as the source of the relativistic effects in the mean–field methods used throughout this work.

2.2 Two–Component Relativistic Mean Field Wave Functions

The power of of the X2C method outlined in Sec. 2.1 is that it allows one to cast mean–field relativistic electronic structure theory into a form which closely resembles non–relativistic

theory. In the case where $\hat{v}$ is an effective many–body potential in the context of mean–field theory, the X2C method dictates that the transformation only be performed using the density–independent terms of the Fock operator [41], i.e. $\hat{H}^{\text{core}}$ of Eq. (1.87). Otherwise, the transformation described by $\boldsymbol{U}^{\text{X2C}}$ would have to be performed as each step of the wave function optimization procedure outlined at the end of Sec. 1.6.1; rendering the method impractical. It is for this reason that the X2C is only exact in that case of a single electron in an external potential; the effective many–body terms in the mean–field Fock operator are neglected in the relativistic treatment. To remedy this somewhat egregious approximation, $\boldsymbol{h}^{\text{X2C}}$ is transformed in such a way as to effectively include these many–body effects by way of the Böttger scaling,

$$\boldsymbol{h}^{\text{X2C}} \mapsto \boldsymbol{\Lambda}^{B\dagger}\boldsymbol{h}^{\text{X2C}}\boldsymbol{\Lambda}^{B}, \tag{2.20}$$

where $\boldsymbol{\Lambda}^{B}$ is the sparse matrix of Böttger scaling factors [49]. This scaling method has become the field standard for approximately accounting for many–body relativistic effects in effective 2C relativistic methods.

With our utilization of the DC Hamiltonian, the two–body part of the electronic Hamiltonian in the effective 2C framework is the same as it was in the non–relativistic case, i.e. the mean–field operators $\hat{J}$, $\hat{K}$ and $\hat{V}^{xc}$ and their basis representations $\underline{\boldsymbol{J}}$, $\underline{\boldsymbol{K}}$ and $\underline{\boldsymbol{V}}^{xc}$, are the same as in Eqs. (1.145) and (1.146). This is due to the fact that for the electronic eigenvectors of Eq. (2.8), the X2C transformation also block diagonalizes the bispinor MO coefficients,

$$\begin{bmatrix} \boldsymbol{h}^{\text{X2C}} & \boldsymbol{0} \\ \boldsymbol{0} & \boldsymbol{h}^{-} \end{bmatrix} \begin{bmatrix} \boldsymbol{C}^{\text{X2C}} & \boldsymbol{0} \\ \boldsymbol{0} & \boldsymbol{C}^{-} \end{bmatrix} = \begin{bmatrix} \boldsymbol{S} & \boldsymbol{0} \\ \boldsymbol{0} & \boldsymbol{S}^{-} \end{bmatrix} \begin{bmatrix} \boldsymbol{C}^{\text{X2C}} & \boldsymbol{0} \\ \boldsymbol{0} & \boldsymbol{C}^{-} \end{bmatrix} \begin{bmatrix} \boldsymbol{\epsilon}^{\text{X2C}} & \boldsymbol{0} \\ \boldsymbol{0} & \boldsymbol{\epsilon}^{-} \end{bmatrix}. \tag{2.21}$$

In effect, this block diagonalization manifests in the same manner as Eq. (1.119). Denoting

the bispinor orbitals which may be expanded in terms of $\boldsymbol{C}^{\mathrm{X2C}}$ as

$$\mathcal{C}^{\mathrm{X2C}} = \left\{ \psi_p(\boldsymbol{r},\sigma) = \begin{bmatrix} \phi_i^{\alpha}(\boldsymbol{r})\alpha(\sigma) \\ \phi_i^{\beta}(\boldsymbol{r})\beta(\sigma) \\ 0 \\ 0 \end{bmatrix} = \sum_{\mu} \begin{bmatrix} C_{\mu p}^{\mathrm{X2C},\alpha}\alpha(\sigma) \\ C_{\mu p}^{\mathrm{X2C},\beta}\beta(\sigma) \\ 0 \\ 0 \end{bmatrix} \chi_{\mu}(\boldsymbol{r}) \right\}, \tag{2.22}$$

we may express the relativistic 1RDM (Eq. (1.162)) which can be constructed from a subset $\mathcal{K}_I^N \subset \mathcal{C}^{\mathrm{X2C}}$ as

$$\overline{\gamma}^1(\boldsymbol{x};\boldsymbol{x}') \sum_{i\in\mathcal{K}_I^N} \begin{bmatrix} \phi_i(\boldsymbol{x})\phi_i^*(\boldsymbol{x}') & 0 \\ 0 & 0 \end{bmatrix}. \tag{2.23}$$

As such, we will introduce a quasi–relativistic 1RDM which simply removes the zeroed out portions of Eq. (2.23),

$$\overline{\gamma}^1(\boldsymbol{x};\boldsymbol{x}') \mapsto \gamma^1(\boldsymbol{x};\boldsymbol{x}') = \sum_{i\in\mathcal{K}_I^N} \phi_i(\boldsymbol{x})\phi_i^*(\boldsymbol{x}'). \tag{2.24}$$

Using this definition of γ^1, we may define the analogous mean–field operators exactly as in Eqs. (1.87) and (1.113), thus yielding the same expressions for $\boldsymbol{J}$, $\boldsymbol{K}$, and $\boldsymbol{V}^{xc}$.

The key difference between the X2C method and non–relativistic mean–field methods is in the definition of the core Hamiltonian. In the four–component treatment of relativistic theory, the density–independent term is described by the Dirac Hamiltonian in Eq. (1.155). However, in the X2C method, the basis representation of the core Hamiltonian is simply given by $\boldsymbol{h}^{\mathrm{X2C}}$ in Eq. (2.19). Thus the basis representation of the Fock matrix for HF and KS mean–field wave functions (X2C-HF and X2C-KS), respectively) are given by

$$\underline{\boldsymbol{F}}^{\mathrm{X2C-HF}} = \underline{\boldsymbol{h}}^{\mathrm{X2C}} + \underline{\boldsymbol{J}} - \underline{\boldsymbol{K}} \quad \text{s.t.} \quad \underline{\boldsymbol{F}}^{\mathrm{X2C-HF}}\underline{\boldsymbol{C}}^{\mathrm{X2C-HF}} = \underline{\boldsymbol{S}}\,\underline{\boldsymbol{C}}^{\mathrm{X2C-HF}}\underline{\boldsymbol{\epsilon}}^{\mathrm{X2C-HF}}, \tag{2.25}$$

$$\underline{\boldsymbol{F}}^{\mathrm{X2C-KS}} = \underline{\boldsymbol{h}}^{\mathrm{X2C}} + \underline{\boldsymbol{J}} + \underline{\boldsymbol{V}}^{xc} \quad \text{s.t.} \quad \underline{\boldsymbol{F}}^{\mathrm{X2C-KS}}\underline{\boldsymbol{C}}^{\mathrm{X2C-KS}} = \underline{\boldsymbol{S}}\,\underline{\boldsymbol{C}}^{\mathrm{X2C-KS}}\underline{\boldsymbol{\epsilon}}^{\mathrm{X2C-KS}}, \tag{2.26}$$

such that we may decompose into the Pauli components of the Fock matrix

$$\boldsymbol{F}^0 = \boldsymbol{h}^{\mathrm{X2C},0} + \boldsymbol{J}^0 + \boldsymbol{X}^0, \tag{2.27}$$

$$\boldsymbol{F}^k = \boldsymbol{h}^{\mathrm{X2C},k} + \boldsymbol{X}^k, \qquad k \in \{1,2,3\}, \tag{2.28}$$

where $\underline{\boldsymbol{F}} \in \{\underline{\boldsymbol{F}}^{\mathrm{X2CHF}}, \underline{\boldsymbol{F}}^{\mathrm{X2CKS}}\}$ and $\underline{\boldsymbol{X}}$ is $-\underline{\boldsymbol{K}}$ for X2C-HF wave functions and $\underline{\boldsymbol{V}}^{xc}$ for X2C-KS wave functions. Thus, unlike the non–relativistic case of Eq. (1.152) where the spin components of the Fock matrix are completely determined by the 1PDM, the X2C Fock matrix explicitly admits spin into its Pauli components through the Pauli components of the X2C core Hamiltonian. As such, X2C Fock matrix is of the form Eq. (1.118), and thus a GSCF procedure must be used in general.

2.3 An Efficient and Scalable Implementation of Non-Collinear Density Functional Theory

2.3.1 Motivation

DFT (Sec. 1.6.2) has become the primary investigative tool for quantum chemical calculations regarding systems at large, experimentally relevant scales. The primary reason for its success has been its excellent balance of accuracy and computational cost and the vast availability through the development of efficient and reliable DFT software capable of leveraging the latest advances in high–performance computing [50]. Efficient and robust numerical integration techniques for the xc potential (Eq. (1.113)) have been thoroughly studied throughout the years [51–57], and their proper application is crucial to the practicality and applicability of DFT methods. The wide adoption of DFT in the scientific community as a whole has enabled routine, *ab initio* characterization of both ground and excited state properties for large macro molecular systems such as those of biological [58–60] and materials [61–66] interest and their transient behavior [67–70].

Recently, there has been a resurgence of interest in the materials community for the development and design of materials which exploit properties of electronic spin in their applications, such as magnetic materials, spintronic devices, and catalytic active sites [71–74]. As such, there is a strong need for electronic structure theories that are capable of treating electronic spins in large scale systems. Thus, motivated by its success in other aspects of materials research, there has been a large emphasis in recent years on the extension of existing DFT methods to properly include electronic spin and spin interactions.

At its core, a rigorous treatment of electronic spin and its interaction with materials in quantum systems must be rooted in relativistic quantum mechanics [26–28, 75]. As was discussed in Sec. 1.8, the introduction of spin couplings into the relativistic Hamiltonian has been demonstrated to yield profound effects even in light elements [26], which may be physically realized in systems such as doped nanodiamonds which have recently been recognized as fantastic candidates for the next generation of spintronic devices and q-bits in quantum computers [63,76–80]. Due to this centralized importance in the treatment of electronic spin, there has been a lot of effort in recent years to extend existing electronic structure methods to include relativistic effects, chief among them being extensions of DFT–based methods in both the ground [40, 81–83] and excited [84–88] electronic states. Relativistic analogues to the Hohenberg–Kohn theorems require the exact energy functional not only to be a functional of the electronic density, but also of the current density [27, 28, 89–96]. While some work has gone into the development of these types of functionals [97–103], the bulk of widely used exchange correlation functionals do not include these effects due to the fact that their contribution is typically small.

One of the central challenges in relativistic DFT is that the introduction of spin couplings into the Hamiltonian necessarily introduces spin non–collinearity in the electronic density for open–shell systems, i.e. the spin magnetization vector is no longer restricted to coincide with the z–axis (see Secs. 1.6.4 and 2.2). In this regard, unlike the collinear theory, non-collinear DFT requires the functional to depend on scalar and magnetization densities (Eq. (1.51)). Unfortunately, density functionals commonly employed in quantum chemistry have been developed for collinear densities, and therefore, there is no straightforward way to employ them in non-collinear systems. In this context, any generalization of collinear DFT to non-collinear densities must adhere to the so called zero–torque theorem [104], namely that the xc magnetic field (see Appendix B Eq. (B.2)) cannot exert a net torque on the magnetization density. However, if such a generalization does not admit local torque by the xc magnetic field, one cannot resolve proper time–evolution of the magnetization density in the absence of fields [88, 104–109]. Several efforts have been made to adapt common density functionals

developed for collinear densities for use relativistic calculations in this manner, both in the context of relativistic two-component [7, 82, 88, 107–111] and four-component [81, 82, 112–114] methods. However, in stark contrast to its non–relativistic collinear counterpart, no work has gone into developing highly optimized numerical integration techniques for these relativistic DFT methods. Thus, in this work, we outline an efficient algorithm and practical considerations for the integration of the xc potential in non–collinear relativistic DFT.

2.3.2 Assembly of the Exchange–Correlation Potential for Spinor Densities

In this section, we examine the integration and assembly of the $\tilde{E}^{xc}$ (Eq. (1.104)) dependent terms of the KS Fock matrix using a spinor density (see Sec. 2.2). In this work, we will limit our discussion to those functionals which may be characterized under the hybrid generalized gradient approximation (hybrid GGA), where $\tilde{E}^{xc}$ takes the form

$$\tilde{E}^{xc}[\gamma^1] = E^{GGA}[\boldsymbol{\rho}^1, \nabla\boldsymbol{\rho}^1] - c_x K[\gamma^1]. \tag{2.29}$$

Here, the full $\tilde{E}^{xc}$ has been partitioned into a pure GGA exchange correlation functional, E^{GGA}, which is a functional of the electronic density ($\boldsymbol{\rho}^1$) and its gradient (see Eq. (1.51)), and a scaled ($c_x \in [0, 1]$) Hartree–Fock exchange energy (Eq. (1.83)). In general, the exchange correlation contribution to the electronic energy may be written as an integral over an exchange correlation (xc) integration kernel, f,

$$E^{GGA}[\boldsymbol{\rho}^1, \nabla\boldsymbol{\rho}^1] = \int \mathrm{d}^3\boldsymbol{r}\ f(\{U(\boldsymbol{r})\}), \tag{2.30}$$

where we have introduced a set of auxiliary "U"–variables, $\{U(\boldsymbol{r})\}$, upon which the xc kernel depends. These need not be the density variables ($\boldsymbol{\rho}^1, \nabla\boldsymbol{\rho}^1$) directly, which we will refer to as "V"–variables, $\{V(\boldsymbol{r})\}$, but rather have complete flexibility in functional form. In non–relativistic, spin–polarized (collinear) DFT, these sets of variables may be defined as

$$\{V^{col}(\boldsymbol{r})\} = \{\rho^{1,\alpha\alpha}(\boldsymbol{r}), \rho^{1,\beta\beta}(\boldsymbol{r}), \nabla\rho^{1,\alpha\alpha}(\boldsymbol{r}), \nabla\rho^{1,\beta\beta}(\boldsymbol{r})\} \tag{2.31}$$

and

$$\{U^{col}(\boldsymbol{r})\} = \{\rho^{1,\alpha\alpha}(\boldsymbol{r}), \rho^{1,\beta\beta}(\boldsymbol{r}), \varphi^{\alpha\alpha}(\boldsymbol{r}), \varphi^{\alpha\beta}(\boldsymbol{r}), \varphi^{\beta\beta}(\boldsymbol{r})\} \tag{2.32}$$

where

$$\varphi^{\sigma\sigma'}(\boldsymbol{r}) = \nabla\rho^{1,\sigma\sigma}(\boldsymbol{r}) \cdot \nabla\rho^{1,\sigma'\sigma'}(\boldsymbol{r}) \tag{2.33}$$

The practical utility for the use of these two separate sets of variables is especially apparent in the context of two–component density functional theory as it allows for a simple retrofitting of standard xc functionals for relativistic calculations by simply redefining the transformations from the V variables of relativistic theory.

Defining the scalar and magnetization densities as in Eq. (1.51), we may define 2C analogues to the collinear auxiliary variables as

$$\{V^{NC}(\boldsymbol{r})\} = \{\rho^{1,0}(\boldsymbol{r}), \mathbf{m}(\boldsymbol{r}), \nabla\rho^{1,0}(\boldsymbol{r}), \nabla\mathbf{m}(\boldsymbol{r})\} \tag{2.34}$$

$$\{U^{NC}(\boldsymbol{r})\} = \{n^{+}(\boldsymbol{r}), n^{-}(\boldsymbol{r}), \varphi^{++}(\boldsymbol{r}), \varphi^{+-}(\boldsymbol{r}), \varphi^{--}(\boldsymbol{r})\} \tag{2.35}$$

where we have used NC to denote non–collinearity. The connection between $\{U^{col}\}$ and $\{U^{NC}\}$ is clear by making the substitution $\alpha \leftrightarrow +$ and $\beta \leftrightarrow -$. $\{V^{col}\}$ and $\{V^{NC}\}$ may be related by recognizing $\{\rho^{1,\alpha\alpha}, \rho^{1,\beta\beta}\}$ as the diagonal contributions of the spinor density, and thus

$$\{\rho^{1,\alpha\alpha}(\boldsymbol{r}), \rho^{1,\beta\beta}(\boldsymbol{r})\} \mapsto \{\rho^{1,0}(\boldsymbol{r}), \mathbf{m}^{col}(\boldsymbol{r})\} \tag{2.36}$$

where $\mathbf{m}^{col}(\boldsymbol{r}) = \{0, 0, \rho^{1,3}(\boldsymbol{r})\}$. Given the components of the spinor density matrix, spatial evaluation of the V–variables is given by (Eq. (1.114) assuming $\{\chi_\mu : \mathbb{R} \to \mathbb{R}\ \}$)

$$\rho^{1,K}(\boldsymbol{r}) = \sum_{\mu\nu} \mathrm{Re}[P^K_{\mu\nu}]\chi_\mu(\boldsymbol{r})\chi_\nu(\boldsymbol{r}) \qquad K \in 0, 1, 2, 3 \tag{2.37}$$

$$\nabla\rho^{1,K}(\boldsymbol{r}) = 2\sum_{\mu\nu} \mathrm{Re}[P^K_{\mu\nu}]\chi_\mu(\boldsymbol{r})\nabla\chi_\nu(\boldsymbol{r}) \quad K \in 0, 1, 2, 3 \tag{2.38}$$

where the matrices $\boldsymbol{P}^K$ are defined as in Eq. (1.115) and $\mathrm{Re}[x]$ denotes the real part of x. Remark that the evaluation of $\{V^{\mathrm{NC}}(\boldsymbol{r})\}$ may then be practically evaluated using strictly real arithmetic.

Given a transformation, $\{V^{NC}(\boldsymbol{r})\} \mapsto \{U^{NC}(\boldsymbol{r})\}$, it is possible to perform practical density functional calculations using standard implementations of collinear xc functionals,

such as those provided by `libxc` [115, 116]. However, defining such a transformation is not a trivial task, as the added spin degrees of freedom in the non–collinear spinor density and Fock matrix must obey to stricter conditions than their collinear counterparts, such as orientation invariance and adhering to the zero–torque theorem for the xc potential [104]. Several definitions of the generalized density variables have been proposed [7, 107–109, 117]. In this work, we utilize the transformation method which meets such conditions from Ref. [88]

$$n^{\pm}(\boldsymbol{r}) = \rho^{1,0}(\boldsymbol{r}) \pm |\mathbf{m}(\boldsymbol{r})| \tag{2.39a}$$

$$\varphi^{\pm\pm}(\boldsymbol{r}) = D^{00}(\boldsymbol{r}) + \sum_{k=1}^{3} D^{kk}(\boldsymbol{r}) \pm f_{\nabla}(\boldsymbol{r}) \sqrt{\sum_{k=1}^{3} D^{0k}(\boldsymbol{r})^2} \tag{2.39b}$$

$$\varphi^{+-}(\boldsymbol{r}) = D^{00}(\boldsymbol{r}) - \sum_{k=1}^{3} D^{kk}(\boldsymbol{r}) \tag{2.39c}$$

where

$$f_{\nabla}(\boldsymbol{r}) = sgn\left(\nabla\rho^{1,0}(\boldsymbol{r}) \cdot \left(\sum_{k=1}^{3} \nabla\rho^{1,k}(\boldsymbol{r})\rho^{1,k}(\boldsymbol{r})\right)\right) \tag{2.40}$$

$$D^{KL}(\boldsymbol{r}) = \nabla\rho^{1,K}(\boldsymbol{r}) \cdot \nabla\rho^{1,L}(\boldsymbol{r}) \tag{2.41}$$

Using this set of transformations, we may define an electronic energy and Fock matrix which has no dependence on the global orientation of $\mathbf{m}(\boldsymbol{r})$ and which satisfies the zero torque theorem (see Appendix B) for the xc potential within in the GGA framework.

In the limit of small $\mathbf{m}(\boldsymbol{r})$ ($|\mathbf{m}(\boldsymbol{r})| < 10^{-12}$, in this work), the transformations outlined in Eq. (2.39) yield numerically unstable expressions for the exchange correlation potential [88]. Thus one must define another set of transformations for practical implementations of non–collinear DFT to ensure proper convergence in the limit of small $\mathbf{m}(\boldsymbol{r})$. In summary, this

change for small $\mathbf{m}(\boldsymbol{r})$ may be described by the following substitutions in Eq. (2.39),

$$|\mathbf{m}(\boldsymbol{r})| \mapsto m_s(\boldsymbol{r}) = \frac{1}{3}\sum_{k=1}^{3}\rho^{1,k}(\boldsymbol{r}), \tag{2.42a}$$

$$\sqrt{\sum_{k=1}^{3}\left(D^{0k}(\boldsymbol{r})\right)^2} \mapsto \nabla\rho^{1,0}(\boldsymbol{r})\cdot\nabla m_s(\boldsymbol{r}). \tag{2.42b}$$

Using these mappings ensures no orientation dependence of $\mathbf{m}$ while maintaining numerical stability in the resulting expression for the xc potential. While Eq. (2.42) formally violates the zero torque theorem, its influence on the over all nature of the electronic density has been shown to be negligible [88].

Differentiating Eq. (2.30) with respect to the elements of the density matrix, we obtain for Eq. (1.113) (or more specifically its Pauli components)

$$V_{\mu\nu}^{xc,L} = V_{\mu\nu}^{GGA,L} - c_{HF}K_{\mu\nu}^{L}, \quad L \in \{0,1,2,3\}, \tag{2.43}$$

where $\underline{\boldsymbol{K}}$ is the HF exchange matrix (Eq. (1.146c)) and

$$\begin{aligned} V_{\mu\nu}^{GGA,K} &= \sum_{\Gamma\Gamma'}\int \mathrm{d}^3\boldsymbol{r}\ \frac{\partial f}{\partial U^{\mathrm{NC},\Gamma}(\mathbf{r})}\frac{\partial U^{\mathrm{NC},\Gamma}(\mathbf{r})}{\partial V^{\mathrm{NC},\Gamma'}(\mathbf{r})}\frac{\partial V^{\mathrm{NC},\Gamma'}(\mathbf{r})}{\partial P_{\mu\nu}^{K}} \\ &= \int \mathrm{d}^3\boldsymbol{r}\ V_{\mu\nu}^{GGA,K}(\boldsymbol{r}) \end{aligned} \tag{2.44}$$

where the partial derivatives of f are the same as in collinear DFT, and the partial derivatives of $\{V^{\mathrm{NC}}(\boldsymbol{r})\}$ may be identified through differentiating Eq. (2.37) for a particular spin component. We refer the reader to the Appendix of Ref. [88] for explicit expressions for the Jacobians between $\{U^{\mathrm{NC}}(\boldsymbol{r})\}$ and $\{V^{\mathrm{NC}}(\boldsymbol{r})\}$.

In practice, Eqs. (2.30) and (2.44) are evaluated numerically using a molecular quadrature scheme [51–57],

$$E^{GGA}[\boldsymbol{\rho},\nabla\boldsymbol{\rho}] \approx \sum_i w(\boldsymbol{r}_i) f(\{U(\boldsymbol{r}_i)\}) \tag{2.45}$$

$$V_{\mu\nu}^{GGA,K} \approx \sum_i w(\boldsymbol{r}_i) V_{\mu\nu}^{GGA,K}(\boldsymbol{r}_i) \tag{2.46}$$

where $\{w(\boldsymbol{r}_i)\}$ is a set of quadrature weights. In this work, we utilize the Becke multi-center numerical integration scheme [51], where the integral is evaluated on series of overlapping atomic centered grids, transformed, through their weights, into "fuzzy", overlapping, and analytically continuous cells instead. We refer the reader to a more thorough discussion regarding specific details of the numerical integration [51,55]. The evaluation of Eq. (2.45) is straight forward as it is a scalar function. In the spirit of the intermediates used in Ref. [57], by substituting the definitions of the partial derivatives of the U and V variables, we arrive at a concise expressions for assembly of Eq. (2.46)

$$V_{\mu\nu}^{GGA,K} = \sum_i Z_\mu^K(\boldsymbol{r}_i)\chi_\nu(\boldsymbol{r}_i) + Z_\nu^K(\boldsymbol{r}_i)\chi_\mu(\boldsymbol{r}_i) \tag{2.47}$$

$$Z_\mu^K(\boldsymbol{r}) = w(\boldsymbol{r})\left(\frac{1}{2}\mathcal{Z}_\rho^K(\boldsymbol{r})\chi_\mu(\boldsymbol{r}) + \sum_\xi \mathcal{Z}_{\nabla,\xi}^K(\boldsymbol{r})\nabla_\xi\chi_\mu(\boldsymbol{r})\right) \tag{2.48}$$

where $\xi \in \{x, y, z\}$ and

$$\mathcal{Z}_\rho^K = \frac{\partial f}{\partial \rho^{1,K}} = \begin{cases} \left(\dfrac{\partial f}{\partial n^+} + \dfrac{\partial f}{\partial n^-}\right) & K = 0 \\ \left(\dfrac{\partial f}{\partial n^+} - \dfrac{\partial f}{\partial n^-}\right)\mathfrak{K}^K & K \neq 0 \end{cases} \tag{2.49a}$$

$$\mathcal{Z}_{\nabla,\xi}^K = \frac{\partial f}{\partial \nabla_\xi \rho^{1,K}} = \begin{cases} \nabla_\xi\rho^{1,0}\left(\dfrac{\partial f}{\partial \varphi^{++}} + \dfrac{\partial f}{\partial \varphi^{+-}} + \dfrac{\partial f}{\partial \varphi^{--}}\right) + \sum_{k=1}^3 \nabla_\xi\rho^{1,k}\mathfrak{H}^k\left(\dfrac{\partial f}{\partial \varphi^{++}} - \dfrac{\partial f}{\partial \varphi^{--}}\right) & K = 0 \\ \nabla_\xi\rho^{1,0}\mathfrak{H}^K\left(\dfrac{\partial f}{\partial \varphi^{++}} - \dfrac{\partial f}{\partial \varphi^{--}}\right) + \nabla_\xi\rho^{1,K}\left(\dfrac{\partial f}{\partial \varphi^{++}} - \dfrac{\partial f}{\partial \varphi^{+-}} + \dfrac{\partial f}{\partial \varphi^{--}}\right) & K \neq 0 \end{cases} \tag{2.50a}$$

where we have dropped the explicit dependence on $\boldsymbol{r}$ for brevity. To consolidate the trans-

formation rules of Eqs. (2.39) and (2.42), we now define

$$\mathfrak{K}^K = \begin{cases} \dfrac{\rho^{1,K}}{|\mathbf{m}|} & \text{(Significant } \mathbf{m}\text{)} \\ \dfrac{1}{6} & \text{(Small } \mathbf{m}\text{)} \end{cases} \tag{2.51a}$$

$$\mathfrak{H}^K = \begin{cases} \dfrac{f_\nabla D^{0K}}{\sqrt{\sum_{k=1}^{3} \left(D^{0k}\right)^2}} & \text{(Significant } \mathbf{m}\text{)} \\ \dfrac{f_\nabla}{6} & \text{(Small } \mathbf{m}\text{)} \end{cases} \tag{2.51b}$$

2.3.3 Implementation

On modern computing architectures, there are three primary facets one must consider when developing high–performance scientific software: parallelism, cache utilization, and exploitation of micro-architecture specific floating point operations (μ-ops) such as single instruction–multiple data (SIMD) and fused multiply–add (FMA) operations. We refer the reader to the work of Goto, *et al* [118] for an excellent discussion of these considerations in the context of matrix operations. In the context of density functional theory, maximal exploitation of computational cache and μ-ops is achieved through batching groups of integration points together to maximize screening capability and memory contingency. There exist many batching schemes for various molecular integration quadratures in the literature [51–57]. We provide the following discussion without loss of generality.

As the point–wise function evaluations required for numerical integration are completely independent, it constitutes what is called an *embarrassingly parallel task*, i.e. no communication is required between the independent operations and thus one should expect near linear speedup with the number of processors used. In the context of electronic structure theory, the final two facets can usually be addressed through the use of highly optimized linear algebra software, such as the optimized BLAS (basic linear algebra subroutines) implementations offered OpenBLAS [119, 120] BLIS [121] and Intel–MKL [122]. However, blind application

of such software without careful consideration will often yield sub-optimal results, thus it is often the case that one must perform some level of algorithmic rearrangement to maximally utilize such capability. To demonstrate this point, we examine the assembly of the exchange correlation potential in Eq. (2.47). One may immediately recognize that the operation on the left of Eq. (2.47) is a sum over symmetric rank–2 updates (SYR2) of column vectors, $\mathbf{z}$ and $\boldsymbol{\chi}$, i.e.

$$\mathbf{V}^{GGA,I} = \sum_i \mathbf{z}_i^I \boldsymbol{\chi}_i^T + \boldsymbol{\chi}_i \left(\mathbf{z}_i^I\right)^T, \tag{2.52}$$

where $\mathbf{z}_i^I$ and $\boldsymbol{\chi}_i$ are of length of the number of basis functions, N_b. While Eq. (2.52) is a valid scheme for the assembly of Eq. (2.47), for large N_b this scheme will be drastically sub-optimal. This is due to the fact that, for large N_b, $\mathbf{V}^{GGA,I}$, $\mathbf{z}_i^I$ and $\boldsymbol{\chi}_i$ occupy a significant portion of the computational caches for each point. This means that the probability of the program attempting to access a memory address, i.e. an element of $\mathbf{z}_i^I$ or $\boldsymbol{\chi}_i$, between integration points and finding that it does not currently reside in the cache, i.e. a "cache miss", is rather high relative to other memory access patterns. This yields a large degradation in performance as whenever a cache miss occurs, the program must then move that address in some manner to the cache from main memory before it can perform any operations on it. Moving data to and from main memory is disproportional more expensive than floating point operations, thus it must be kept to a minimum to obtain optimal efficiency.

We may instead factor out a portion of the sum in Eq. (2.52) such that we may partition it into sum over batches of points. In this work, we utilize a macrobatch approach [55], where the grid points of each atoms are grouped into Lebedev spheres [**?**] of several radial quadrature points. This scheme is pictorially represented in Fig. 2.1. Denoting the set of all batches as $\mathfrak{B}$, we obtain

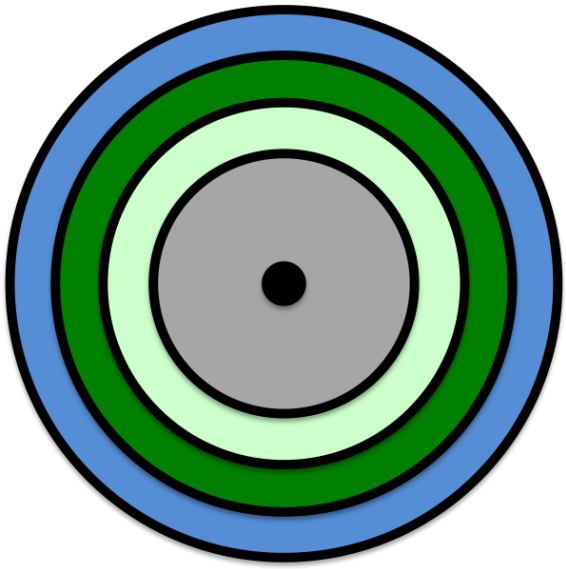


Figure 2.1: Pictorial representation of the integrand macrobatching scheme for the xc potential integration. Each of the colored regions represent a set of Lebedev spheres over several radial quadrature points, with the solid black dot representing the atomic nucleus. In the batching scheme, the scalar and matrix integrands are evaluated over the entire batch simultaneously to improving caching and μ-op behavior.

$$\begin{aligned}\mathbf{V}^{GGA,I} &= \sum_{S_j \in \mathfrak{B}} \left(\sum_{i \in S_j} \mathbf{z}_i^I \boldsymbol{\chi}_i^T + \boldsymbol{\chi}_i \left(\mathbf{z}_i^I\right)^T \right) \\ &= \sum_{S_j \in \mathfrak{B}} \mathbf{Z}^{I(j)} \left(\mathbf{X}^{(j)}\right)^T + \mathbf{X}^{(j)} \left(\mathbf{Z}^{I(j)}\right)^T \end{aligned} \tag{2.53}$$

where

$$\mathbf{Y}^{(j)} = \begin{bmatrix} \mathbf{y}_1 & \mathbf{y}_2 & \cdots & \mathbf{y}_i & \cdots & \mathbf{y}_{|S_j|} \end{bmatrix} \quad \forall i \in S_j, \tag{2.54}$$

and $\mathbf{y}$ is either $\mathbf{z}$ or $\boldsymbol{\chi}$. Equation (2.53) is a sum over symmetric rank–$2k$ updates (SYR2K), where $k = |S_j|$. By tuning k, one improves caching behavior dramatically. This is due to the fact that optimized implementations of SYR2K operations utilized efficient block operations to optimize the flow of data to and from the computational caches. Similar schemes may developed for the evaluation of the V variables (Eq. (2.37)) over batches using

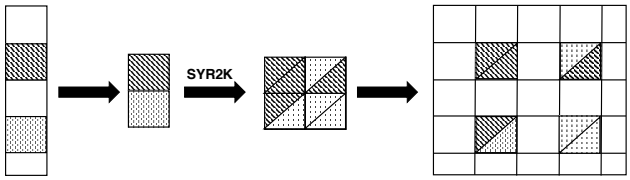


Figure 2.2: Pictorial representation of the screening and updating scheme for each batch in the numerical integration of the xc potential. A list of significant basis functions in the batch (colored patterns in the figure) is selected and then partitioned out for integration of that batch. The accumulation of the matrix integrand over the batch is evaluated by SYR2K and then the final, unscreened result is updated as shown. This scheme allows for only sequential memory access in the performance critical section of the integration and is responsible for drastic performance increases.

optimized matrix–matrix multiplication routines. However, while the caching behavior is improved with increasing k, this is not the only consideration one needs take into account when partitioning the integration grid into batches.

The scheme in Eq. (2.53) may be further improved by recognizing the fact that the basis functions typically used for molecular calculations carry a degree of spatial locality. A pictorial representation of the screening and updating scheme is given in Fig. 2.2. For each batch, we create a list of basis functions that effectively overlaps it (colored subset of basis functions in Fig. 2.2). This list of significant basis functions will be different for each batch, but the number of basis functions in each list becomes independent of size for sufficiently large molecules, given the spatial localization nature of Gaussian atom–centered basis sets. This reduced list of basis functions, evaluated for all points in the batch, is stored in contiguous blocks of memory, and used (along with the corresponding submatrices of the density matrix, when required) for the evaluation of the potential, $\mathbf{Z}$ (see Eq. (2.48)), by exploiting a sub-sequential series of vectorized operations. An important note here is that the maximum values for the batch of basis functions, $\chi_{max}(batch)$, and potential, $Z_{max}(batch)$, can be used to screen the entire contribution of the points in the batch to the integration. In this case, the integration can move to the next batch, avoiding the rank-2k update, that is the

computationally most expensive part of the process, without loosing accuracy. Otherwise, recognizing that $\mathbf{Z}$ and $\mathbf{X}$ exhibit the same sparsity pattern, we may define

$$\tilde{\mathbf{V}}_{(j)}^{GGA,K} = \tilde{\mathbf{Z}}^{K(j)} \left(\tilde{\mathbf{X}}^{(j)}\right)^T + \tilde{\mathbf{X}}^{(j)} \left(\tilde{\mathbf{Z}}^{K(j)}\right)^T \tag{2.55}$$

where moieties denoted with a tilde are the packed quantities where only the basis functions which have been chosen to be evaluated for the batch are represented. The packed $\tilde{\mathbf{V}}_{(j)}^{GGA,K}$ may then be used to update the full $\mathbf{V}^{GGA,K}$ by mapping its elements to those in the full basis dimension.

2.3.4 Discussion

In this section, we will provide validation and computational performance results for the proposed X2C-KS method. The proposed method was implemented in a locally modified version of the open–source `ChronusQ` [123] electronic structure software package. All calculations were performed using Intel Haswell compute nodes (14×2 Intel®Xeon E5–2680 v4 CPUs @ 2.40 GHz, 32k L1 cache, 256k L2 cache, 35840k L3 cache) without the exploitation of molecular point group symmetry. All numerical integrations were carried out with the Becke molecular integration scheme using 100 Euler–Maclaurin [53] quadrature points for the radial integration and 302 Lebedev [**?**] points for the angular integration around each atom.

Validation

A series of geometrically frustrated hydrogen rings were used to gauge the validity of the proposed X2C-KS implementation. Geometrically frustrated systems provide an excellent test case for the validation of non–collinear electronic structure methods as their lowest energy mean–field solutions break $\hat{S}_z$ symmetry to minimize Pauli repulsion [18, 106–109, 124–127] . Unlike their collinear counter parts (such as RKS and UKS), X2C-KS (or more generally GKS) is able to support this broken symmetry due to its explicit treatment of the full spinor nature of the electronic density. To this end, a series of six hydrogen rings

ranging from 3 to 8 hydrogens were constructed such that each hydrogen was placed at 1 Å spacing around an equidistant circle (see Fig. 2.3). Thus only the odd membered rings may be considered geometrically frustrated. All calculations involving hydrogen rings were performed using the X2C-B3LYP/6-311+G(D,P) level of theory [128–130]. The scalar and spin densities of the hydrogen rings solutions have been examined in Fig. 2.3.

In comparison to the thorough discussion of geometric frustration of hydrogen rings in Ref. [18], we can see that for the even numbered hydrogen rings, the symmetrical distribution of the spin and scalar densities indicates an anti–ferromagnetic spin alignment; the same as one would get in a collinear solutions. This is further confirmed by the fact that the expectation value of $\hat{S}$ for these solutions was found to be zero, thus all spins must be antialligned. While is this perhaps not the most interesting result in the context of non–collinear calculations, it does indicate that our implementation collapses to the expected collinear behavior if needed. Further, in the case that the spin density is small in all space (the six–membered hydrogen ring), we can see that the the choice for the generalized auxiliary variables in Eq. (2.42) is a robust and accurate choice even in the worst case scenario. The primary result of Fig. 2.3 is that both the spin and scalar densities adopt a symmetrical distribution even for the odd membered rings; a property which would be impossible in a collinear solution due to the geometrical frustration of the system. An anti–ferromagnetic solution (the lowest energy solution within the unrestricted formalism for the Slater determinant ground state) would yield an asymmetric spin density [18]. Thus, our implementation of X2C-KS is able to reproduce the expected symmetries of the non–collinear solutions for both even– and odd–membered hydrogen rings, ensuring the robustness and reliability of the proposed method.

Computational Performance

In this section, we examine the computational performance of the proposed X2C-KS method. All the following tests presented were performed using X2C-B3LYP/6-311+G(2D,P). All times refer to the combined wall time for the numerical evaluation of E^{GGA} and the matrix elements $V_{\mu\nu}^{GGA,K}$ (Eq. (2.45) and Eq. (2.46)) as an average over 5 SCF steps in the X2C-KS

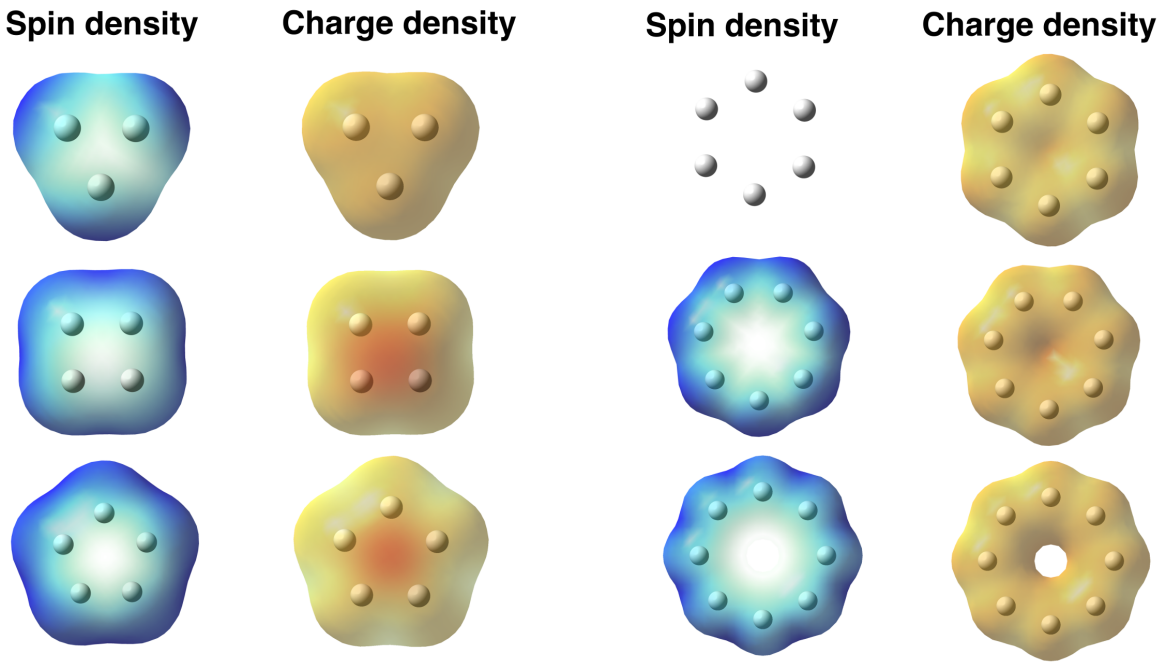


Figure 2.3: X2C-B3LYP 6-311+g(D,P) spin ($|\boldsymbol{m}(\boldsymbol{r})|$, left) and scalar ($\rho^{1,0}(\boldsymbol{r})$, right) densities for a series of hydrogen rings. Blue and Red represent regions of greater density magnitude respectively.

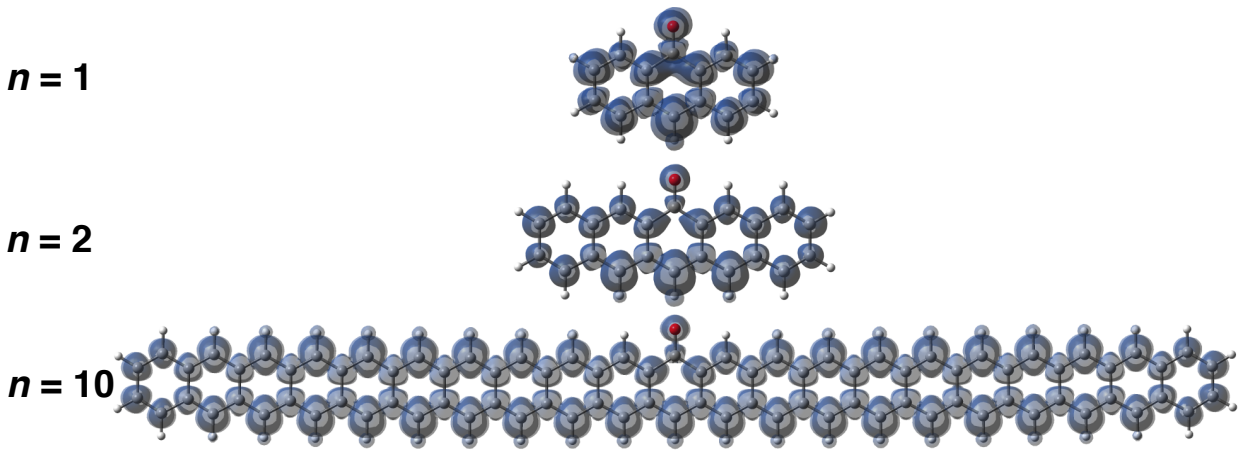


Figure 2.4: X2C-B3LYP 6-311+G(2D,P) spin densities ($|\boldsymbol{m}(\boldsymbol{r})|$) for phenoxy radicals with an increasing number of fused benzene rings (n=1-10, where n represents the number of fused benzene rings on each side).

optimization.

To demonstrate the efficacy of our method relative to standard UKS methods, we examine the relative scaling of UKS and X2C-KS with respect to system size. For this numerical experiment we have chooses a set of phenoxy radicals shown in Fig. 2.4. These systems were chosen as they exhibit highly delocalized spin–density across their entire spatial extent. This allows for a true comparison between UKS and X2C-KS as UKS will only support a particular (z) orientation of the magnetization vector while X2C-KS will not have this restriction. Wall timings for single–node (28 CPU core) performance on these systems are presented in Fig. 2.5. As can be seen, the scaling of UKS and X2C-KS is identical with X2C-KS having a slightly larger prefactor. In terms of raw wall timings, this increase in prefactor does not amount to a significant computational overhead over UKS. This is to be expected as there are (linearly) more spin components of $\underline{\boldsymbol{V}}^{xc}$ is X2C-KS over UKS (per Eq. (1.129)), thus the only difference should amount to a prefactor.

To demonstrate the practicality of the proposed method, we examine the parallel performance of our implementation using the largest phenoxy radical from the previous numerical experiment. Wall time as a function of the number of parallel processes utilized (1, 2, 4, 8, 12 nodes, for a total of 28, 56, 112, 224, 336 CPU cores) for this system is are presented in Fig. 2.6. The implementation of X2C-KS is shown to exhibit linear scaling over parallel processors (a slope of -1.01). As previously discussed in Sec. 2.3.3, this behavior is expected for a proper implementation of any KS method as the operations which are to be performed are completely independent. In out implementation, distributed memory parallelism was achieved by placing each atomic integrand (per the Becke scheme) on an individual MPI process while performing each atomic integrand using shared–memory parallelism (OpenMP) of each node.

2.3.5 Conclusions

In this work, we developed an efficient and scalable protocol for the integration and assembly of the xc potential in non–collinear KS-DFT. Initial numerical experiments demonstrate

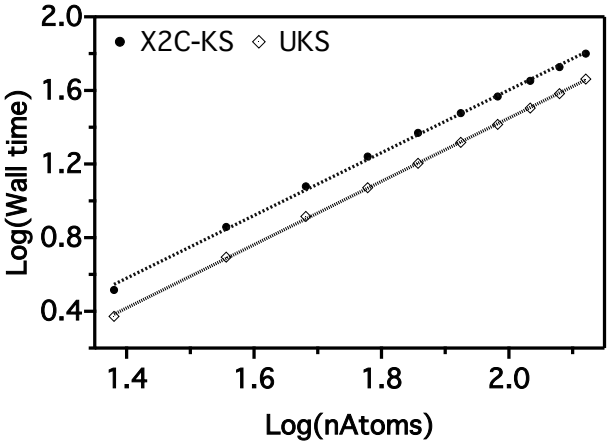


Figure 2.5: Relative scaling with respect to system size on a set of phenoxy radicals for the UKS and proposed X2C-KS methods. Times are presented logarithmically to demonstrate identical scaling with differing prefactors for the two methods. Times presented are the average wall times for the numerical integration of E^{GGA} and $V_{\mu\nu}^{GGA,K}$ over 5 SCF steps.

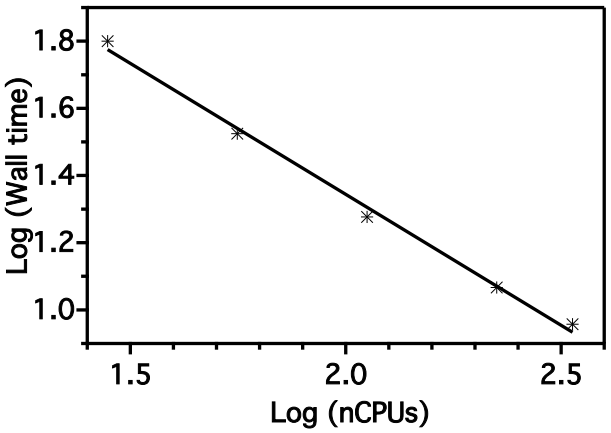


Figure 2.6: Wall times for the distributed memory parallel performance of the proposed implementation of X2C-KS on a large phenoxy radical. Times are presented logarithmically to demonstrate the linear (-1.01) scaling of the proposed method. Times presented are the average wall times for the numerical integration of E^{GGA} and $V_{\mu\nu}^{GGA,K}$ over 5 SCF steps.

numerical stability and robustness for the proposed method on a set of challenging molecular systems which exhibit non–collinearity due to geometrical frustration. We have demonstrated excellent performance of the proposed method both from the perspective of scaling with system size and linear parallel scaling on distributed memory architectures. Further, we have shown that with the proposed algorithm, the computational cost relative to UKS is not significant. We hope that the proposed algorithm will inspire development in relativistic DFT to move past proof of concept and towards leveraging the latest advances in high–performance computing.

2.4 The Relativistic Particle–Particle Tamm-Dancoff Approximation

At times, the KS-DFT description is not sufficient for the proper description of the electronic wave function. This case is encountered in general when the wave function cannot be described properly as a single Slater determinant. As such, in this section is outlined a two–component many–body expansion method (ala Eq. (1.62)) which includes relativistic effects and tackles the electron correlation problem though representing the wave function as a linear combination of several Slater determinants. The following sections have been adapted and reproduced with permission from David B. Williams–Young, Franco Egidi, and Xiaosong Li. Relativistic Two–Component Particle–Particle Tamm–Dancoff Approximation. *J. Chem. Theory Comput.* **2016**, 12(11), pp 5379-5384. Copyright 2016 American Chemical Society.

2.4.1 Motivation

The ability to accurately predict and characterize the electronically excited states of molecular systems is paramount to a complete understanding of many chemical phenomena. As such, excited states are the central focus of many fields of physical chemistry, most prominent being that of spectroscopy. Due to this centralized importance and the need to efficiently and accurately predict excited states properties, much effort has been devoted over the years towards the modeling of excitation energies and oscillator strengths.

Recently, the particle-particle random phase approximation (pp-RPA) and Tamm-Dancoff approximation (pp-TDA), which have been standard trade tools of the nuclear physics community in the treatment of the many–body correlation energy for low matter density systems for some time [4], have been extended to the treatment the correlation energy and excitation energies of quantum molecular systems within a finite basis set [131–137]. Although the introduction into the quantum chemistry community is relatively recent, a wealth of effort has been afforded to the rigorous investigation of these methods in a variety of different contexts, including the evaluation of excitation energies [131–133], excited–state properties and geometry optimizations [138], and the treatment of non-adiabatic phenomena such as non-adiabatic dynamics [139] and the description of conical intersections [140]. So far in their development, however, these methods have only seen application in molecular systems using strictly collinear (RSCF and USCF) references, disallowing extension to systems with non–collinear (GSCF) reference, such as those that arise in spin-frustrated systems (see Sec. 2.3.4) or whenever spin-orbit effects are included in the treatment of the electronic structure.

Recent years have also seen new developments in the realm of relativistic quantum chemistry. Relativistic effects, while often neglected in most standard treatment of electronic structure, can have profound consequences in chemical systems [26]. Scalar relativistic effects cause the contraction of the core electron shells of heavy atoms, but perhaps of even more consequence is the introduction of spin couplings in the Hamiltonian. Spin-spin and spin-orbit interactions can affect the electronic spin dynamics even in light atoms, and a direct consequence of these couplings on excited states is the loss of degeneracies of spin-eigenstates, giving rise to fine structure splittings (FSS) in atoms and molecules with symmetry-induced degeneracies. It is therefore desirable to develop accurate and cost-effective relativistic electronic structure methods able to model such effects.

Thus, in this work, we extend the pp-TDA formalism for use with relativistic GSCF reference determinants, specifically the X2C-HF reference of Secs. 2.1 and 2.2. However, the presented formalism may be employed in any case where the GSCF method must be employed, such as the spin-frustrated systems explored in Sec. 2.3.4, even in the absence of

relativistic effects.

2.4.2 The Particle-Particle Tamm-Dancoff Approximation

The pp-TDA is a non-particle-number conserving many–body expansion method, i.e. the approximation of the excitation operator of Eq. (1.62) it employs does not commute with the number operator. To model a system with N electrons, the pp-TDA starts from a reference determinant for a system with $N-2$ electrons, and adds two electrons back using an appropriate excitation operator. The ground and excited states of the N-particle system are thus obtained as "excited states" of the $N-2$ electron reference, and the desired excitation energies can be written as simple energy differences. A general formalism for the treatment of the pp-TDA within a finite basis of spin–collinear MOs has described rigorously elsewhere [131, 132, 134]. Here, we review this formalism for completeness and present the working expressions for the relativistic X2C pp-TDA (X2C-pp-TDA) within the basis of MO spinors as well as describe some caveats in the practical application of this method within the context of a spinor reference.

From an (exact) M-particle ground state, $\left|\Psi_0^M\right\rangle$, the excitation operator of Eq. (1.62) which constructs all ground and excited N-particle states ($\left|\Psi_0^N\right\rangle$ and $\left|\Psi_n^N\right\rangle$ respectively) may be written conveniently as a projector $\hat{R}_n^{N,M\dagger} = \left|\Psi_n^N\right\rangle\left\langle\Psi_0^M\right|$, such that

$$\left|\Psi_n^N\right\rangle = \hat{R}_n^{N,M\dagger}\left|\Psi_0^M\right\rangle. \tag{2.56}$$

Given such an ansatz, it is possible to construct an equation-of-motion (EOM) [4] for $\hat{R}_n^{N,M\dagger}$, affording some corresponding probing de-excitation operator $\delta\hat{R}$, to obtain the eigenenergies of $\left|\Psi_n^N\right\rangle$,

$$\left[\delta\hat{R}, \left[\hat{H}, \hat{R}_n^{N,M\dagger}\right]\right] = (E_n^N - E_0^M)\left[\delta\hat{R}, \hat{R}_n^{N,M\dagger}\right]. \tag{2.57}$$

Equation (2.57) is formally exact and completely independent of the chosen reference, provided one has access to the exact N- and M-particle states, or equivalently a closed form expression for the projector (such as Eq. (1.63)). In practice, one may take the expectation value of Eq. (2.57) using some approximate M-particle ground state, which in the present

work will be a Slater determinant, $\left|\Phi_0^M\right\rangle$, to obtain *approximate* energy differences between N- and M-particle states given some explicit (truncated) form of $\hat{R}_n^{N,M\dagger}$. As has been previously discussed, if the N and M systems differ by exactly two–particles ($M = N - 2$), the X2C-pp-TDA equation may be obtained by postulating that the excitation operator take the form of all (unique) 2-particle additions to obtain N-particle states from an $(N-2)$-particle reference,

$$\hat{R}_n^{N,(N-2)\dagger} = \sum_{a<b} X_{ab}^n \tau^{ab}, \tag{2.58}$$

while the de-excitation operator takes the form

$$\delta\hat{R} = \tau_{ab} \quad . \tag{2.59}$$

Here, τ is defined in Eq. (1.59) and X_{ab}^n is an expansion coefficient that describes the contribution to the n-th N-particle state of the addition of 2 particles into single-particle virtual states, a and b, of the $(N-2)$-particle ground state reference. By taking the expectation value of Eq. (2.57) in a single X2C-HF Slater determinant (e.g. by using Wick's theorem) given Eq. (2.58), one obtains the Hermitian eigenvalue problem of the X2C-pp-TDA

$$\sum_{c<d} A_{ab,cd} X_{cd}^n = \Omega_n X_{ab}^n \quad (a<b), \tag{2.60}$$

$$\Omega_n = (E_n^N - E_0^{N-2}) \tag{2.61}$$

$$A_{ab,cd} = \delta_{ac}\delta_{bd}(\epsilon_a^{\mathrm{X2C-HF}} + \epsilon_b^{\mathrm{X2C-HF}}) + \left\langle ab \left| r_{12}^{-1} \right| cd \right\rangle - \left\langle ab \left| r_{12}^{-1} \right| dc \right\rangle \quad , \tag{2.62}$$

where $\{\epsilon_p^{\mathrm{X2C-HF}}\}$ is the set of orbital eigenenergies obtained from solving the X2C-HF equation in Eq. (2.25) and

$$\left\langle ab \left| r_{12}^{-1} \right| cd \right\rangle = \sum_{\mu\nu\lambda\kappa} \sum_{\sigma\sigma'} C_{\mu a}^{\sigma *} C_{\mu b}^{\sigma' *} C_{\mu c}^{\sigma} C_{\mu d}^{\sigma'} \left\langle \mu\nu \left| r_{12}^{-1} \right| \lambda\kappa \right\rangle \tag{2.63}$$

where $\left\langle \mu\nu \left| r_{12}^{-1} \right| \lambda\kappa \right\rangle$ is defined in Eq. (1.149) and $\underline{\boldsymbol{C}} = \underline{\boldsymbol{C}}^{\mathrm{X2C-HF}}$. One may obtain neutral N-particle excitations by examining the eigen spectrum of Eq. (2.60). By variationally optimizing the wave function of the $(N-2)$-particle system via X2C-HF, both the N-particle

ground and excited–state energies are obtained via

$$E_n^N = E_0^{N-2} + \Omega_n \quad . \tag{2.64}$$

Thus the excitation energy between N-particle ground and excited states, ω_n^N, described via the X2C-pp-TDA may be written as differences of the eigenenergies,

$$\omega_n^N = E_n^N - E_0^N = \Omega_n - \Omega_0 \quad (n > 0). \tag{2.65}$$

These working expressions in Eqs. (2.60), (2.62), (2.64) and (2.65) are similar to those previously expressed for the spin-collinear reference [131, 132, 134]. The key difference is that all of the above equations are expressed in a non–collinear GSCF spinor basis rather than a collinear (RSCF / USCF) orbital basis, and that the orbitals have been optimized in the presence of relativistic spin-orbit effects via the X2C method. Unlike the collinear case, where significat simplification of Eq. (2.60) is achieved through exploitation of the spin orthogonality of the reference [131,133], the general non-collinear case presented in this work cannot be further simplified.

2.4.3 Results and Discussion

All calculations were performed with a locally modified version of the Gaussian quantum chemistry suite of programs [141], and employed the taug-cc-pVTZ-DK Gaussian basis set [142] with the diffuse f-functions removed. Relativistic effects were accounted for by means of the variational X2C method outlined in Secs. 2.1 and 2.2. In order to partially account for two-electron spin-orbit interaction in the Hamiltonian, we employed a scheme based on the scaling of the nuclear charge according to the angular momenta of the basis functions (Eq. (2.20)). The atomic nuclei, rather than being treated as point charges, were described using s-type Gaussian charge distribution (Eq. (1.143)). The stability of the two-component ground state wave function was also tested before X2C-pp-TDA calculations were performed [18].

Single Excitations

In order to highlight the capability of the pp-TDA method to describe excited states within a relativistic framework, in this section we examine the FSS of some atomic systems. The presence of spin-orbit couplings lifts some of the energetic degeneracies that would be expected in the ground or excited electronic states in non–relativistic theory. We therefore calculate the excitation energies of selected atomic systems and compare the obtained fine structure splittings with experimental reference values [143] to assess the accuracy of the method. In this section we restrict ourselves to states describable by single excitations (with respect to the N-electron system) which allows us to also compare our results with the results obtained using the two-component particle-hole Random-Phase Approximation (X2C-ph-RPA), also known as Time-Dependent Hartree-Fock method (X2C-TDHF), as well as with results obtained using the X2C-ph-TDA method [38]. Results for these FSS estimations are collected in Tab. 2.1.

It can be seen that, in general, the three methods perform similarly with respect to the reference values insofar as the order of magnitude of the error is concerned. A general trend may be observed in that the X2C-pp-TDA consistently overestimates the splittings as the atomic charge of the underlying nucleus increases. This effect is magnified in the low–energy transitions while it is less apparent in the higher–energy transitions. This is due to the fact that the frontier orbitals of the $(N-2)$-reference being used become sub-optimal in the proper description of the N-electron system due to a contraction in the presence of higher nuclear charge. This leads to an unphysically small energetic separation between the frontier orbitals of the N-electron system which causes increasing errors due to an unphysical increase in mixing. This problem is less obvious in higher–energy excitation because the higher–lying orbitals are not as affected. These orbitals are properly optimized in the X2C-ph-RPA/TDA due to orbital occupancy of the resulting wave function. The general out-performance of the X2C-ph-TDA over the X2C-ph-RPA may be attributed to an over estimation of electron correlation in the ground and excited states via the RPA [144]. The presence of the de-

excitation amplitudes in the X2C-ph-RPA allow for an over-mixing for the low-lying excited states with the ground state which give rise to an overestimate of the FSS, much the same as the case for the X2C-pp-TDA.

The main advantage of the particle-particle over the particle-hole formalism is that, in the former, both the ground and electronically excited N-particle states are described on equal footing with respect to correlation, being a linear combination of several Slater determinants. Conversely, in the ph-TDA or ph-RPA method, the ground state is described as a single determinant, while excited states are described as linear combinations of single excitations (and possibly de-excitations). That being said, the excitation space spanned by the X2C-pp-TDA solutions does not include all chemically relevant excitations, many of which can be found using the more traditional ph-RPA or ph-TDA methods. This is due to the fact that the X2C-pp-TDA is, in its traditional form, incapable of accessing excitations that involve contributions from below the Fermi level. Some work has been done in attempts to resolve this problem [131], but these alterations to the pp-TDA method have not been explored in this work.

Triplet References and Double Excitations

In this section we wish to highlight other advantages of X2C-pp-TDA over conventional X2C-ph-RPA. In the previous section we presented results for atomic systems that are characterized by being closed shell in both the N and $N-2$ systems. This is important because if the reference state has unpaired electrons then, as a consequence of the single–reference nature of the Hartree-Fock wave function, excited states will in general be spin-contaminated, affecting one's ability to extract meaningful fine structure splittings from the results, though adaptations to remedy this problem in the general case exist [145–149]. By using X2C-pp-TDA it is possible to treat systems with N electrons with any odd spin multiplicity, provided they become closed shell upon the addition or removal of two electrons. Molecules which possess triplet ground states as well as diradical moieties may be taken as examples. To demonstrate this feature we compare the FSS of one set of excited states of molecular oxy-

Table 2.1: Calculated and reference excited-state fine structure splittings (in meV) for single excitations of some atomic systems. The presence of a superscript "$\circ$" in the term symbol denotes an odd state with respect to space inversion.

Method	Level	Mg	Al^+	Si^{2+}
X2C-ph-RPA		4.89	10.49	19.85
X2C-ph-TDA	$^3P_1^\circ - ^3P_0^\circ$	2.41	7.94	16.62
X2C-pp-TDA		2.77	9.13	18.97
Ref		2.49	7.55	15.94
X2C-ph-RPA		9.75	21.02	39.96
X2C-ph-TDA	$^3P_2^\circ - ^3P_1^\circ$	4.82	15.96	33.50
X2C-pp-TDA		5.55	18.40	38.40
Ref [143]		5.05	15.36	32.45
X2C-ph-RPA		0.33	1.82	4.43
X2C-ph-TDA	$^3P_1^\circ - ^3P_0^\circ$	0.33	1.82	4.31
X2C-pp-TDA		0.42	2.17	5.08
Ref [143]		0.41	1.73	4.10
X2C-ph-RPA		0.67	3.67	9.09
X2C-ph-TDA	$^3P_2^\circ - ^3P_1^\circ$	0.67	3.68	8.86
X2C-pp-TDA		0.84	4.50	11.04
Ref [143]		0.84	3.65	9.07

	MSE	MAE
X2C-ph-RPA	2.32	2.28
X2C-ph-TDA	0.32	0.19
X2C-pp-TDA	1.55	1.55

gen with experimental data in Tab. 2.2. The difference between the calculated and measured value is just 2.5 meV, notwithstanding the approximations intrinsic in our method (e.g. the approximate treatment of electron correlation and the two-electron spin-orbit contributions, or the finite basis set). Of course, the same reasoning can also be applied in reverse: X2C-ph-RPA theory can be readily used to find excited-state FSS of systems with a singlet ground state, however if the addition or removal of two electrons produces an open-shell molecule, then X2C-pp-TDA will present some spin-contamination in the computed excited-states.

One advantage that X2C-pp-TDA always has over X2C-ph-RPA theory, however, is its ability to describe double excitations. Table 2.2 compares calculated and reference excited-state FSS of doubly-excited states of some atomic moieties. The performance of the method is similar as in the case of single excitations presented in the previous section. Such states cannot be found among the excited states computed via X2C-ph-RPA.

Table 2.2: Excited-state fine structure splittings (in meV) for singly excited triplet and doubly excited singlet electronic states calculated by the X2C-pp-TDA method.

System	Level	X2C-pp-TDA	Ref [143, 150]
O_2	$^3\Delta_3 - {}^3\Delta_2$	20.58	18.09
Al^+	$^3P_1 - {}^3P_0$	9.20	7.75
	$^3P_2 - {}^3P_1$	17.93	15.03
Si^{2+}	$^3P_1 - {}^3P_0$	19.46	16.55
	$^3P_2 - {}^3P_1$	37.88	32.06

2.4.4 Conclusions

In this work, a scheme for the extension of the pp-TDA method to relativistic two-component wave functions has been presented. This scheme involves the approximate decoupling of the large and small components of the relativistic wave function by means of the X2C method, followed by an Hartree-Fock SCF calculation on the system obtained by removing two elec-

trons, in order to obtain a set of complex spinor molecular orbitals. The two-component reference system is then used in the X2C-pp-TDA calculation that yields the ground and excited states for the N-electron system. The extension of the pp-TDA to a two-component reference comes at the cost of the employing complex spinor orbitals, and not being able to separate the problem into smaller sub-problems as is done in the case of RHF or UHF references via spin integration. The increased computational cost highlights the ever pressing need for direct and parallel implementations of post-SCF electronic structure methods, which is exaggerated in the case of relativistic electronic structure calculations.

It has been shown that the X2C-pp-TDA method exhibits excellent results in the prediction of the fine-structure splittings of the atomic and molecular species considered here. The results are comparable and at times better than those obtained using X2C-ph-RPA [38]. In addition, the X2C-pp-TDA is able to capture electronic excitations traditionally inaccessible by the X2C-ph-RPA/TDA thanks to the 2-particle reference shift, such as double excitations and those that would be described as spin-contaminated in particle-number conserving methods. While these results are promising, the general applicability of the X2C-pp-TDA method, as with the spin-collinear variant, is limited as it is traditionally unable to capture excitations that involve contributions of orbitals from below the Fermi level. That being said, there are many systems, such as triplet and diradical systems, where the X2C-pp-TDA provides a suitable method for the accurate description of the electronic manifold.

Chapter 3

MOLECULAR RESPONSE PROPERTIES THROUGH MODEL ORDER REDUCTION

The previous sections have developed the formal theory to practically obtain the stationary (Eq. (1.70)) electronic ground and excited states of molecular systems. While such developments provide the basis of any practical quantum theory, the majority of interesting chemical phenomena result for the departure from the a stationary state through the action of some external perturbation, i.e. light. In this chapter we will focus on the interaction and response of molecular systems with external electromagnetic fields which will allow us to probe many physically observable quantities such as the photoabsorption cross section. The following sections have been adapted and reproduced in part with permission from Roel van Beeumen, David B. Williams-Young, Joeseph M. Kasper, Chao Yang, Esmond G. Ng, and Xiaosong Li. Model Order Reduction Algorithm for Estimating the Absorption Spectrum. *J. Chem. Theory Comput.* **2017**, 13(10), pp 4950-4961. Copyright 2017 American Chemical Society.

3.1 Motivation

With recent advances in laser light source technology, X-ray absorption spectroscopy (XAS) has become an important probative tool in chemical physics [151]. The ability of XAS to simultaneously characterize both the electronic and geometrical structure of chemical systems has made it indispensable in the fields of catalysis and photophysics [152–156]. However, despite the capability of XAS to obtain a wealth of chemically relevant information, the complexity of experimentally obtained XAS spectra often requires a theoretical supplement to obtain a meaningful interpretation of the query phenomenon [157, 158]. Thus, the ability

to properly describe the high-energy electronic excitations of molecular systems theoretically is critical in modern electronic structure theory.

In light of its importance in physical chemistry, the prediction of XAS properties poses an interesting challenge for traditional electronic structure methods. This challenge is rooted in the fact that the X-Ray region is buried deep within the eigenspectrum of the Hamiltonian and is often spectrally dense. For example, in near–edge X-Ray absorption fine structure (NEXAFS) spectroscopy, the spectrum consists of many excited states that correspond to excitations of core electrons to diffuse quasi–bound levels. Thus, as system sizes increase, the number of states in the given energy region increases dramatically. Further, it is important to note that, because very large basis sets are often required to properly describe the rather diffuse nature of these excited states, the increase in complexity leads to poor scaling with system size.

Many electronic structure methods have been extended to the description of high-energy, X-ray electronic excitations in recent years. In the time domain, real-time density functional theory [159–161] has been shown to excellently reproduce the X-ray K-edge for molecules within relatively short simulation times [162, 163]. For large systems, however, time-domain methods have difficulty taking full advantage of concurrency on modern computing architectures, and are thus not yet a sustainable avenue in routine theoretical inquiry of these phenomena. In contrast, frequency domain approaches are often favored in these types of calculations as they may be cast as computationally scalable linear algebra problems which are well suited for massive concurrency. Frequency domain approaches to treat electronic excitations may be separated into two categories which obtain equivalent information: methods which aim to obtain a spectral decomposition of the quantum propagator, i.e., eigenproblem–based methods, and methods which solve the response problem directly through the solution of linear systems of equations.

Recasting electronic structure methods into eigenproblems has long been the de facto standard frequency domain method for electronically excited states. Through knowledge of the poles (eigenroots) of the quantum propagator, one has direct access to information

regarding the electronic excitations (resonances) of the molecular system. In addition, such a spectral decomposition may be used to treat off-resonant perturbations through interpolation schemes known as sum-over-states expressions [164]. Much work has gone into the development of these methods in both wave function theory, such as those based on the coupled-cluster (CC) [165–169] and algebraic diagrammatic construction (ADC) [170, 171] expansions of the many-body wave function, and self-consistent field theory, such as the linear response time-dependent Hartree–Fock (TD-HF) [4, 172–174] and density functional theory (TD-DFT) [15,16]. These methods have been shown to accurately predict and reproduce both low- [175, 176] and high-energy [162, 177–182] electronic excitations in molecular systems. Despite their accuracy, however, eigenproblem–based methods possess an inherent challenge in the description of high-energy excited states when the eigenroots of interest are buried deep in the eigenspectrum. Traditional methods used to partially diagonalize the propagator, such as the block-Davidson method [183–185], are designed to converge to the extreme ends of the eigenspectrum with no built-in mechanism to establish the spectrum's interior. Several approaches have been described to overcome this problem [186], including energy specific [177, 179] and restricted energy window methods [180–182] when the eigenroots of interest are well-separated. Further, in spectrally dense regions of the propagator's eigenspectrum, iterative diagonalization algorithms require the resolution of many more roots than is often practical to ensure smooth convergence.

Methods which solve the response problem through the solutions of linear systems offer an attractive alternative to eigenproblem–based approaches in the description of high-energy excitations because they have an intrinsic mechanism to probe the interior of the energy spectrum. In these methods, the probing frequency of the applied perturbation is a chosen parameter [172,175]. Thus, the interior of the spectrum is easily probed through a number of solutions of linear system of equations in the desired frequency domain. This simplicity does, however, come at a seemly significant computational cost compared to eigenproblem–based methods. While eigenproblems are able to directly obtain many poles of the eigenspectrum simultaneously, one must solve the linear problem many times over some discretization of the

frequency domain to obtain similar results. In general, this discretization must be quite dense to achieve a reasonable accuracy and thus can be more expensive than their eigenproblem based counterparts. Approaches using linear systems and based on the complex polarization propagator (CPP), such as CPP-CC [187–189] and CPP-SCF, [164, 175, 190, 191] have been shown to be successful in the description of both high [192–196] and low [197] energy properties of molecular systems and have been extended to relativistic Hamiltonians as well [198].

In this work, we introduce a general framework for the prediction of spectrally interior molecular response properties based on model order reduction (MOR) via interpolation. MOR techniques have been successfully applied in different fields of computation science and engineering, where it reduces the computational complexity of mathematical models in numerical simulations. Examples include structural dynamics, sound and vibration analysis, and control theory [199–201]. The MOR algorithm proposed in this paper aims to overcome the large computational overhead associated with the spectral discretization required by linear system based methods while maintaining the accuracy associated with eigenproblem based methods. Further, the proposed algorithm will be shown to allow for the massively scalable parallelism that is well suited for modern computing architectures.

3.2 Linear response and absorption spectrum

In the semi-classical theory of molecular light-matter interaction within the electric dipole approximation, the isotropic absorption cross section for the interaction with plane-polarized light, $\sigma(\omega)$, at a particular perturbing frequency, ω, is proportional to the trace of the dynamic polarizability tensor, $\boldsymbol{\alpha}(\omega)$,

$$\sigma(\omega) \propto \omega \,\mathrm{Im}\left(\mathrm{Tr}\left[\boldsymbol{\alpha}(\widetilde{\omega})\right]\right), \qquad \widetilde{\omega} = \omega + i\eta, \tag{3.1}$$

where $\eta > 0$ is a small damping parameter to ensure the convergence of $\boldsymbol{\alpha}$ in the spectral neighborhoods of resonant perturbations. Within the linear response regime of the first-order polarization propagator approximation (FOPPA) [164], the dynamic polarizability tensor

may be written as

$$\boldsymbol{\alpha}(\widetilde{\omega}) = \mathbf{d}^{\top}\mathbf{G}^{-1}(\widetilde{\omega})\mathbf{d}, \qquad \mathbf{d} = \begin{bmatrix} \mathbf{d}_x & \mathbf{d}_y & \mathbf{d}_z \\ \mathbf{d}_x & \mathbf{d}_y & \mathbf{d}_z \end{bmatrix}. \tag{3.2}$$

Here, $\{\mathbf{d}_\xi \mid \xi \in \{x, y, z\}\}$ is the set of dipole operators expressed in the MO basis. In the following algorithmic developments, we restrict the discussion to the FOPPA using a Hartree–Fock reference (TD-HF), although the algorithm presented is completely general to any choice of propagator or reference. Within TD-HF, $\mathbf{G}(\widetilde{\omega})$ may be written as

$$\mathbf{G}(\widetilde{\omega}) = \mathbf{H} - \widetilde{\omega}\mathbf{S}, \tag{3.3}$$

where

$$\mathbf{H} = \begin{bmatrix} \mathbf{A} & \mathbf{B} \\ \mathbf{B}^* & \mathbf{A}^* \end{bmatrix}, \qquad \mathbf{S} = \begin{bmatrix} \mathbf{I} & \mathbf{0} \\ \mathbf{0} & -\mathbf{I} \end{bmatrix}, \tag{3.4}$$

with $\mathbf{S} = \mathbf{S}^{\top} = \mathbf{S}^{-1}$ and

$$A_{ai,bj} = \left\langle 0^{\mathrm{HF}} \middle| [\tau_a^i, [\hat{H}_{el}^{\mathrm{BO}}, \tau_j^b]] \middle| 0^{\mathrm{HF}} \right\rangle = \delta_{ij}\delta_{ab}(\epsilon_a^{\mathrm{HF}} - \epsilon_i^{\mathrm{HF}}) + \left\langle aj \left| r_{12}^{-1} \right| ib \right\rangle - \left\langle aj \left| r_{12}^{-1} \right| bi \right\rangle \tag{3.5a}$$

$$B_{ai,bj} = \left\langle 0^{\mathrm{HF}} \middle| [\tau_i^a, [\hat{H}_{el}^{\mathrm{BO}}, \tau_j^b]] \middle| 0^{\mathrm{HF}} \right\rangle = \left\langle ab \left| r_{12}^{-1} \right| ij \right\rangle - \left\langle ab \left| r_{12}^{-1} \right| ji \right\rangle \tag{3.5b}$$

$$d_{\xi,ai} = \left\langle 0^{\mathrm{HF}} \middle| [\hat{O}^1, \tau_i^a] \middle| 0^{\mathrm{HF}} \right\rangle = \left\langle \phi_a \left| \hat{r}_\xi \right| \phi_i \right\rangle \tag{3.5c}$$

Here, we have denoted $\left|0^{\mathrm{HF}}\right\rangle$ as the HF ground state and $\{\hat{r}_\xi\}$ as to components of the position operator. $\{\epsilon_p^{\mathrm{HF}}\}$ is obtained by solving Eq. (1.98) and the integrals $\left\langle \cdot \left| r_{12}^{-1} \right| \cdot \right\rangle$ are given as in Eq. (2.63). Further, we have adopted the index convention for occupied and unoccupied HF-MOs as in Sec. 1.4. The definitions in Eq. (3.5) are general to both two-component relativistic and non-relativistic HF references. However, in the following, we will restrict our treatment to that of non-relativistic theory such that we may employ the use of strictly real HF-MOs. Further, due to the fact that the Born–Oppenheimer Hamiltonian is spin-independent, we may utilize RHF / UHF wave functions (Sec. 1.6.4) for the reference determinant. This will allow for significant simplification of the resulting expressions due to spin orthogonality [164].

In order to study the spectrum of the pencil $(\mathbf{H}, \mathbf{S})$ let

$$\boldsymbol{\Omega} = \mathbf{S}^{-1}\mathbf{H} = \begin{bmatrix} \mathbf{A} & \mathbf{B} \\ -\mathbf{B} & -\mathbf{A} \end{bmatrix}. \tag{3.6}$$

Although the matrix $\boldsymbol{\Omega}$ is non-symmetric, it has a number of special properties [165,202,203]. If $\mathbf{H}$ is positive definite, it may be shown that $\boldsymbol{\Omega}$ possesses a structured eigendecomposition [173, 204], i.e.,

$$\begin{bmatrix} \mathbf{A} & \mathbf{B} \\ -\mathbf{B} & -\mathbf{A} \end{bmatrix} = \begin{bmatrix} \mathbf{U} & \mathbf{V} \\ \mathbf{V} & \mathbf{U} \end{bmatrix} \begin{bmatrix} \boldsymbol{\Lambda} & \mathbf{0} \\ \mathbf{0} & -\boldsymbol{\Lambda} \end{bmatrix} \begin{bmatrix} \mathbf{U} & -\mathbf{V} \\ -\mathbf{V} & \mathbf{U} \end{bmatrix}^{\top} \tag{3.7}$$

where $\boldsymbol{\Lambda} = \mathrm{diag}(\lambda_1, \ldots, \lambda_n)$ consists of strictly positive eigenvalues, and the eigenvectors are normalized with respect to the metric $\mathbf{S}$,

$$\begin{bmatrix} \mathbf{U} & -\mathbf{V} \\ -\mathbf{V} & \mathbf{U} \end{bmatrix}^{\top} \begin{bmatrix} \mathbf{U} & \mathbf{V} \\ \mathbf{V} & \mathbf{U} \end{bmatrix} = \mathbf{I}. \tag{3.8}$$

As $\mathbf{H}$ is taken to be real in this work, it possesses additional properties that may be exploited in the development of efficient algorithms for estimating the absorption spectrum of the target system. In particular, we may apply the following similarity transformation

$$\mathbf{T} = \frac{1}{\sqrt{2}} \begin{bmatrix} \mathbf{I} & \mathbf{I} \\ -\mathbf{I} & \mathbf{I} \end{bmatrix}, \qquad \mathbf{T}^{-1} = \mathbf{T}^{\top}, \tag{3.9}$$

to $\mathbf{G}(\widetilde{\omega})$, yielding

$$\mathbf{T}^{\top}\mathbf{G}(\widetilde{\omega})\mathbf{T} = \begin{bmatrix} \mathbf{K} & \mathbf{0} \\ \mathbf{0} & \mathbf{M} \end{bmatrix} - \widetilde{\omega} \begin{bmatrix} \mathbf{0} & \mathbf{I} \\ \mathbf{I} & \mathbf{0} \end{bmatrix}, \tag{3.10}$$

where

$$\mathbf{M} \equiv \mathbf{A} + \mathbf{B}, \tag{3.11}$$

$$\mathbf{K} \equiv \mathbf{A} - \mathbf{B}, \tag{3.12}$$

which are, in most cases, positive definite. In this case, the polarizability tensor may be reformulated as

$$\boldsymbol{\alpha}(\widetilde{\omega}) = \widetilde{\mathbf{d}}^{\top}\widetilde{\mathbf{G}}^{-1}(\widetilde{\omega})\widetilde{\mathbf{d}}, \qquad \widetilde{\mathbf{d}} = \begin{bmatrix} \mathbf{d}_x & \mathbf{d}_y & \mathbf{d}_z \end{bmatrix}, \tag{3.13}$$

where

$$\widetilde{\mathbf{G}}(\widetilde{\omega}) = \mathbf{MK} - \widetilde{\omega}^2\mathbf{I}. \tag{3.14}$$

Note that the dimension of $\widetilde{\mathbf{G}}(\widetilde{\omega})$ is only half the dimension of $\mathbf{G}(\widetilde{\omega})$. Furthermore, it can be shown that

$$\mathbf{M} = (\mathbf{X} - \mathbf{Y})\mathbf{\Lambda}(\mathbf{X} - \mathbf{Y})^\top, \tag{3.15}$$

$$\mathbf{K} = (\mathbf{X} + \mathbf{Y})\mathbf{\Lambda}(\mathbf{X} + \mathbf{Y})^\top, \tag{3.16}$$

and

$$(\mathbf{X} - \mathbf{Y})^\top(\mathbf{X} + \mathbf{Y}) = \mathbf{I}, \tag{3.17}$$

such that the eigenvalues $\pm\mathbf{\Lambda}$ may be computed by

$$\mathbf{MK} = (\mathbf{X} - \mathbf{Y})\mathbf{\Lambda}^2(\mathbf{X} + \mathbf{Y})^\top. \tag{3.18}$$

Remark that by making use of $\mathbf{MK}$, the dimension of the eigenvalue problem is also reduced by a factor of 2 [205, 206].

3.3 Interpolatory Model Order Reduction of Linear Dynamical Systems

In this section, we briefly review the theory of model order reduction for linear dynamical systems. The next section will examine its connection to the computation of the absorption spectrum within the FOPPA.

3.3.1 Linear dynamical systems

We consider the linear multiple-input multiple-output (MIMO) system

$$\mathbf{\Sigma} = \begin{cases} (\mathbf{H} - s\mathbf{S})\,\mathbf{x}(s) = \mathbf{b}\,u(s) \\ \mathbf{y}(s) = \mathbf{c}^\top\mathbf{x}(s) \end{cases}, \tag{3.19}$$

where s is a derivative or shift operator, $\mathbf{H} \in \mathbb{R}^{n\times n}$ and $\mathbf{S} \in \mathbb{R}^{n\times n}$ are the system matrices, $\mathbf{b} \in \mathbb{R}^{n\times m}$, and $\mathbf{c} \in \mathbb{R}^{n\times p}$. We call n the dimension (order) of the system $\mathbf{\Sigma}$, $\mathbf{x} \in \mathbb{R}^{n\times m}$ the

state vector, $u \in \mathbb{R}$ the input, and $\mathbf{y} \in \mathbb{R}^{p \times m}$ the output [199]. Note that the system $\mathbf{\Sigma}$ is completely characterized by the quadruple $(\mathbf{H}, \mathbf{S}, \mathbf{b}, \mathbf{c})$.

The transfer function, $\boldsymbol{\varpi}(s)$, of $\mathbf{\Sigma}$ is defined as

$$\boldsymbol{\varpi}(s) = \mathbf{c}^\top \left(\mathbf{H} - s\mathbf{S}\right)^{-1} \mathbf{b}, \tag{3.20}$$

and describes the relation between the input and output of $\mathbf{\Sigma}$, i.e., $\mathbf{y}(s) = \boldsymbol{\varpi}(s)u(s)$. For the remainder, we will assume that $n \gg 1$, $m \ll n$, $p \ll n$, and $u(s) \equiv 1$ for all s.

3.3.2 State space transformation

In some cases, it might be more advantageous to describe the system from a different point of view as the original one. In these cases, we may perform a non-singular state transformation $\mathbf{T}$, i.e., $\det(\mathbf{T}) \neq 0$, yielding the transformed state

$$\widetilde{\mathbf{x}} = \mathbf{T}^{-1}\mathbf{x}, \tag{3.21}$$

of the transformed system

$$\widetilde{\mathbf{\Sigma}} = \begin{cases} \left(\widetilde{\mathbf{H}} - s\widetilde{\mathbf{S}}\right)\widetilde{\mathbf{x}}(s) = \widetilde{\mathbf{b}}\, u(s) \\ \mathbf{y}(s) = \widetilde{\mathbf{c}}^\top \widetilde{\mathbf{x}}(s) \end{cases}, \tag{3.22}$$

where $\widetilde{\mathbf{H}} = \mathbf{T}^{-1}\mathbf{H}\mathbf{T}$, $\widetilde{\mathbf{S}} = \mathbf{T}^{-1}\mathbf{S}\mathbf{T}$, $\widetilde{\mathbf{b}} = \mathbf{T}^{-1}\mathbf{b}$, and $\widetilde{\mathbf{c}}^\top = \mathbf{c}^\top\mathbf{T}$. Remark that $\mathbf{\Sigma}$ and $\widetilde{\mathbf{\Sigma}}$ admit the same transfer function as well as the same output. Therefore, we call the systems $\mathbf{\Sigma}$ and $\widetilde{\mathbf{\Sigma}}$ equivalent.

3.3.3 Reduced–order models

The evaluation of the transfer function of a system $\mathbf{\Sigma}$ requires a linear system solve for every value of s. In cases where the system dimension n is large and a high resolution is required, i.e., a high number of values of s, the evaluation of the transfer function is very expensive. In this work, we examine the effectiveness of model order reduction (MOR) techniques to circumvent this expense. MOR for linear dynamical systems is a technique that approximates

a system $\mathbf{\Sigma}$ by another system $\widehat{\mathbf{\Sigma}}$ of the same form but of a much lower dimension (order) $k \ll n$. Consequently, evaluating the transfer function of $\widehat{\mathbf{\Sigma}}$ is relatively inexpensive as it only involves linear system solves of dimension k instead of linear system solves of dimension n for $\mathbf{\Sigma}$.

Let the system $\mathbf{\Sigma}$ be given by Eq. (3.19) and define a non-singular matrix $\mathbf{V} \in \mathbb{R}^{n\times k}$ with orthonormal columns, i.e., $\mathbf{V}^\top\mathbf{V} = \mathbf{I}$. Then, a reduced–order model $\widehat{\mathbf{\Sigma}}$ can be constructed by applying a Galerkin projection $\mathbf{P} = \mathbf{V}\mathbf{V}^\top$ onto $\mathbf{\Sigma}$, yielding

$$\widehat{\mathbf{\Sigma}} = \begin{cases} \left(\widehat{\mathbf{H}} - s\widehat{\mathbf{S}}\right)\widehat{\mathbf{x}}(s) = \widehat{\mathbf{b}}\,u(s) \\ \qquad\qquad \widehat{\mathbf{y}}(s) = \widehat{\mathbf{c}}^\top\widehat{\mathbf{x}}(s) \end{cases}, \tag{3.23}$$

where $\widehat{\mathbf{H}} = \mathbf{V}^\top\mathbf{H}\mathbf{V}$, $\widehat{\mathbf{S}} = \mathbf{V}^\top\mathbf{S}\mathbf{V}$, $\widehat{\mathbf{b}} = \mathbf{V}^\top\mathbf{b}$, and $\widehat{\mathbf{c}}^\top = \mathbf{c}^\top\mathbf{V}$. Note that the length of the state vector $\widehat{\mathbf{x}}$ and the dimension of $\widehat{\mathbf{\Sigma}}$ are only $k \ll n$. The purpose of MOR is to construct a $\mathbf{V}$ such that the transfer function of $\widehat{\mathbf{\Sigma}}$ approximates very well the one of $\mathbf{\Sigma}$,

$$\varpi_{\mathbf{\Sigma}}(s) \approx \varpi_{\widehat{\mathbf{\Sigma}}}(s), \tag{3.24}$$

for all query s.

3.3.4 Model order reduction via moment matching

One way to construct a matrix $\mathbf{V}$ such that Eq. (3.24) holds is by examining the concepts of moments and moment matching [199]. Let the transfer function ϖ of $\mathbf{\Sigma}$ be given by Eq. (3.20). Then the ℓth moment of ϖ around the point $s = s_\star$ is defined as the ℓth derivative of ϖ evaluated at $s_\star$, i.e.,

$$\mathbf{m}_\ell(s_\star) := (-1)^\ell \left.\frac{d^\ell}{ds^\ell}\varpi(s)\right|_{s=s_\star}, \tag{3.25}$$

for $\ell \geq 0$. Consequently, since $\varpi(s) = \mathbf{c}^\top\left(\mathbf{H} - s\mathbf{S}\right)^{-1}\mathbf{b}$, the moments at $s_\star$ are

$$\mathbf{m}_\ell(s_\star) = \mathbf{c}^\top\left(\mathbf{H} - s_\star\mathbf{S}\right)^{-(\ell+1)}\mathbf{b}, \qquad \ell > 0.$$

Note also that the moments determine the coefficients of the Taylor series expansion of the transfer function $\boldsymbol{\varpi}$ in the neighborhood of $s_\star$

$$\boldsymbol{\varpi}(s) = \mathbf{m}_0(s_\star) + \mathbf{m}_1(s_\star)\frac{s - s_\star}{1!} + \mathbf{m}_2(s_\star)\frac{(s - s_\star)^2}{2!} + \cdots \tag{3.26}$$

Model order reduction via moment matching consists of constructing a subspace $\mathbf{V} \in \mathbb{R}^{n \times km}$ such that the original and reduced–order model match moments

$$\mathbf{m}_{i_j}(s_j) = \widehat{\mathbf{m}}_{i_j}(s_j), \qquad j = 1, \ldots, k. \tag{3.27}$$

If all moments to be matched are chosen at zero, i.e., $s_j = 0$ for $j = 1, 2, \ldots, k$, the corresponding model is known as a Padé approximation. In the general case, the problem Eq. (3.27) is known as rational interpolation and can be solved by choosing the projection matrix $\mathbf{V}$ such that

$$\mathbf{V} = \text{span}\left[(\mathbf{H} - s_1\mathbf{S})^{-1}\,\mathbf{b} \quad (\mathbf{H} - s_2\mathbf{S})^{-1}\,\mathbf{b} \quad \cdots \quad (\mathbf{H} - s_k\mathbf{S})^{-1}\,\mathbf{b}\right]. \tag{3.28}$$

It can be shown that the matrix $\mathbf{V}$ defined in Eq. (3.28) spans a rational Krylov subspace and matches all the 0th moments at s_j. For more information about the connections between moment matching and rational interpolation, we refer the interested reader to Section 11 of Antoulas' model order reduction book [199].

3.4 Estimating absorption spectrum without explicitly computing eigenvalues and eigenvectors

The most straightforward way to evaluate the absorption spectrum is to compute eigenvalues and the corresponding eigenvectors of $(\mathbf{H}, \mathbf{S})$. However, as we indicated earlier, when the dimension of $\mathbf{H}$ and $\mathbf{S}$ becomes large (spectrally dense), this approach can be prohibitively expensive (complicated).

It has been shown [207] that a special $\mathbf{K}$-inner product Lanczos algorithm can be used to provide a good approximation to the overall structure of the absorption spectrum without explicitly computing the eigenvalues and eigenvectors of $(\mathbf{H}, \mathbf{S})$. In particular, the Lanczos

algorithm can reveal major absorption peaks in the low frequency region of the spectrum without too many iterations. However, the algorithm gives limited resolution of the absorption spectrum in the spectral interior as the Krylov subspace constructed by the Lanczos iteration contains little spectral information associated with interior eigenvalues of $(\mathbf{H}, \mathbf{S})$.

We now propose an alternative way to evaluate the absorption spectrum without explicitly computing the eigenvalues and eigenvectors of $(\mathbf{H}, \mathbf{S})$. This scheme focuses on approximating the dynamic polarizability tensor $\boldsymbol{\alpha}(\widetilde{\omega})$ defined in Eq. (3.2) and the absorption spectrum $\sigma(\omega)$ defined in Eq. (3.1) within a specific energy window directly.

Firstly, observe that the dynamic polarizability tensor Eq. (3.2) may be viewed simply as the expectation value of the inverse of $\mathbf{H} - \widetilde{\omega}\mathbf{S}$. Hence, the evaluation of $\boldsymbol{\alpha}(\widetilde{\omega})$ may be recast into a problem of solving linear equations, i.e., for a specific frequency ω, we can directly evaluate the absorption spectrum Eq. (3.1) as follows

$$\sigma(\omega) \propto \omega \,\mathrm{Im}\left(\mathrm{Tr}\left[\mathbf{d}^{\top}\mathbf{x}(\widetilde{\omega})\right]\right), \tag{3.29}$$

where $\mathbf{x}$ is the solution of the linear system

$$(\mathbf{H} - \widetilde{\omega}\mathbf{S})\,\mathbf{x}(\widetilde{\omega}) = \mathbf{d}. \tag{3.30}$$

Secondly, the dynamic polarizability tensor Eq. (3.2) may also be viewed as the transfer function, i.e., the relation between input and output, of the linear dynamical system (see Sec. 3.3.1)

$$\begin{cases} (\mathbf{H} - \widetilde{\omega}\mathbf{S})\,\mathbf{x}(\widetilde{\omega}) = \mathbf{d} \\ \qquad\qquad\quad \mathbf{y}(\omega) = \mathbf{d}^{\top}\mathbf{x}(\widetilde{\omega}) \end{cases}. \tag{3.31}$$

Consequently, the absorption spectrum can directly be obtained from the output variable $\mathbf{y}$

$$\sigma(\omega) \propto \omega \,\mathrm{Im}\left(\mathrm{Tr}\left[\mathbf{y}(\omega)\right]\right). \tag{3.32}$$

In order to evaluate the output $\mathbf{y}$ of system Eq. (3.31) for a given frequency, we again need to solve a linear system of the form Eq. (3.30).

Finally, by exploiting the block structure of $\mathbf{H}$ and performing a state space transformation with Eq. (3.9) (see Sec. 3.3.2), we obtain an equivalent linear dynamical system for Eq. (3.31), but with a halved order,

$$\begin{cases} \left(\mathbf{MK} - \widetilde{\omega}^2\mathbf{I}\right)\widetilde{\mathbf{x}}(\widetilde{\omega}) = \widetilde{\mathbf{d}} \\ \mathbf{y}(\omega) = 2\,\widetilde{\mathbf{d}}^\top\mathbf{K}\,\widetilde{\mathbf{x}}(\widetilde{\omega}) \end{cases}, \tag{3.33}$$

such that we obtain the following, compact expressions for the dynamic polarizability tensor

$$\boldsymbol{\alpha}(\widetilde{\omega}) = 2\,\widetilde{\mathbf{d}}^\top\mathbf{K}\left(\mathbf{MK} - \widetilde{\omega}^2\mathbf{I}\right)^{-1}\widetilde{\mathbf{d}}, \tag{3.34}$$

and the absorption spectrum

$$\sigma(\omega) \propto \omega\,\mathrm{Im}\left(\mathrm{Tr}\left[\widetilde{\mathbf{d}}^\top\mathbf{K}\left(\mathbf{MK} - \widetilde{\omega}^2\mathbf{I}\right)^{-1}\widetilde{\mathbf{d}}\right]\right). \tag{3.35}$$

Note that the dimension of the linear systems to be solved in Eq. (3.35) is only half of the dimension of the linear system shown in Eq. (3.30).

Clearly, we cannot afford to evaluate $\sigma(\omega)$ for all ω's of interest. However, this connection to linear dynamical systems allows us to employ MOR techniques (see Sec. 3.3.3) to reduce the number of $\sigma(\omega)$ evaluations in the full dimension. More precisely, we construct a function $\hat{\sigma}(\omega)$ that approximates $\sigma(\omega)$ within a specific energy window $[\omega_{\min}, \omega_{\max}]$, but is much cheaper to evaluate. The construction of such an approximate function only requires solving a few linear systems of the form Eq. (3.30) or Eq. (3.33) at a few selected frequencies $\tau_j,\ j = 1, 2, \ldots, k$. The solutions of these linear systems are then used to construct a reduced–order model which interpolates the full dynamic polarizability at τ_j, and provides an approximation to the dynamic polarizability tensor Eq. (3.2) at other frequencies within the predefined energy window. When k is small, both the construction and the evaluation of the reduced–order model is significantly lower than other approaches that are either based on solving an eigenvalue problem or Eq. (3.30) at many different frequencies.

3.5 Interpolation–based algorithms

Let the dimension of the matrix $\mathbf{H}$ defined in Eq. (3.4) be $2n \times 2n$. The dimension of the lower dimensional matrix $\widehat{\mathbf{H}}$ that we construct for the reduced–order model is $3k \times 3k$, where

$k \ll n$. One way to construct such a matrix is to first construct a subspace spanned by orthonormal columns of a matrix $\mathbf{V} \in \mathbb{R}^{2n \times 3k}$ and then project $\mathbf{H}$ onto such a subspace $\mathbf{V}$, i.e.,

$$\widehat{\mathbf{H}} = \mathbf{V}^\top \mathbf{H} \mathbf{V}. \tag{3.36}$$

If we also let $\widehat{\mathbf{S}} = \mathbf{V}^\top \mathbf{S} \mathbf{V}$ and $\widehat{\mathbf{d}} = \mathbf{V}^\top \mathbf{d}$, then the absorption spectrum can be approximated by

$$\widehat{\sigma}(\omega) \propto \omega \operatorname{Im}\left(\operatorname{Tr}\left[\widehat{\mathbf{d}}^\top \left(\widehat{\mathbf{H}} - \widetilde{\omega} \widehat{\mathbf{S}} \right)^{-1} \widehat{\mathbf{d}} \right] \right). \tag{3.37}$$

Clearly, the choice of the subspace $\mathbf{V}$ is crucial in maintaining the fidelity of the reduced–order model. The subspace we use to construct the reduced–order model takes the form

$$\mathbf{V} = \operatorname{span}\left[(\mathbf{H} - \tau_1 \mathbf{S})^{-1} \mathbf{d} \quad (\mathbf{H} - \tau_2 \mathbf{S})^{-1} \mathbf{d} \quad \cdots \quad (\mathbf{H} - \tau_k \mathbf{S})^{-1} \mathbf{d} \right], \tag{3.38}$$

where τ_j, $j = 1, 2, \ldots, k$, are the interpolation frequencies carefully chosen within the energy window of interest to ensure that

$$\sigma(\omega) \approx \widehat{\sigma}(\omega), \tag{3.39}$$

for all ω in the energy window of interest. It follows from the way $\mathbf{V}$ is constructed in Eq. (3.38) that $\widehat{\boldsymbol{\alpha}}$ interpolates $\boldsymbol{\alpha}$ at the interpolation frequencies, i.e.,

$$\boldsymbol{\alpha}(\tau_j) = \widehat{\boldsymbol{\alpha}}(\tau_j), \qquad j = 1, 2, \ldots, k. \tag{3.40}$$

Furthermore, since the linear systems Eq. (3.31) and Eq. (3.33) have symmetric system matrices $(\mathbf{H}, \mathbf{S})$ and $\mathbf{MK}$, respectively, and the input and output matrices $\mathbf{b}$ and $\mathbf{c}$ are linearly dependent, the Galerkin projection becomes a Petrov–Galerkin projection [199]. Hence, the original systems Eq. (3.31) and Eq. (3.33) and its corresponding reduced–order systems of dimension k match $2k$ moments instead of only k moments in the general case [199]. In order words, we can obtain the same accuracy for the reduced–order models with fewer interpolation frequencies than the general (non-linearly dependent) case.

Algorithm 1 summarizes the construction of the reduced–order model and how it is used to obtain an approximation of the absorption spectrum within an energy window of interest.

Clearly, the higher the model order k, the more accurate the approximation. In the next section, we will show that even for a relatively small k, we can obtain a quite accurate approximation for $\sigma(\omega)$ in an interior spectral window that contains thousands of eigenvalues.

Algorithm 1: Absorption spectrum via model order reduction

Input : Matrices $\mathbf{H}, \mathbf{S}, \mathbf{d}$,

Interpolation frequencies $\tau_1, \tau_2 \ldots, \tau_k$,

Frequencies $\omega_1, \omega_2, \ldots, \omega_N$, and η.

Output: Absorption spectrum $\widehat{\sigma}(\omega_1), \widehat{\sigma}(\omega_2), \ldots, \widehat{\sigma}(\omega_N)$.

for $j = 1, 2, \ldots, k$ **do**

1 Linear system solve $\mathbf{x}_j = (\mathbf{H} - \tau_j \mathbf{S})^{-1} \mathbf{d}$.

end

2 QR factorization $\mathbf{X} = \mathbf{VR}$.

3 Construct $\widehat{\mathbf{H}} = \mathbf{V}^\top \mathbf{H} \mathbf{V}$, $\widehat{\mathbf{S}} = \mathbf{V}^\top \mathbf{S} \mathbf{V}$, and $\widehat{\mathbf{d}} = \mathbf{V}^\top \mathbf{d}$.

for $j = 1, 2, \ldots, N$ **do**

4 Compute $\widehat{\sigma}(\omega_j) = \omega \, \mathrm{Im} \left(\mathrm{Tr} \left[\widehat{\mathbf{d}}^\top \left(\widehat{\mathbf{H}} - (\omega_j + i\eta) \widehat{\mathbf{S}} \right)^{-1} \widehat{\mathbf{d}} \right] \right)$.

end

Although Algorithm 1 provides a general framework for constructing a reduced–order model for estimating the absorption spectrum defined by $(\mathbf{H}, \mathbf{S})$, it is more efficient to exploit the structure of $(\mathbf{H}, \mathbf{S})$ and construct a reduced–order model for Eq. (3.33) instead. Such a reduced–order model may be obtained by projecting Eq. (3.33) onto a subspace defined by

$$\widetilde{\mathbf{V}} = \mathrm{span} \left[\left(\mathbf{MK} - \tau_1^2 \mathbf{I} \right)^{-1} \widetilde{\mathbf{d}} \quad \left(\mathbf{MK} - \tau_2^2 \mathbf{I} \right)^{-1} \widetilde{\mathbf{d}} \quad \cdots \quad \left(\mathbf{MK} - \tau_k^2 \mathbf{I} \right)^{-1} \widetilde{\mathbf{d}} \right], \tag{3.41}$$

where τ_j, $j = 1, 2, \ldots, k$, are again the interpolation frequencies. Because the matrix $\mathbf{MK}$ is self-adjoint with respect to the $\mathbf{K}$-inner product, it is more convenient to carry out the

projection using the $\mathbf{K}$-inner product and projecting $\mathbf{MK}$ onto a subspace spanned by a $\mathbf{K}$-orthonormal basis, i.e., $\widetilde{\mathbf{V}}^\top \mathbf{K} \widetilde{\mathbf{V}} = \mathbf{I}$ is satisfied. If we let

$$\widehat{\mathbf{MK}} = \widetilde{\mathbf{V}}^\top \mathbf{K} \mathbf{M} \mathbf{K} \widetilde{\mathbf{V}}, \tag{3.42}$$

$$\widehat{\mathbf{d}} = \widetilde{\mathbf{V}}^\top \mathbf{K} \widetilde{\mathbf{d}}, \tag{3.43}$$

then the approximation to the absorption spectrum provided by the structure exploiting reduced–order model can be expressed by

$$\widehat{\sigma}(\omega) \propto \omega \, \mathrm{Im} \left(\mathrm{Tr} \left[\widehat{\mathbf{d}}^\top \left(\widehat{\mathbf{MK}} - \widetilde{\omega}^2 \mathbf{I} \right)^{-1} \widehat{\mathbf{d}} \right] \right). \tag{3.44}$$

By exploiting the block structure of $\mathbf{H}$, we can prove that Eq. (3.37) and Eq. (3.44) are equivalent. However, the latter is cheaper to construct, both in terms of the number of floating point operations and memory usage, since it only involves matrices of size $n \times n$ and vectors of size n. The structure exploiting model order reduction algorithm for approximating the absorption spectrum is outlined in Algorithm 2.

Note that both Algorithms 1 and 2 require a choice of the interpolation frequencies τ_j. The number of these interpolation frequencies and their locations solely determine the quality of the absorption spectrum approximations. The simplest way to choose these interpolation frequencies is to partition the energy window of interest evenly by a uniform interpolation grid. However, because the absorption spectrum can be highly oscillatory in certain regions within the energy window, a very fine grid may be needed to resolve the high oscillation. As a result, the order of the reduced–order model, which is proportional to the number of interpolation frequencies, can be exceedingly high.

A more effective strategy for choosing the interpolation frequencies is to choose these frequencies in an adaptive fashion. We now propose a refinement strategy, which is graphically illustrated in Fig. 3.1. To start this procedure, we choose in the first level a coarse, uniform grid of interpolation frequencies (marked by ■) to construct the level-1 reduced–order model. The set of interpolation frequencies is refined by adding the midpoints (marked by ▲) between two adjacent level-1 interpolation frequencies. This enlarged set forms the second level

Algorithm 2: Absorption spectrum via structure exploiting model order reduction

Input : Matrices $\mathbf{M}, \mathbf{K}, \widetilde{\mathbf{d}}$,

Interpolation frequencies $\tau_1, \tau_2 \ldots, \tau_k$,

Frequencies $\omega_1, \omega_2, \ldots, \omega_N$, and η.

Output: Absorption spectrum $\widehat{\sigma}(\omega_1), \widehat{\sigma}(\omega_2), \ldots, \widehat{\sigma}(\omega_N)$.

for $j = 1, 2, \ldots, k$ **do**

1 Linear system solve $\widetilde{\mathbf{x}}_j = \left(\mathbf{MK} - \tau_j^2 \mathbf{I}\right)^{-1} \widetilde{\mathbf{d}}$.

end

2 QR factorization $\widetilde{\mathbf{X}} = \widetilde{\mathbf{V}}\widetilde{\mathbf{R}}$, with $\widetilde{\mathbf{V}}^\top \mathbf{K} \widetilde{\mathbf{V}} = \mathbf{I}$.

3 Construct $\widehat{\mathbf{MK}} = \widetilde{\mathbf{V}}^\top \mathbf{KMK} \widetilde{\mathbf{V}}$ and $\widehat{\mathbf{d}} = \widetilde{\mathbf{V}}^\top \mathbf{K} \widetilde{\mathbf{d}}$.

for $j = 1, 2, \ldots, N$ **do**

4 Compute $\widehat{\sigma}(\omega_j) = \omega \operatorname{Im}\left(\operatorname{Tr}\left[\widehat{\mathbf{d}}^\top \left(\widehat{\mathbf{MK}} - (\omega_j + i\eta)^2 \mathbf{I}\right)^{-1} \widehat{\mathbf{d}}\right]\right)$.

end

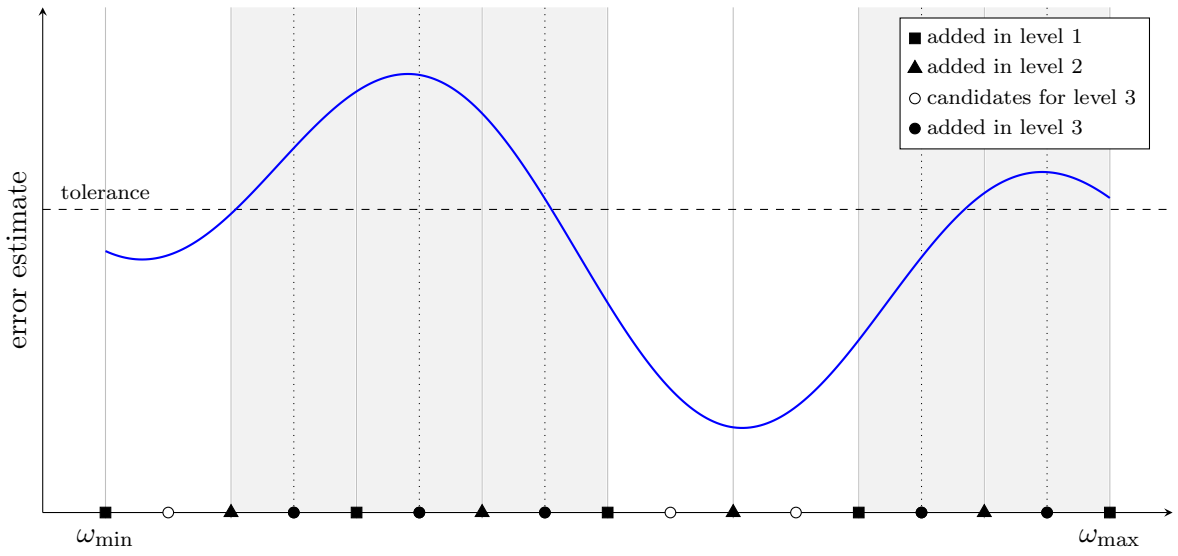


Figure 3.1: Adaptive refinement strategy for selecting the interpolation frequencies.

of interpolation frequencies, yielding a more accurate level-2 reduced–order model. Next, we choose the midpoints between two adjacent level-2 interpolation frequencies as candidates (marked by ∘) to enlarge the set in the third level. We also estimate the approximation error by computing the relative difference between the level-1 and level-2 reduced–order models for the entire energy window. If the error estimate at an interval between two adjacent level-2 interpolation frequencies is above a prescribed error tolerance, the midpoint (marked by •) is added to the existing set of interpolation frequencies. The enlarged set results in an even more accurate level-3 reduced–order model. This refinement process continues until the error estimate at the entire energy window is below the threshold or when the refined model order exceeds an prescribed upper bound.

3.6 Computational results

The proposed automatic MOR algorithm has been implemented in the Chronus Quantum software package [123] and in MATLAB[4]. The following numerical experiments were performed using a single Sandy–Bridge Intel Xeon compute node (E5-2650 v2 @ 2.60 GHz) with 16 cores and 512 GB DDR3 RAM. All of the water cluster test cases were performed using the 6-31G(d) basis set without the use of molecular symmetry and were chosen for their dense spectral character in the X-Ray spectral domain. All of the geometries for the water clusters used in this work may be found in the supplemental information.

The implementation of the MOR utilizes a synchronized approach to the Generalized Minimum Residual (GMRES) [208] algorithm for the solution of the linear systems. In this approach [209], each linear system is solved individually via the standard GMRES algorithm but its matrix-vector products (GEMVs), which constitutes the dominant cost, are synchronized and performed in batches. Hence, the GEMVs become matrix-matrix products (GEMMs) and allow for optimal efficiency and cache utilization through the use of Level 3 BLAS operations. In all experiments we used a block size of 12, coming from

[4]https://bitbucket.org/roelvb/mor4absspectrum

combining the 3 dipole vectors at 4 interpolation frequencies.

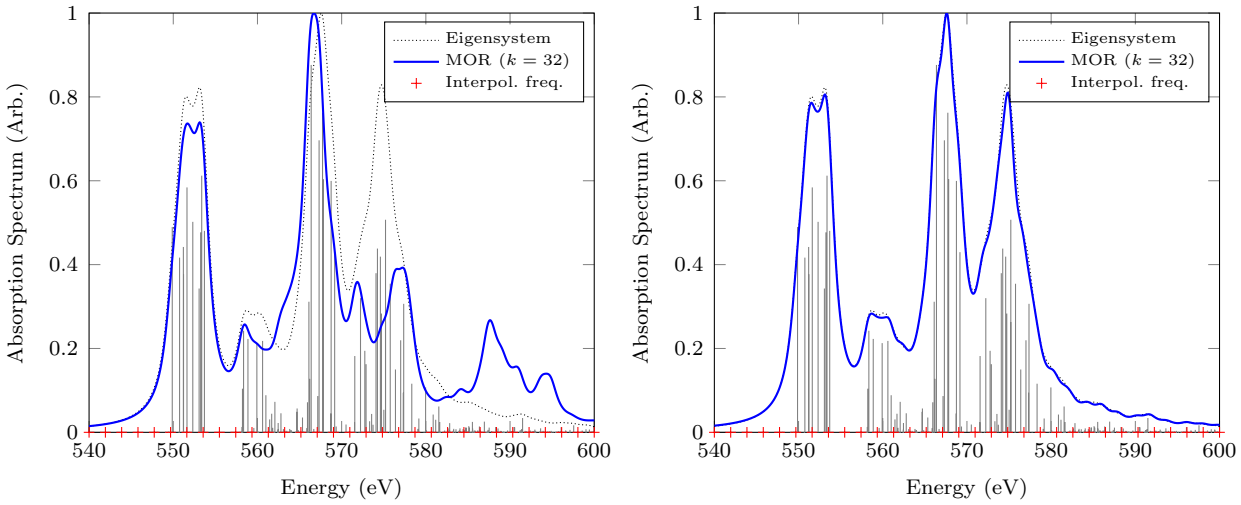
Several numerical experiments were performed to demonstrate the performance and accuracy of the proposed MOR algorithms. Since the interpolation points are merely used to construct a reduced–order model, it is conceivable that we may choose them to be real numbers instead of complex numbers that contain a small imaginary damping factor. The advantage of choosing real interpolation points is that all linear systems can be solved in real arithmetic. However, as we will see below, this approach may not lead to any performance gain and can even lead to a performance degradation.

We also examined how the order of the reduced–order model changes as the damping factor η changes and as the size of the molecular system increases as well as the overall computational scaling of the proposed method using the aforementioned water clusters. Numerical comparisons are made to the Lorentzian broadened poles of the propagator using the oscillator strengths [210–212]. The eigenvalues and oscillator strengths were computed via BSEPACK [204, 213] on a Cray XC40 with Haswell Intel Xeon compute nodes (E5-2698 v3 @2.3 GHz, 2x16 cores, 128 GB DDR4 RAM). The broadening factor was set equal to η for comparison with the approximate MOR experiments.

3.6.1 Real versus complex interpolation frequencies

We start with a cluster of 5 water molecules and are interested in computing the absorption spectrum in the energy window $[540\,\text{eV}, 600\,\text{eV}]$. The dimension of the matrix $\mathbf{H}$ Eq. (3.4) was $2n = 6{,}500$ and $\mathbf{H}$ had 394 eigenvalues in the energy window. The damping factor was $\eta = 1\,\text{eV}$ and the tolerance for solving the linear systems was set to 10^{-6}. The damping factor was chosen to roughly mimic the effects of the core-hole lifetime of the K-edge transitions in oxygen and vibrational broadening [151]. It is important to note that the broadening due to the damping parameter in these simulations is purely phenomenological, as no vibronic effects are being explicitly treated.

In the first experiment, we used a fixed order $k = 32$ for the reduced–order models and only changed the interpolation frequencies τ_j, $j = 1, 2, \ldots, k$. We computed the absorption



(a) Algorithm 1: real τ_j

(b) Algorithm 1: complex τ_j

(c) Algorithm 2: real τ_j

(d) Algorithm 2: complex τ_j

Figure 3.2: Numerical experiments for the evaluation of the XAS spectrum of 5 H_2O clusters by the proposed MOR algorithms using a fixed model order ($k = 32$). The MOR results are compared to the Lorentzian broadened poles of the propagator, labelled Eigensystem. A damping parameter of 1 eV was chosen both for the MOR calculations and the broadening factor of the Lorentzians for the reference. It can be seen that the use of complex interpolation frequencies for the construction of the model basis is important in spectrally dense regions.

spectrum by Algorithms 1 and 2 for both real $\tau_j = \omega_j$ and complex $\tau_j = \omega_j + i\eta$, where ω_j were uniformly selected in the energy window. The corresponding results are presented in Fig. 3.2 and in the top part of Tab. 3.1. Note that by using complex interpolation frequencies τ_j, we obtained good approximations to the absorption spectrum from both Algorithms 1 and 2 even with such a small model size. On the other hand, the use of real τ_j resulted in poor approximations for both algorithms. This is due to the fact that the (real) interpolation frequencies are often very close to the (real) eigenvalues of $(\mathbf{H}, \mathbf{S})$ or $\mathbf{MK}$, resulting in ill-conditioned linear systems to be solved. However, this can be avoided with complex interpolation frequencies.

Next, we repeated the previous experiment but chose the interpolation frequencies via the adaptive refinement strategy introduced in Sec. 3.5. As the error estimates, we used the difference of the normalized absorption spectrum between two consecutive refinement

Table 3.1: The effect of using real and complex interpolation frequencies τ_j on the MOR evaluation of XAS spectra for 5 H_2O clusters. Computational expense for Algorithms 1 and 2. Here k is the reduced–order, GEMMs is the total number of matrix-matrix products, and the total wall-clock time is given in seconds.

Algorithm	k	GEMMs	Wall (s)
Algorithm 1: real τ_j	32	1,052	19.76
Algorithm 1: complex τ_j	32	776	40.97
Algorithm 2: real τ_j	32	985	9.78
Algorithm 2: complex τ_j	32	646	17.5
Algorithm 1: real τ_j	218	7,440	137.01
Algorithm 1: complex τ_j	87	2,285	115.50
Algorithm 2: real τ_j	211	6,541	65.31
Algorithm 2: complex τ_j	87	2,026	52.70
Conventional CPP (1,000 points)		18,126	538.90

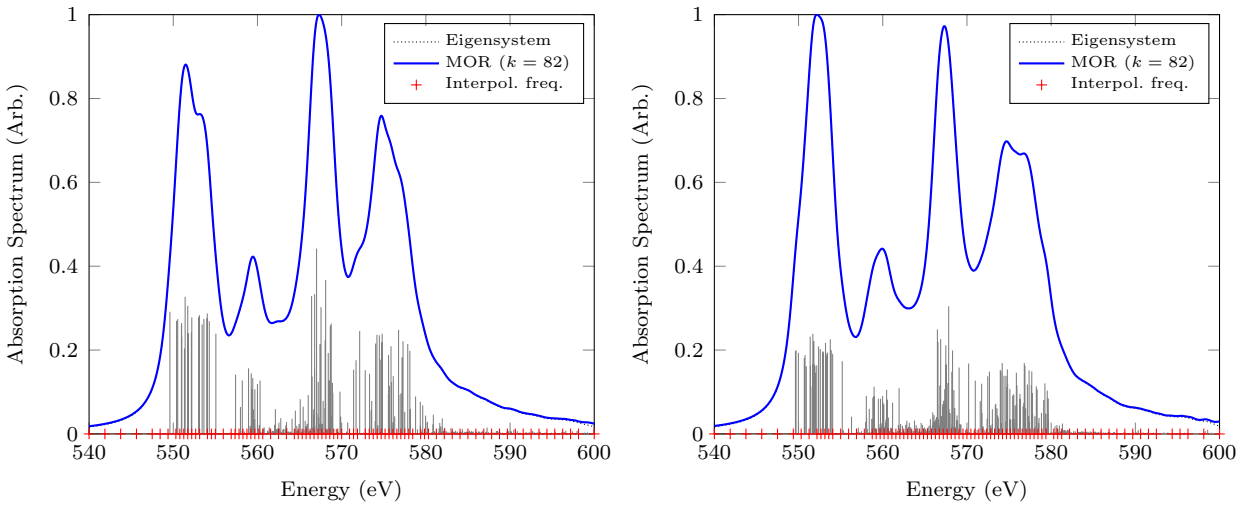
levels. The tolerance was set to 0.01, which corresponds to a 1 percent change in the overall absorption spectrum on the window $[540\,\mathrm{eV}, 600\,\mathrm{eV}]$. This resulted in reduced–order models of different orders k, reported in the middle part of Tab. 3.1. We observe that in terms of the order k, the use of complex interpolation frequencies has a significant advantage over the use of real frequencies. Further, we also observe that the adaptive refinement strategy for Algorithms 1 and 2 resulted in very similar orders k when the same type of interpolation frequencies are used.

The corresponding computational expense for the previous two experiments is reported in Tab. 3.1 using various metrics. We observe that for both fixed and adaptive model orders, the computational cost required for Algorithm 2 was significantly lower than that of Algorithm 1. This is expected as both methods are mathematically equivalent and the former only deals with linear systems of half the dimension of the latter. Furthermore, although *real* interpolation frequencies allow us to solve only *real* linear systems, we observe that in case of adaptively chosen model orders, the drastic decrease in model order required for complex interpolation frequencies over real frequencies offsets this advantage. Finally, we note at the bottom of Tab. 3.1 that the use of Algorithm 2 with complex interpolation frequencies reduces the computational expense by a factor of almost 10 compared to conventional complex polarization propagator calculations on a fine grid.

3.6.2 Computational scaling

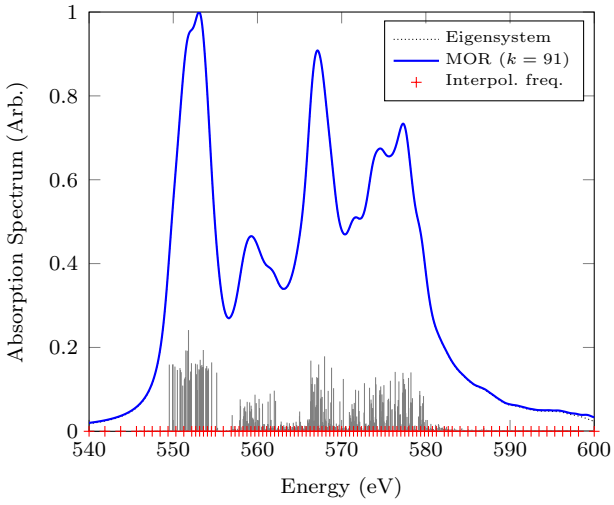
We now consider water clusters consisting of 5, 10, 15, 20, and 25 water molecules. The corresponding matrix dimensions are shown in Tab. 3.2. The energy window $[540\,\mathrm{eV}, 600\,\mathrm{eV}]$ and damping factor $\eta = 1\,\mathrm{eV}$ were the same as for the previous experiments. We computed the absorption spectrum via Algorithm 2 with complex interpolation frequencies chosen adaptively. The obtained absorption spectra are shown in Fig. 3.3.

The MOR results are given in Tab. 3.2, where we present the orders k of the reduced–order models, the total number of GEMMs, and the total wall-clock time for different GMRES convergence tolerances. Firstly, we observe that the order k of the reduced–order models

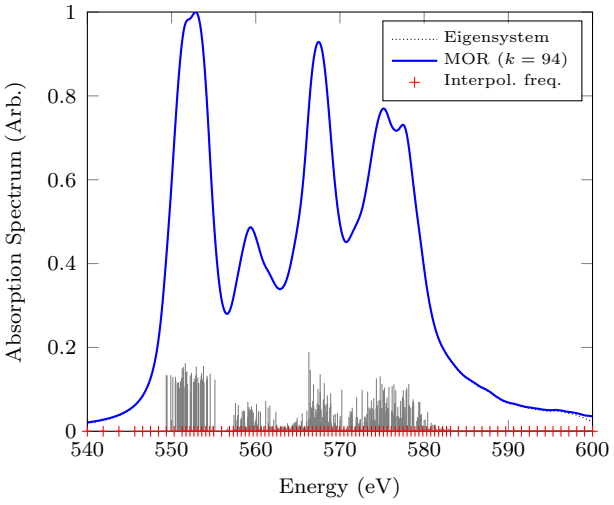


(a) Water cluster $10\,H_2O$

(b) Water cluster $15\,H_2O$



(c) Water cluster $20\,H_2O$



(d) Water cluster $25\,H_2O$

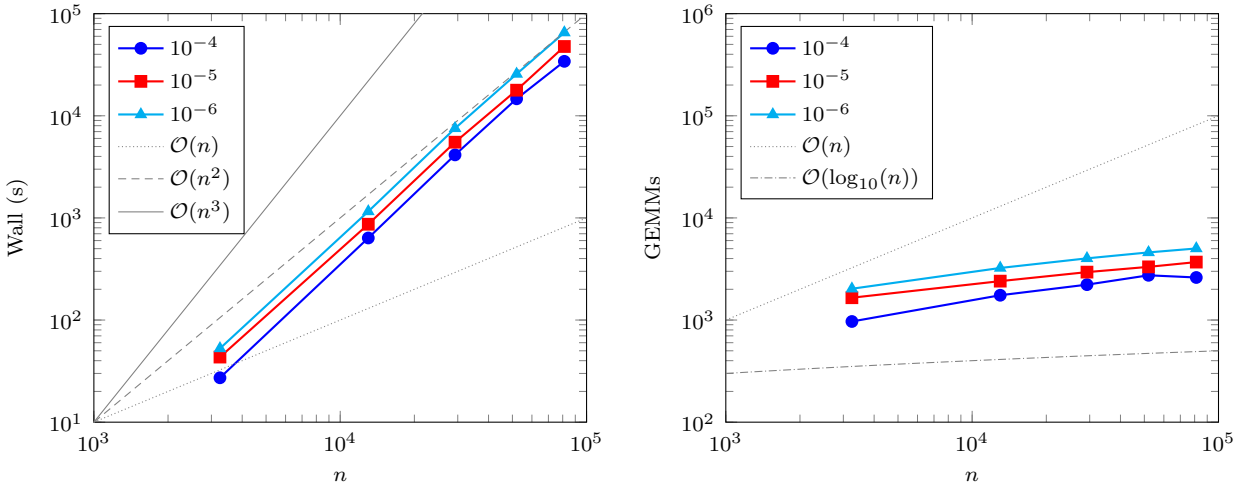
Figure 3.3: Numerical experiments for the evaluation of the XAS spectrum of variably sized H_2O clusters via Algorithm 2 with adaptively chosen complex interpolation frequencies. The MOR results are compared to the Lorentzian broadened poles of the propagator, labelled Eigensystem. A damping parameter of 1 eV was chosen both for the MOR calculations and the broadening factor of the Lorentzians for the reference.

Table 3.2: Numerical experiments for the evaluation of the XAS spectrum of variably sized H_2O clusters via Algorithm 2 with adaptively chosen complex interpolation frequencies. Here, **MK** is of dimension n with $\#\lambda$ eigenvalues lying within the energy window $[540\,\text{eV}, 600\,\text{eV}]$. The comparisons are made for GMRES convergence tolerances of 10^{-4}, 10^{-5}, and 10^{-6}, with k as the reduced model order, GEMMs as the total number of matrix-matrix products, and the total wall-clock time is given in seconds.

Waters			GMRES tol = 10^{-4}			GMRES tol = 10^{-5}			GMRES tol = 10^{-6}		
#	n	$\#\lambda$	k	GEMMs	Wall (s)	k	GEMMs	Wall (s)	k	GEMMs	Wall (s)
5	3,250	394	76	968	27.2	87	1,654	43.4	87	2,025	52.7
10	13,000	1,456	99	1,749	636.2	83	2,404	867.1	82	3,235	1,157.0
15	29,250	3,183	99	2,221	4,141.8	82	2,946	5,511.9	82	4,018	7,534.4
20	52,000	5,524	123	2,742	14,665.8	89	3,317	17,807.0	91	4,594	25,656.5
25	81,250	8,530	123	2,610	34,128.8	95	3,694	47,697.1	94	5,020	65,284.1

increases sub-linearly with the number of waters, whereas the number of eigenvalues inside the energy window, $\#\lambda$, grows linearly with respect to the problem dimension. Secondly, the order k decreases for increasing GMRES convergence tolerances. This is due to the fact that if we solve the linear systems less accurately, we match the moments less accurately and hence we need more interpolation points (a higher value of k) for the same accuracy of the reduced–order model and the corresponding absorption spectra. Moreover, the order k seems to stagnate around GMRES tolerance 10^{-5} and there were no visual differences any more between the obtained absorption spectra for GMRES tolerances 10^{-5} and 10^{-6}.

The total wall-clock time and number of GEMMs are also shown in Fig. 3.4. The left figure illustrates that the wall-clock time scales quadratically with respect to the problem dimension, compared to a cubic scaling for a full diagonalization. Moreover, the right figure shows that the number of GEMMs only scales logarithmically, compared to an expected linear scaling for iterative eigensolvers since the number of eigenvalues inside the energy window grows linearly. It is worth noting that the vector space dimension of the linear



(a) Wall time

(b) Total number of GEMMs

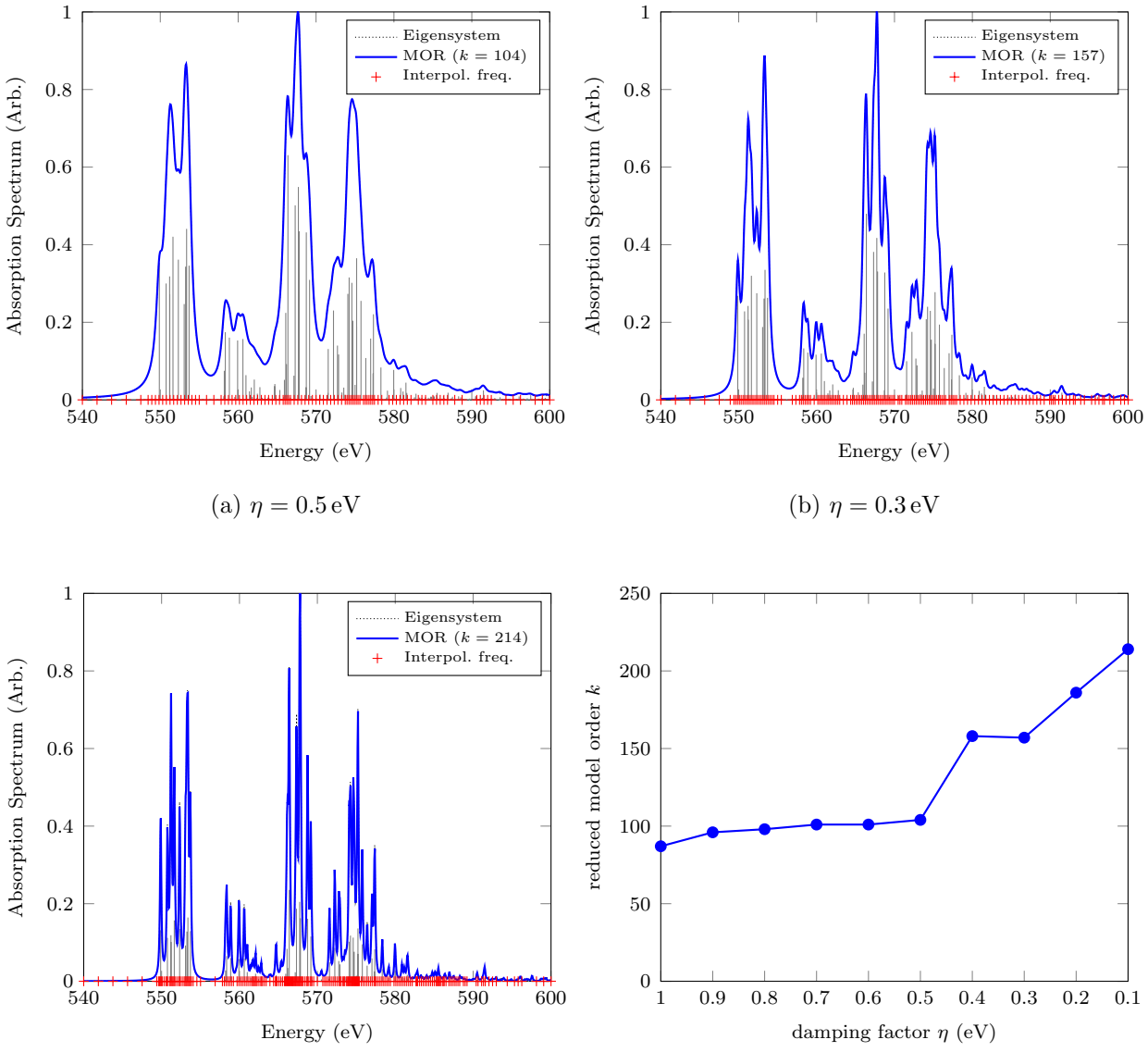
Figure 3.4: Cluster of H_2O molecules: MOR results for the absorption spectra computed via Algorithm 2 with adaptively chosen complex interpolation frequencies. The comparisons are made for GMRES convergence tolerances of 10^{-4}, 10^{-5}, and 10^{-6}.

problem also scales quadratically with system size.

3.6.3 Effect of damping factor

We examine the effect of the damping factor on the overall effectiveness of the proposed MOR algorithm in the low–damping limit. We revisit the case of water clusters containing 5 water molecules from the previous subsections over the same energy widow. Specifically, we examine the effect on the damping parameter $\eta \in [0.1, 1]\,\text{eV}$ on the model order required to achieve a convergence of 1 percent in the absorption spectrum. The MOR results were obtains via Algorithm 2 using adaptively chosen complex interpolation frequencies. The resulting spectra are presented in Fig. 3.5(a)–(c).

The effect of the damping factor on the automatically selected model order is illustrated in Fig. 3.5(d). In this figure, we observe that by decreasing the damping factor the reduced model order k first remains almost constant until 0.5 eV and then slightly starts to increase



(a) $\eta = 0.5\,\mathrm{eV}$

(b) $\eta = 0.3\,\mathrm{eV}$

(c) $\eta = 0.1\,\mathrm{eV}$

(d) k as a function of η

Figure 3.5: Numerical experiments for the evaluation of the XAS spectrum of 5 H_2O clusters by Algorithm 2 using different damping factors η. (a)–(c) The MOR results are compared to the Lorentzian broadened poles of the propagator, labelled Eigensystem. (d) Effect of the damping factor η on the reduced model order k.

for smaller values of η. Even in the low–damping limit (0.1 eV), when the obtained absorption spectrum is exceptionally complicated and oscillatory relative to the previous experiments (1 eV), the required model order is still well within the realm of practicality for routine calculations. Thus the proposed MOR algorithm may be used as a general procedure which requires no assumption of (the smoothness of) the underlying absorption spectrum.

3.7 Conclusions

In this work, we have presented a novel, adaptive algorithm for the *ab initio* prediction of the absorption spectrum based on model order reduction techniques applied to the quantum propagator. While this approach is general to any spectral domain, the power of the proposed method is in those spectral domains which are dense and interior in the propagator's eigenspectrum. The accuracy and efficiency of this method to predict the X-Ray absorption spectrum have been demonstrated using a series of water clusters. Water clusters were chosen as an especially challenging case study as the propagator is spectrally dense in the spectral neighborhood of the water's oxygen K-Edge. The numerical experiments have shown that complex interpolation frequencies should be preferred over real ones and that in this case the order of the reduced order models only slightly increases with the problem dimension, in contrast to the rapid growth of the number of eigenvalues inside the energy window. Moreover, the wall-clock time for the proposed model order reduction algorithm scales only quadratically with respect to the dimension of the problem, compared to cubic scaling for eigenvalue based algorithms. Further, it was shown that, even in the limit of highly oscillatory and low–damping absorption spectra, the proposed algorithm remains practical and thus may be treated as agnostic to the underlying nature of the spectrum. While results were presented only for the TD-HF method, the proposed adaptive MOR algorithm is general to any choice reference, propagator, or perturbation. Further, although it is not expressly considered in this work, this technique is well suited for parallelism on a massive scale as each of the linear system solutions is completely independent from the other, thus allowing for minimal communication. With the proposed MOR algorithm, routine study of X-Ray absorption spectra

for medium-to-large sized systems is simplified.

BIBLIOGRAPHY

[1] J. Von Neumann. *Mathematical Foundations of Quantum Mechanics*. Number 2. Princeton University Press, 1955.

[2] J. M. Lee. *Introduction to Smooth Manifolds*. Springer Science & Business Media, 2003.

[3] A. L. Fetter and J. D. Walecka. *Quantum Theory of Many-Particle Systems*. Courier Corporation, 2012.

[4] P. Ring and P. Schuck. *The Nuclear Many-Body Problem*. Springer Science & Business Media, 2004.

[5] A. Szabo and N. S. Ostlund. *Modern Quantum Chemistry: Introduction to Advanced Electronic Structure Theory*. Courier Corporation, 2012.

[6] R. G. Parr and W. Yang. *Density-Functional Theory of Atoms and Molecules*. Oxford University Press, USA, 1989.

[7] C. Van Wüllen. Spin Densities in Two-Component Relativistic Density Functional Calculations: Noncollinear versus Collinear Approach. *J. Comput. Chem.*, 23(8):779–785, 2002.

[8] E. Dalgaard. Expansion and Completeness Theorems for Operator Manifolds. *Int. J. Quant. Chem.*, 15(2):169–180, 1979.

[9] J. Linderberg and Y. Öhrn. *Propagators in Quantum Chemistry*. Academic Press: London and New York, 1973.

[10] J. J. Sakurai and J. Napolitano. *Modern Quantum Mechanics*. Cambridge University Press, 2017.

[11] C. C. J. Roothaan. New Developments in Molecular Orbital Theory. *Rev. Mod. Phys.*, 23(2):69, 1951.

[12] P. Hohenberg and W. Kohn. Inhomogeneous Electron Gas. *Phys. Rev.*, 136:B864–&, 1964.

[13] T. L. Gilbert. Hohenberg-Kohn Theorem for Nonlocal External Potentials. *Phys. Rev. B*, 12(6):2111, 1975.

[14] W. Kohn and L. J. Sham. Self-Consistent Equations Including Exchange and Correlation Effects. *Phys. Rev.*, 140:A1133–A1138, 1965.

[15] A. Dreuw and M. Head-Gordon. Single-Reference Ab Initio Methods for the Calculation of Excited States of Large Molecules. *Chem. Rev.*, 105(11):4009–4037, 2005.

[16] M. E. Casida. *Recent Advances in Density Functional Methods*, volume 1. World Scientific Publishing, Singapore, 1995.

[17] J. A. Pople, P. M. Gill, and B. G. Johnson. Kohn-Sham Density–Functional Theory within a Finite Basis Set. *Chem. Phys. Lett.*, 199(6):557–560, 1992.

[18] J. J. Goings, F. Ding, M. J. Frisch, and X. Li. Stability of the Complex Generalized Hartree-Fock Equations. *J. Chem. Phys.*, 142(15):154109, 2015.

[19] J. L. Stuber and J. Paldus. Symmetry Breaking in the Independent Particle Model. *Fundamental World of Quantum Chemistry: A Tribute Volume to the Memory of Per-Olov Löwdin*, 1:67–139, 2003.

[20] J. Tully. Mixed Quantum–Classical Dynamics. *Faraday Discussions*, 110:407–419, 1998.

[21] I. N. Levine et al. *Molecular Spectroscopy*. Wiley, 1975.

[22] M. Born and R. Oppenheimer. Zur Quantentheorie der Molekeln. *Annalen der Physik*, 389(20):457–484, 1927.

[23] L. Visscher and K. G. Dyall. Dirac-Fock Atomic Electronic Structure Calculations Using Different Nuclear Charge Distributions. 67:207–224, 1997.

[24] H. M. Quiney, J. K. Laerdahl, K. Fægri, Jr., and T. Saue. Ab Initio Dirac-Hartree-Fock Calculations of Chemical Properties and PT-Odd Effects in Thallium Fluoride. *Phys. Rev. A*, 57:920–944, 1998.

[25] J.-M. Lévy-Leblond. Nonrelativistic Particles and Wave Equations. *Communications in Mathematical Physics*, 6(4):286–311, 1967.

[26] P. Pyykkö. Relativistic Effects in Chemistry: More Common Than You Thought. *Annu. Rev. Phys. Chem.*, 63:45–64, 2012.

[27] M. Reiher and A. Wolf. *Relativistic Quantum Chemistry: The Fundamental Theory of Molecular Science*. Wiley-VCH Verlag GmbH & Co. KGaA, Weinheim, Germany, 2015.

[28] K. G. Dyall and K. Fægri, Jr. *Introduction to Relativistic Quantum Chemistry*. Oxford University Press, Oxford, U.K., 2007.

[29] R. P. Feynman. The Theory of Positrons. *Phys. Rev.*, 76(6):749, 1949.

[30] W. Liu. Perspective: Relativistic Hamiltonians. *Int. J. Quant. Chem.*, 114(15):983–986, 2014.

[31] W. Liu. Effective Quantum Electrodynamics Hamiltonians: A Tutorial Review. *Int. J. Quant. Chem.*, 115(10):631–640, 2015.

[32] T. Saue and L. Visscher. Four-Component Electronic Structure Methods for Molecules. In *Theoretical Chemistry and Physics of Heavy and Superheavy Elements*, pages 211–267. Springer, 2003.

[33] F. Wang and W. Liu. Benchmark Four-Component Relativistic Density Functional Calculations on Cu_2, Ag_2, and Au_2. *Chem. Phys.*, 311(1-2):63–69, 2005.

[34] W. Kutzelnigg and W. Liu. Quasirelativistic Theory Equivalent to Fully Relativistic Theory. *J. Chem. Phys.*, 123(24):241102, 2005.

[35] L. L. Foldy and S. A. Wouthuysen. On the Dirac Theory of Spin 1/2 Particles and its Non-Relativistic Limit. *Phys. Rev.*, 78(1):29, 1950.

[36] T. D. Newton and E. P. Wigner. Localized States for Elementary Systems. *Rev. Mod. Phys.*, 21(3):400, 1949.

[37] W. Liu and D. Peng. Infinite-Order Quasirelativistic Density Functional Method Based on the Exact Matrix Quasirelativistic Theory. *J. Chem. Phys.*, 125(4):044102, 2006.

[38] F. Egidi, J. J. Goings, M. J. Frisch, and X. Li. Direct Atomic-Orbital-Based Relativistic Two-Component Linear Response Method for Calculating Excited-State Fine Structures. *J. Chem. Theor. Comput.*, 12(8):3711–3718, 2016.

[39] M. Ilia and T. Saue. An Infinite-Order Two-Component Relativistic Hamiltonian by a Simple One-Step Transformation. *J. Chem. Phys.*, 126(6):064102, 2007.

[40] D. Peng, W. Liu, Y. Xiao, and L. Cheng. Making Four- and Two-Component Relativistic Density Functional Nethods Fully Equivalent Based on the Idea of "from Atoms to Molecule". *J. Chem. Phys.*, 127(10):104106, 2007.

[41] D. Peng, N. Middendorf, F. Weigend, and M. Reiher. An Efficient Implementation of Two-Component Relativistic Exact-Decoupling Methods for Large Molecules. *J. Chem. Phys.*, 138(18):184105, 2013.

[42] W. Liu. Big Picture of Relativistic Molecular Quantum Mechanics. 3(2):204–221, 2016.

[43] A. Wolf, M. Reiher, and B. A. Hess. The Generalized Douglas–Kroll Transformation. *J. Chem. Phys.*, 117(20):9215–9226, 2002.

[44] W. Liu. Ideas of Relativistic Quantum Chemistry. *Mol. Phys.*, 108(13):1679–1706, 2010.

[45] M. Douglas and N. M. Kroll. Quantum Electrodynamical Corrections to the Fine Structure of Helium. *Ann. Phys.*, 82(1):89–155, 1974.

[46] B. A. Hess. Relativistic Electronic-Structure Calculations Employing a Two-Component No-Pair Formalism with External-Field Projection Operators. *Phys. Rev. A*, 33(6):3742, 1986.

[47] K. G. Dyall. Interfacing Relativistic and Nonrelativistic Methods. I. Normalized Elimination of the Small Component in the Modified Dirac Equation. *J. Chem. Phys.*, 106(23):9618–9626, 1997.

[48] E. van Lenthe, E. J. Baerends, and J. G. Snijders. Relativistic Regular Two-Component Hamiltonians. *J. Chem. Phys.*, 99(6):4597–4610, 1993.

[49] J. C. Böttger. Approximate Two-Electron Spin-Orbit Coupling Term For Density-Functional-Theory DFT Calculations Using The Douglas-Kroll-Hess Transformation. *Phys. Rev. B*, 62:7809–7815, 2000.

[50] L. E. Ratcliff, S. Mohr, G. Huhs, T. Deutsch, M. Masella, and L. Genovese. Challenges in Large Scale Quantum Mechanical Calculations. *Wiley Interdiscip. Rev. Comput. Mol. Sci.*, 7(1):e1290, 2017.

[51] A. D. Becke. A Multicenter Numerical Integration Scheme for Polyatomic Molecules. *J. Chem. Phys.*, 88(4):2547–2553, 1988.

[52] M. R. Pederson and K. A. Jackson. Variational Mesh for Quantum-Mechanical Simulations. *Phys. Rev. B*, 41:7453–7461, Apr 1990.

[53] C. W. Murray, N. C. Handy, and G. J. Laming. Quadrature Schemes for Integrals of Density Functional Theory. *Mol. Phys.*, 78(4):997–1014, 1993.

[54] B. G. Johnson. Development, Implementation and Applications of Efficient Methodologies for Density Functional Calculations. In J. Seminario and P. Politzer, editors, *Modern Density Functional Theory: A Tool for Chemistry*, volume 2 of *Theoretical and Computational Chemistry*, pages 169 – 219. Elsevier, Amsterdam, The Netherlands, 1995.

[55] R. Stratmann, G. E. Scuseria, and M. J. Frisch. Achieving Linear Scaling in Exchange-Correlation Density Functional Quadratures. *Chem. Phys. Lett.*, 257(3):213 – 223, 1996.

[56] A. M. Köster, R. Flores-Moreno, and J. U. Reveles. Efficient and Reliable Numerical Integration of Exchange-Correlation Energies and Potentials. *J. Chem. Phys.*, 121(2):681–690, 2004.

[57] A. M. Burow and M. Sierka. Linear Scaling Hierarchical Integration Scheme for the Exchange-Correlation Term in Molecular and Periodic Systems. *J. Chem. Theor. Comput.*, 7(10):3097–3104, 2011.

[58] G. Lever, D. J. Cole, R. Lonsdale, K. E. Ranaghan, D. J. Wales, A. J. Mulholland, C.-K. Skylaris, and M. C. Payne. Large-Scale Density Functional Theory Transition State Searching in Enzymes. *J. Phys. Chem. Lett.*, 5(21):3614–3619, 2014.

[59] C. Curutchet and B. Mennucci. Quantum Chemical Studies of Light Harvesting. *Chem. Rev.*, 117(2):294–343, 2017.

[60] G. Donati, A. Petrone, P. Caruso, and N. Rega. The Mechanism of a Green Fluorescent Protein Proton Shuttle Unveiled in the Time-Resolved Frequency Domain by Excited State Ab Initio Dynamics. *Chem. Sci.*, 9:1126–1135, 2018.

[61] J. Hafner, C. Wolverton, and G. Ceder. Toward Computational Materials Design: the Impact of Density Functional Theory on Materials Research. *MRS Bull.*, 31(9):659–668, 2006.

[62] J. Aarons, M. Sarwar, D. Thompsett, and C.-K. Skylaris. Perspective: Methods for Large-Scale Density Functional Calculations on Metallic Systems. *J. Chem. Phys.*, 145(22):220901, 2016.

[63] A. Petrone, J. J. Goings, and X. Li. Quantum Confinement Effects on Optical Transitions in Nanodiamonds Containing Nitrogen Vacancies. *Phys. Rev. B*, 94:165402, 2016.

[64] G. Donati, D. B. Lingerfelt, A. Petrone, N. Rega, and X. Li. "Watching" Polaron Pair Formation from First-Principles Electron-Nuclear Dynamics. *J. Phys. Chem. A*, 120(37):7255–7261, 2016.

[65] N. Li, Z. Zhu, C.-C. Chueh, H. Liu, B. Peng, A. Petrone, X. Li, L. Wang, and A. K.-Y. Jen. Mixed Cation $FA_xPEA_{1-x}PbI_3$ with Enhanced Phase and Ambient Stability toward High-Performance Perovskite Solar Cells. *Adv. Energy Mater.*, 7:1601307, 2016.

[66] D. C. Gary, A. Petrone, X. Li, and B. M. Cossairt. Investigating the Role of Amine in InP Nanocrystal Syntheses: Destabilizing Cluster Intermediates by Z-Type Ligand Displacement. *Chem. Commun.*, 53:161–164, 2017.

[67] J. J. Goings, J. M. Kasper, F. Egidi, S. Sun, and X. Li. Real Time Propagation of the Exact Two Component Time-Dependent Density Functional Theory. *J. Chem. Phys.*, 145(10):104107, 2016.

[68] D. B. Lingerfelt, D. B. Williams-Young, A. Petrone, and X. Li. Direct Ab Initio (Meta-)Surface-Hopping Dynamics. *J. Chem. Theor. Comput.*, 12:935–945, 2016.

[69] A. Petrone, D. B. Lingerfelt, D. B. Williams-Young, and X. Li. Ab Initio Transient Vibrational Spectral Analysis. *J. Phys. Chem. Lett.*, 7:4501–4508, 2016.

[70] A. Petrone, D. B. Williams-Young, D. B. Lingerfelt, and X. Li. Ab Initio Excited State Transient Raman Analysis. *J. Phys. Chem. A*, 121:3958–3965, 2017.

[71] A. L. Buchachenko and V. L. Berdinsky. Electron Spin Catalysis. *Chem. Rev.*, 102(3):603–612, 2002.

[72] I. D'Amico and C. A. Ullrich. Spin Coulomb Drag: An Intrinsic Dissipation Mechanism in Spintronics. *Phys. Status Solidi B*, 243(10):2285–2289, 2006.

[73] S. Sanvito. Molecular Spintronics. *Chem. Soc. Rev.*, 40:3336–3355, 2011.

[74] P. J. Hore and H. Mouritsen. The Radical-Pair Mechanism of Magnetoreception. *Annu. Rev. Biophys.*, 45(1):299–344, 2016.

[75] E. K. U. Gross and R. M. Dreizler. *Relativistic Density Functional Theory*, pages 353–379. Springer US, Boston, MA, 1984.

[76] V. A. Soltamov, A. A. Soltamova, P. G. Baranov, and I. I. Proskuryakov. Room Temperature Coherent Spin Alignment of Silicon Vacancies in 4H- and 6H-SiC. *Phys. Rev. Lett.*, 108:226402, May 2012.

[77] G. Thiering and A. Gali. Ab Initio Calculation of Spin-Orbit Coupling for an NV Center in Diamond Exhibiting Dynamic Jahn-Teller Effect. *Phys. Rev. B*, 96:081115, Aug 2017.

[78] J. R. Weber, W. F. Koehl, J. B. Varley, A. Janotti, B. B. Buckley, C. G. Van de Walle, and D. D. Awschalom. Quantum Computing with Defects. *Proc. Natl. Acad. Sci. U.S.A.*, 107(19):8513–8518, 2010.

[79] T. D. Ladd, F. Jelezko, R. Laflamme, Y. Nakamura, C. Monroe, and J. L. OBrien. Quantum Computers. *Nature*, 464(7285):45, 2010.

[80] D. D. Awschalom, L. C. Bassett, A. S. Dzurak, E. L. Hu, and J. R. Petta. Quantum Spintronics: Engineering and Manipulating Atom-Like Spins in Semiconductors. *Science*, 339(6124):1174–1179, 2013.

[81] T. Saue and T. Helgaker. Four-Component Relativistic Kohn-Sham Theory. *J. Comput. Chem.*, 23(8):814–823, 2002.

[82] F. Wang and W. Liu. Comparison of Different Polarization Schemes in Open-shell Relativistic Density Functional Calculations. *J. Chin. Chem. Soc.*, 50(3B):597–606, 2003.

[83] T. Saue. Relativistic Hamiltonians for Chemistry: A Primer. *ChemPhysChem*, 12(17):3077–3094, 2011.

[84] T. Saue and H. J. A. Jensen. Linear Response at the 4-Component Relativistic Level: Application to the Frequency-Dependent Dipole Polarizabilities of the Coinage Metal Dimers. *J. Comput. Phys.*, 118(2):522–536, 2003.

[85] J. Gao, W. Liu, B. Song, and C. Liu. Time-Dependent Four-Component Relativistic Density Functional Theory for Excitation Energies. *J. Chem. Phys.*, 121(14):6658–6666, 2004.

[86] R. Bast, H. J. A. Jensen, and T. Saue. Relativistic Adiabatic Time-Dependent Density Functional Theory Using Hybrid Functionals and Noncollinear Spin Magnetization. *Int. J. Quant. Chem.*, 109(10):2091–2112, 2009.

[87] D. Williams-Young, F. Egidi, and X. Li. Relativistic Two-Component Particle-Particle Tamm–Dancoff Approximation. *J. Chem. Theor. Comput.*, 12:5379–5384, 2016.

[88] F. Egidi, S. Sun, J. J. Goings, G. Scalmani, M. J. Frisch, and X. Li. Two-Component Non-Collinear Time-Dependent Spin Density Functional Theory for Excited State Calculations. *J. Chem. Theor. Comput.*, 13:2591–2603, 2017.

[89] G. Vignale. Current density functional theory and orbital magnetism. In *Density Functional Theory*, pages 485–511. Springer, Boston, MA, 1995.

[90] T. Kreibich, E. K. U. Gross, and E. Engel. Approximate Relativistic Optimized Potential Method. *Phys. Rev. A*, 57:138–148, Jan 1998.

[91] W. Kohn, A. Savin, and C. A. Ullrich. Hohenberg-Kohn Theory Including Spin Magnetism and Magnetic Fields. *Int. J. Quant. Chem.*, 100(1):20–21, 2004.

[92] F. A. Buot, J. Dobson, R. Dreizler, E. Engel, E. Gross, M. Petersilka, and A. Rajagopal. *Density Functional Theory II: Relativistic and Time Dependent Extensions*, volume 2. Springer, Berlin, Germany, 1996.

[93] G. Vignale and M. Rasolt. Density-Functional Theory in Strong Magnetic Fields. *Phys. Rev. Lett.*, 59:2360–2363, Nov 1987.

[94] P. Romaniello and P. L. de Boeij. Relativistic Two-Component Formulation of Time-Dependent Current-Density Functional Theory: Application to the Linear Response of Solids. *J. Chem. Phys.*, 127(17):174111, 2007.

[95] S. Sharma, S. Pittalis, S. Kurth, S. Shallcross, J. K. Dewhurst, and E. K. U. Gross. Comparison of Exact-Exchange Calculations for Solids in Current-Spin-Density- and Spin-Density-Functional Theory. *Phys. Rev. B*, 76:100401, Sep 2007.

[96] N. Helbig, S. Kurth, S. Pittalis, E. Räsänen, and E. K. U. Gross. Exchange-Correlation Orbital Functionals in Current-Density Functional Theory: Application to a Quantum Dot in Magnetic Fields. *Phys. Rev. B*, 77:245106, Jun 2008.

[97] A. Soncini, A. M. Teale, T. Helgaker, F. D. Proft, and D. J. Tozer. Maps of Current Density Using Density-Functional Methods. *J. Chem. Phys.*, 129(7):074101, 2008.

[98] A. M. Lee, N. C. Handy, and S. M. Colwell. The Density Functional Calculation of Nuclear Shielding Constants Using London Atomic Orbitals. *J. Chem. Phys.*, 103(23):10095–10109, 1995.

[99] L. M. Sandratskii. Noncollinear Magnetism in Itinerant-Electron Systems: Theory and Applications. *Adv. Phys.*, 47(1):91–160, 1998.

[100] C. A. Ullrich. Excitation Energies in Time-Dependent (Current-) Density-Functional Theory: A Simple Perspective. *J. Chem. Theor. Comput.*, 5(4):859–865, 2009.

[101] F. G. Eich and E. K. U. Gross. Transverse Spin-Gradient Functional for Noncollinear Spin-Density-Functional Theory. *Phys. Rev. Lett.*, 111:156401, Oct 2013.

[102] J. E. Bates and F. Furche. Harnessing the Meta-Generalized Gradient Approximation for Time-Dependent Density Functional Theory. *J. Chem. Phys.*, 137(16):164105, 2012.

[103] J. W. Furness, J. Verbeke, E. I. Tellgren, S. Stopkowicz, U. Ekstrm, T. Helgaker, and A. M. Teale. Current Density Functional Theory Using Meta-Generalized Gradient Exchange-Correlation Functionals. *J. Chem. Theor. Comput.*, 11(9):4169–4181, 2015.

[104] K. Capelle, G. Vignale, and B. L. Györffy. Spin Currents and Spin Dynamics in Time-Dependent Density-Functional Theory. *Phys. Rev. Lett.*, 87:206403, Oct 2001.

[105] K. Capelle and B. L. Gyorffy. Exploring Dynamical Magnetism with Time–Dependent Density–Functional Theory: From Spin Fluctuations to Gilbert Damping. *Europhys. Lett.*, 61(3):354–360, 2003.

[106] S. Sharma, J. K. Dewhurst, C. Ambrosch-Draxl, S. Kurth, N. Helbig, S. Pittalis, S. Shallcross, L. Nordström, and E. K. U. Gross. First-Principles Approach to Noncollinear Magnetism: Towards Spin Dynamics. *Phys. Rev. Lett.*, 98:196405, May 2007.

[107] J. E. Peralta, G. E. Scuseria, and M. J. Frisch. Noncollinear Magnetism in Density Functional Calculations. *Phys. Rev. B*, 75:125119, Mar 2007.

[108] G. Scalmani and M. J. Frisch. A New Approach to Noncollinear Spin Density Functional Theory beyond the Local Density Approximation. *J. Chem. Theor. Comput.*, 8(7):2193–2196, 2012.

[109] I. W. Bulik, G. Scalmani, M. J. Frisch, and G. E. Scuseria. Noncollinear Density Functional Theory Having Proper Invariance and Local Torque Properties. *Phys. Rev. B*, 87:035117, Jan 2013.

[110] F. Wang and T. Ziegler. Time-Dependent Density Functional Theory Based on a Noncollinear Formulation of the Exchange-Correlation Potential. *J. Chem. Phys.*, 121(24):12191–12196, 2004.

[111] D. Peng, W. Zou, and W. Liu. Time-Dependent Quasirelativistic Density-Functional Theory Based on the Zeroth-Order Regular Approximation. *J. Chem. Phys.*, 123(14):144101, 2005.

[112] O. Fossgaard, O. Gropen, M. C. Valero, and T. Saue. On the Performance of Four-Component Relativistic Density Functional Theory: Spectroscopic Constants and Dipole Moments of the Diatomics HX and XY (X,Y=F, Cl, Br, and I). *J. Chem. Phys.*, 118(23):10418–10430, 2003.

[113] H. Eschrig and V. D. P. Servedio. Relativistic Density Functional Approach to Open Shells. *J. Comput. Chem.*, 20(1):23–30, 1999.

[114] J. Anton, B. Fricke, and E. Engel. Noncollinear and Collinear Relativistic Density-Functional Program for Electric and Magnetic Properties of Molecules. *Phys. Rev. A*, 69:012505, Jan 2004.

[115] M. A. Marques, M. J. Oliveira, and T. Burnus. Libxc: A Library of Exchange and Correlation Functionals for Density Functional Theory. *Comp. Phys. Comm.*, 183(10):2272–2281, 2012.

[116] S. Lehtola, C. Steigemann, M. J. Oliveira, and M. A. Marques. Recent Developments in Libxc: A Comprehensive Library of Functionals for Density Functional Theory. *SoftwareX*, 7:1–5, 2018.

[117] C. A. Ullrich. Nonuniqueness in Spin-Density-Functional Theory on Lattices. *Phys. Rev. B*, 72:073102, Aug 2005.

[118] K. Goto and R. A. Geijn. Anatomy of High-Performance Matrix Multiplication. 34(3):12, 2008.

[119] Q. Wang, X. Zhang, Y. Zhang, and Q. Yi. Augem: Automatically generate high performance dense linear algebra kernels on x86 cpus. In *Proceedings of the International Conference on High Performance Computing, Networking, Storage and Analysis*, page 25. ACM, 2013.

[120] Z. Xianyi, W. Qian, and Z. Yunquan. Model-driven level 3 blas performance optimization on loongson 3a processor. In *2012 IEEE 18th International Conference on Parallel and Distributed Systems (ICPADS)*, pages 684–691. IEEE, 2012.

[121] F. G. Van Zee and R. A. van de Geijn. BLIS: A Framework for Rapidly Instantiating BLAS Functionality. 41(3):14:1–14:33, June 2015.

[122] Intel(R) Math Kernel Library 18.0. Update 1 for Linux.

[123] X. Li, E. F. Valeev, D. Williams-Young, A. Petrone, J. Goings, J. Kasper, F. Ding, H. Liu, S. Sun, and P. Lestrange. Chronus Quantum, Beta 2 Version, 2017. http://www.chronusquantum.org.

[124] S. Yamanaka, D. Yamaki, Y. Shigeta, H. Nagao, and K. Yamaguchi. Noncollinear Spin Density Functional Theory for Spin-Frustrated and Spin-Degenerate Systems. *Int. J. Quant. Chem.*, 84(6):670–676, 2001.

[125] J. Schimpl, H. M. Petrilli, and P. E. Blöchl. Nitrogen Binding to the FeMo-Cofactor of Nitrogenase. *J. Am. Chem. Soc.*, 125(51):15772–15778, 2003.

[126] S. Luo, I. Rivalta, V. Batista, and D. G. Truhlar. Noncollinear Spins Provide a Self-Consistent Treatment of the Low-Spin State of a Biomimetic Oxomanganese Synthetic Trimer Inspired by the Oxygen Evolving Complex of Photosystem II. *J. Phys. Chem. Lett.*, 2(20):2629–2633, 2011.

[127] S. Luo and D. G. Truhlar. Noncollinear Spin States for Density Functional Calculations of Open-Shell and Multi-Configurational Systems: Dissociation of MnO and NiO and Barrier Heights of O_3, BeH_2, and H_4. *J. Chem. Theor. Comput.*, 9(12):5349–5355, 2013.

[128] A. D. Becke. Density-Functional Thermochemistry. III. The Role of Exact Exchange. *J. Chem. Phys.*, 98:5648, 1993.

[129] C. Lee, W. Yang, and R. G. Parr. Development of the Colle-Salvetti Correlation-Energy Formula into a Functional of the Electron Density. *Phys. Rev. B*, 37(2):785, 1988.

[130] B. Miehlich, A. Savin, H. Stoll, and H. Preuss. Results Obtained with the Correlation Energy Density Functionals of Becke and Lee, Yang and Parr. *Chem. Phys. Lett.*, 157(3):200–206, 1989.

[131] Y. Yang, H. van Aggelen, and W. Yang. Double, Rydberg and Charge Transfer Excitations from Pairing Matrix Fluctuation and Particle-Particle Random Phase Approximation. *J. Chem. Phys.*, 139:224105, 2013.

[132] D. Peng, H. van Aggelen, Y. Yang, and W. Yang. Linear-Response Time-Dependent Density-Functional Theory with Pairing Fields. *J. Chem. Phys.*, 140:18A522, 2014.

[133] Y. Yang, H. van Aggelen, S. N. Steinmann, D. Peng, and W. Yang. Benchmark Tests and Spin Adaption for the Particle-Particle Random Phase Approximation. *J. Chem. Phys.*, 139:174110, 2013.

[134] D. Peng, P. N. Steinmann, H. van Aggelen, and W. Yang. Equivalence of the Particle-Particle Random Phase Approximation Correlation Energy and Ladder-Coupled-Coupled-Cluster Doubles. *J. Chem. Phys.*, 139:104112, 2013.

[135] H. van Aggelen, Y. Yang, and W. Yang. Exchange-Correlation Energy from Pairing Matrix Fluctuation and the Particle-Particle Random-Phase Approximation. *Phys. Rev. A*, 88:030501, 2013.

[136] P. Mori-Sánchez, A. J. Cohen, and W. Yang. Discontinuous Nature of the Exchange-Correlation Functional in Strongly Correlated Systems. *Phys. Rev. Lett.*, 102:066403, 2009.

[137] G. E. Scuseria, T. M. Henderson, and I. W. Bulik. Particle-Particle and Quasiparticle Random Phase Approximations: Connections to Coupled Cluster Theory. *J. Chem. Phys.*, 139:104113, 2013.

[138] D. Zhang, D. Peng, P. Zhang, and W. Yang. Analytic Gradients, Geometry Optimization and Excited State Potential Energy Surfaces from the Particle-Particle Random Phase Approximation. *Phys. Chem. Chem. Phys.*, 17(2):1025–1038, 2015.

[139] Z. Li, B. Suo, and W. Liu. First Order Nonadiabatic Coupling Matrix Elements Between Excited States: Implementation and Application at the TD-DFT and pp-TDA Levels. *J. Chem. Phys.*, page 244105, 2014.

[140] Y. Yang, L. Shen, D. Zhang, and W. Yang. Conical Intersections from Particle-Particle Random Phase and Tamm-Dancoff Approximations. *J. Phys. Chem. Lett.*, 7(13):2407–2411, 2016.

[141] M. J. Frisch, G. W. Trucks, H. B. Schlegel, G. E. Scuseria, M. A. Robb, J. R. Cheeseman, G. Scalmani, V. Barone, B. Mennucci, G. A. Petersson, H. Nakatsuji, M. Caricato, X. Li, H. P. Hratchian, A. F. Izmaylov, J. Bloino, G. Zheng, J. L. Sonnenberg, W. Liang, M. Hada, M. Ehara, K. Toyota, R. Fukuda, J. Hasegawa, M. Ishida, T. Nakajima, Y. Honda, O. Kitao, H. Nakai, T. Vreven, J. J. A. Montgomery, J. E. Peralta, F. Ogliaro, M. Bearpark, J. J. Heyd, E. Brothers, K. N. Kudin, V. N. Staroverov, T. Keith, R. Kobayashi, J. Normand, K. Raghavachari, A. Rendell, J. C. Burant, S. S. Iyengar, J. Tomasi, M. Cossi, N. Rega, J. M. Millam, M. Klene, J. E. Knox, J. B. Cross, V. Bakken, C. Adamo, J. Jaramillo, R. Gomperts, R. E. Stratmann, O. Yazyev, A. J. Austin, R. Cammi, C. Pomelli, J. W. Ochterski, R. L. Martin, K. Morokuma, V. G.

Zakrzewski, G. A. Voth, P. Salvador, J. J. Dannenberg, S. Dapprich, P. V. Parandekar, N. J. Mayhall, A. D. Daniels, O. Farkas, J. B. Foresman, J. V. Ortiz, J. Cioslowski, and D. J. Fox. Gaussian Development Version Revision I.04.

[142] W. A. de Jong, R. J. Harrison, and D. A. Dixon. Parallel Douglas-Kroll Energy and Gradients in NWChem: Estimating Scalar Relativistic Effects Using Douglas-Kroll Contracted Basis Sets. *J. Chem. Phys.*, 114:48–53, 2001.

[143] A. Kramida, Y. Ralchenko, J. Reader, and NIST ASD Team. NIST Atomic Spectra Database (ver. 5.2); National Institute of Standards and Technology (NIST): Gaithersburg, MD, 2014. Available via the Internet at: `http://physics.nist.gov/asd`, accessed July 26, 2016., 2014.

[144] A. Dreuw and M. Head-Gordon. Single-Reference Ab Initio Methods for the Calculation of Excited States of Large Molecules. *Chem. Rev.*, 105:4009–4037, 2005.

[145] Z. Li and W. Liu. Spin-adapted Open-Shell Random Phase Approximation and Time-Dependent Density Functional Theory. I. Theory. *J. Chem. Phys.*, 133:064106, 2010.

[146] Z. Li, W. Liut, Y. Zhang, and B. Suo. Spin-adabpted Open-Shell Time-Dependent Density Functional Theory. II. Theory and Piolet Application. *J. Chem. Phys.*, 134:134101, 2011.

[147] Z. Li and W. Liu. Spin-adabpted Open-Shell Time-Dependent Density Functional Theory. III. An Even Better and Simpler Formulation. *J. Chem. Phys.*, 135:194106, 2011.

[148] Z. Li and W. Liu. Theoretical and Numerical Assessments of Spin-Flip Time-Dependent Density Functional Theory. *J. Chem. Phys.*, 136:024107, 2012.

[149] Z. Li, B. Suo, Y. Ziang, Y. Xiao, and W. Liu. Combining Spin-Adapted Open-Shell TD-DFT with Spin-Orbit Coupling. *Mol. Phys.*, 111:3741, 2013.

[150] P. H. Krupenie. The Spectrum of Molecular Oxygen. *J. Phys. Chem. Ref. Data*, 1:423–534, 1972.

[151] J. Stöhr. *NEXAFS Spectroscopy*, volume 25. Springer Science & Business Media, 2013.

[152] P. Yannoulis, R. Dudde, K. Frank, and E. Koch. Orientation of Aromatic Hydrocarbons on Metal Surfaces as Determined by NEXAFS. *Surf. Sci.*, 189:519–528, 1987.

[153] U. Aygül, D. Batchelor, U. Dettinger, S. Yilmaz, S. Allard, U. Scherf, H. Peisert, and T. Chassé. Molecular Orientation in Polymer Films for Organic Solar Cells Studied by NEXAFS. *J. Phys. Chem. C*, 116(7):4870–4874, 2012.

[154] S. E. Shadle, B. Hedman, K. O. Hodgson, and E. I. Solomon. Ligand K-Edge X-Ray Absorption Spectroscopic Studies. Metal-Ligand Covalency in a Series of Transition Metal Tetrachlorides. *J. Am. Chem. Soc.*, 117(8):2259–2272, 1995.

[155] J. L. DuBois, P. Mukherjee, T. Stack, B. Hedman, E. I. Solomon, and K. O. Hodgson. A Systematic K-Edge X-Ray Absorption Spectroscopic Study of Cu (III) Sites. *J. Am. Chem. Soc.*, 122(24):5775–5787, 2000.

[156] L. X. Chen, W. J. Jäger, G. Jennings, D. J. Gosztola, A. Munkholm, and J. P. Hessler. Capturing a Photoexcited Molecular Structure Through Time-Domain X-Ray Absorption Fine Structure. *Science*, 292(5515):262–264, 2001.

[157] L. X. Chen, M. L. Shelby, P. J. Lestrange, N. E. Jackson, K. Haldrup, M. W. Mara, A. B. Stickrath, D. Zhu, H. Lemke, M. Chollet, B. M. Hoffman, and X. Li. Imaging Ultrafast Excited State Pathways in Transition Metal Complexes by X-Ray Transient Absorption and Scattering Using X-Ray Free Electron Laser Source. *Faraday Discuss.*, 194:639–658, 2016.

[158] M. L. Shelby, P. J. Lestrange, N. E. Jackson, K. Haldrup, M. W. Mara, A. B. Stickrath, D. Zhu, H. T. Lemke, M. Chollet, B. M. Hoffman, X. Li, and L. X. Chen. Ultrafast Excited State Relaxation of a Metalloporphyrin Revealed by Femtosecond X-Ray Absorption Spectroscopy. *J. Am. Chem. Soc.*, 138(28):8752–8764, 2016.

[159] X. Li, S. M. Smith, A. N. Markevitch, D. A. Romanov, R. J. Levis, and H. B. Schlegel. A Time-Dependent Hartree-Fock Approach for Studying the Electronic Optical Response of Molecules in Intense Fields. *Phys. Chem. Chem. Phys.*, 7:233–239, 2005.

[160] X. Li and J. C. Tully. Ab Initio Time-Resolved Density Functional Theory for Lifetimes of Excited Adsorbate States at Metal Surfaces. *Chem. Phys. Lett.*, 439(1-3):199–203, 2007.

[161] W. Liang, C. T. Chapman, and X. Li. Efficient First-Principles Electronic Dynamics. *J. Chem. Phys.*, 134(18):184102, 2011.

[162] K. Lopata, B. E. Van Kuiken, M. Khalil, and N. Govind. Linear-Response and Real-Time Time-Dependent Density Functional Theory Studies of Core-level Near-Edge X-Ray Absorption. *J. Chem. Theor. Comput.*, 8(9):3284–3292, 2012.

[163] A. Bruner, D. LaMaster, and K. Lopata. Accelerated Broadband Spectra using Transition Dipole Decomposition and Padé Approximants. *J. Chem. Theor. Comput.*, 12(8):3741–3750, 2016.

[164] J. Oddershede, P. Jørgensen, and D. L. Yeager. Polarization Propagator Methods in Atomic and Molecular Calculations. *Comp. Phys. Rep.*, 2(2):33–92, 1984.

[165] J. Olsen, H. J. A. Jensen, and P. Jørgensen. Solution of the Large Matrix Equations which Occur in Response Theory. *J. Comput. Phys.*, 74(2):265–282, feb 1988.

[166] H. J. Monkhorst. Calculation of Properties with the Coupled-Cluster Method. *Int. J. Quant. Chem.*, 12(S11):421–432, 1977.

[167] H. Koch and P. Jørgensen. Coupled Cluster Response Functions. *J. Chem. Phys.*, 93(5):3333–3344, 1990.

[168] J. F. Stanton and R. J. Bartlett. The Equation of Motion Coupled-Cluster Method. A Systematic Biorthogonal Approach to Molecular Excitation Energies, Transition Probabilities, and Excited State Properties. *J. Chem. Phys.*, 98(9):7029–7039, 1993.

[169] D. C. Comeau and R. J. Bartlett. The Equation-of-Motion Coupled-Cluster Method. Applications to Open-and Closed-Shell Reference States. *Chem. Phys. Lett.*, 207(4-6):414–423, 1993.

[170] J. Wenzel, M. Wormit, and A. Dreuw. Calculating X-Ray Absorption Spectra of Open-Shell Molecules with the Unrestricted Algebraic-Diagrammatic Construction Scheme for the Polarization Propagator. *J. Chem. Theor. Comput.*, 10:4583, 2014.

[171] J. Wenzel, M. Wormit, and A. Dreuw. Calculating Core-Level Excitations and X-Ray Absorption Spectra of Large and Medium Sized Closed-Shell Molecules with the Algebraic-Diagrammatic Construction Scheme for the Polarization Propagator. *J. Chem. Theor. Comput.*, 35:1900, 2014.

[172] O. Christiansen, P. Jørgensen, and C. Hättig. Response Functions from Fourier Component Variational Perturbation Theory Applied to a Time-Averaged Quasienergy. *Int. J. Quant. Chem.*, 68(1):1–52, 1998.

[173] P. Jørgensen and J. Simmons. *Second Quantization–Based Methods in Quantum Chemistry.* Academic Press Inc., 1981.

[174] D. Rowe. Equations-of-Motion Method and the Extended Shell Model. *Rev. Mod. Phys.*, 40(1):153, 1968.

[175] T. Helgaker, S. Coriani, P. Jørgensen, K. Kristensen, J. Olsen, and K. Ruud. Recent Advances in Wave Function-Based Methods of Molecular-Property Calculations. *Chem. Rev.*, 112(1):543–631, 2012.

[176] I. Shavitt and R. J. Bartlett. *Many-Body Methods in Chemistry and Physics: MBPT and Coupled-Cluster Theory*. Cambridge university press, 2009.

[177] W. Liang, S. A. Fischer, M. J. Frisch, and X. Li. Energy-Specific Linear Response TDHF/TDDFT for Calculating High-Energy Excited States. *J. Chem. Theor. Comput.*, 7(11):3540–3547, 2011.

[178] P. J. Lestrange, P. D. Nguyen, and X. Li. Calibration of Energy-Specific TDDFT for Modeling K-Edge XAS Spectra of Light Elements. *J. Chem. Theor. Comput.*, 11:2994–2999, 2015.

[179] B. Peng, P. J. Lestrange, J. J. Goings, M. Caricato, and X. Li. Energy-Specific Equation-of-Motion Coupled-Cluster Methods for High-Energy Excited States: Application to K-Edge X-Ray Absorption Spectroscopy. *J. Chem. Theor. Comput.*, 11(9):4146–4153, 2015.

[180] M. Stener, G. Fronzoni, and M. De Simone. Time Dependent Density Functional Theory of Core Electrons Excitations. *Chem. Phys. Lett.*, 373(1):115–123, 2003.

[181] K. Ray, S. DeBeer George, E. I. Solomon, K. Wieghardt, and F. Neese. Description of the Ground-State Covalencies of the Bis (dithiolato) Transition-Metal Complexes from X-Ray Absorption Spectroscopy and Time-Dependent Density-Functional Calculations. *Chem. Eur. J.*, 13(10):2783–2797, 2007.

[182] N. A. Besley and F. A. Asmuruf. Time-Dependent Density Functional Theory Calculations of the Spectroscopy of Core Electrons. *Phys. Chem. Chem. Phys.*, 12(38):12024–12039, 2010.

[183] E. R. Davidson. The Iterative Calculation of a Few of the Lowest Eigenvalues and Corresponding Eigenvectors of Large Real–Symmetric Matricies. *J. Comput. Phys.*, 17:87, 1975.

[184] R. B. Morgan and D. S. Scott. Generalizations of Davidson's Method for Computing Eigenvalues of Sparse Symmetric Matricies. *SIAM J. Sci. Statist. Comput.*, 7:817–825, 1986.

[185] R. B. Morgan. Generalizations of Davidson's Method for Computing Eigenvalues of Large Non–Symmetric Matricies. *J. Comput. Phys.*, 101:287–291, 1992.

[186] D. Zuev, E. Vecharynski, C. Yang, N. Orms, and A. I. Krylov. New Algorithms for Iterative Matrix-Free Eigensolvers in Quantum Chemistry. *J. Comput. Chem.*, 36(5):273–284, 2015.

[187] S. Coriani, T. Fransson, O. Christiansen, and P. Norman. Asymmetric-Lanczos-Chain-Driven Implementation of Electronic Resonance Convergent Coupled-Cluster Linear Response Theory. *J. Chem. Theor. Comput.*, 8(5):1616–1628, 2012.

[188] T. Fransson, S. Coriani, O. Christiansen, and P. Norman. Carbon X-Ray Absorption Spectra of Fluoroethenes and Acetone: A Study at the Coupled Cluster, Density Functional, and Static-exchange Levels of Theory. *J. Chem. Phys.*, 138(12):124311, 2013.

[189] J. Kauczor, P. Norman, O. Christiansen, and S. Coriani. Communication: A Reduced-Space Algorithm for the Solution of the Complex Linear Response Equations used in Coupled Cluster Damped Response Theory, 2013.

[190] M. A. Marques, N. T. Maitra, F. M. Nogueira, E. K. Gross, and A. Rubio. *Fundamentals of Time-Dependent Density Functional Theory*, volume 837. Springer Science & Business Media, 2012.

[191] P. Norman, D. M. Bishop, H. Jørgen Aa. Jensen, and J. Oddershede. Near-Resonant Absorption in the Time-Dependent Self-Consistent Field and Multiconfigurational Self-Consistent Field Approximations. *J. Chem. Phys.*, 115(22):10323–10334, 2001.

[192] T. Fahleson, H. Ågren, and P. Norman. A Polarization Propagator for Nonlinear X-Ray Spectroscopies. *J. Phys. Chem. Lett.*, 7(11):1991–1995, 2016.

[193] S. Coriani, O. Christiansen, T. Fransson, and P. Norman. Coupled-Cluster Response Theory for Near-Edge X-Ray-Absorption Fine Structure of Atoms and Molecules. *Phys. Rev. A*, 85(2):022507, 2012.

[194] M. Linares, S. Stafstrom, Z. Rinkevicius, H. Ågren, and P. Norman. Complex Polarization Propagator Approach in the Restricted Open-Shell, Self-Consistent Field Approximation: The Near K-Edge X-Ray Absorption Fine Structure Spectra of Allyl and Copper Phthalocyanine. *J. Phys. Chem. B*, 115(18):5096–5102, 2010.

[195] U. Ekström, P. Norman, V. Carravetta, and H. Ågren. Polarization Propagator for X-Ray Spectra. *Phys. Rev. Lett.*, 97(14):143001, 2006.

[196] T. Fransson, D. Burdakova, and P. Norman. K-and L-Edge X-Ray Absorption Spectrum Calculations of Closed-Shell Carbon, Silicon, Germanium, and Sulfur Compounds

using Damped Four-Component Density Functional Response Theory. *Phys. Chem. Chem. Phys.*, 18(19):13591–13603, 2016.

[197] P. Norman, J. Parello, P. L. Polavarapu, and M. Linares. Predicting Near-UV Electronic Circular Dichroism in Nucleosomal DNA by Means of DFT Response Theory. *Phys. Chem. Chem. Phys.*, 17(34):21866–21879, 2015.

[198] S. Villaume, T. Saue, and P. Norman. Linear Complex Polarization Propagator in a Four-Component Kohn–Sham Framework. *J. Chem. Phys.*, 133(6):064105, 2010.

[199] A. C. Antoulas. *Approximation of Large-Scale Dynamical Systems*. Number 6 in Advances in Design and Control. SIAM, 2005.

[200] U. Hetmaniuk, R. Tezaur, and C. Farhat. Review and Assessment of Interpolatory Model Order Reduction Methods for Frequency Response Structural Dynamics and Acoustics Problems. *International Journal for Numerical Methods in Engineering*, 90(13):1636–1662, 2012.

[201] U. Hetmaniuk, R. Tezaur, and C. Farhat. An Adaptive Scheme for a Class of Interpolatory Model Reduction Methods for Frequency Response Problems. *International Journal for Numerical Methods in Engineering*, 93(10):1109–1124, 2013.

[202] P. Benner, V. Mehrmann, and H. Xu. A Numerically Stable, Structure Preserving Method for Computing the Eigenvalues of Real Hamiltonian or Symplectic Pencils. *Numer. Math.*, 78(3):329–358, 1998.

[203] Z. Bai and R.-C. Li. Minimization Principles for the Linear Response Eigenvalue Problem I: Theory. *SIAM J. Mat. Anal. Appl.*, 33(4):1075–1100, 2012.

[204] M. Shao, F. H. da Jornada, C. Yang, J. Deslippe, and S. G. Louie. Structure Preserving Parallel Algorithms for Solving the Bethe–Salpeter Eigenvalue Problem. *Linear Algebra Appl.*, 488:148–167, 2016.

[205] H. Weiss, R. Ahlrichs, and M. Häser. A Direct Algorithm for SelfConsistentField Linear Response Theory and Application to C60: Excitation Energies, Oscillator Strengths, and FrequencyDependent Polarizabilities. *J. Chem. Phys.*, 99(2):1262–1270, 1993.

[206] R. E. Stratmann, G. E. Scuseria, and M. J. Frisch. An Efficient Implementation of Time-Dependent Density-Functional Theory for the Calculation of Excitation Energies of Large Molecules. *J. Chem. Phys.*, 109(19):8218–8224, 1998.

[207] J. Brabec, L. Lin, M. Shao, N. Govind, C. Yang, Y. Saad, and E. G. Ng. Efficient Algorithms for Estimating the Absorption Spectrum within Linear Response TDDFT. *J. Chem. Theor. Comput.*, 11(11):5197–5208.

[208] H. F. Walker. Implementation of the GMRES Method using Householder Transformations. *SIAM J. Sci. Stat. Comp.*, 9(1):152–163, 1988.

[209] M. Shao, H. M. Aktulga, C. Yang, E. G. Ng, P. Maris, and J. P. Vary. Accelerating Nuclear Configuration Interaction Calculations through a Preconditioned Block Iterative Eigensolver. *arXiv*, abs/1609.01689, 2016.

[210] A. McLachlan and M. Ball. Time-Dependent Hartree–Fock Theory for Molecules. *Rev. Mod. Phys.*, 36(3):844, 1964.

[211] R. A. Harris. Oscillator Strengths and Rotational Strengths in Hartree–Fock Theory. *J. Chem. Phys.*, 50(9):3947–3951, 1969.

[212] D. Yeager, M. Nascimento, and V. McKoy. Some Applications of Excited-State-Excited-State Transition Densities. *Phys. Rev. A*, 11(4):1168, 1975.

[213] M. Shao and C. Yang. BSEPACK User's Guide, 2016. https://sites.google.com/a/lbl.gov/bsepack/.

Appendix A

PAULI ALGEBRA ON EVEN RANK SPINORS

In this section, we develop the necessary spin–algebra on even–ranked tensors over the spin basis (spinor) to supplement the development of non–collinear formulations of quantum mechanics. Let $X(2)$ be a rank-2 spinor, such that

$$X(2) = \begin{bmatrix} X(2)^{\alpha\alpha} & X(2)^{\alpha\beta} \\ X(2)^{\beta\alpha} & X(2)^{\beta\beta} \end{bmatrix}, \tag{A.1}$$

where $\left\{X(2)^{\sigma\sigma'} \in S \mid \sigma, \sigma' \in \{\alpha, \beta\}\right\}$ is a set of tensor components over some vector space S. In this work, the state of affairs will typically dictate $S = \mathrm{GL}(\mathbb{C}, N)$: the set of complex linear operators of dimension N. However, for the proposes of this appendix, a general space S will suffice. From Eq. (A.1), it is clear $X(2) \in S \times \mathrm{GL}(\mathbb{C}, 2)$. Choosing the standard basis of $\mathrm{GL}(\mathbb{C}, 2)$ as $U^2 \times U^2$, we may recast Eq. (A.1) as

$$X(2) = \sum_{\sigma\sigma'} X(2)^{\sigma\sigma'} \otimes \boldsymbol{e}_\sigma \otimes \boldsymbol{e}_{\sigma'} \qquad \boldsymbol{e}_\alpha = \begin{bmatrix} 1 \\ 0 \end{bmatrix}, \quad \boldsymbol{e}_\beta = \begin{bmatrix} 0 \\ 1 \end{bmatrix}. \tag{A.2}$$

In this work, we rely on a change of basis to simplify the subsequent derivations and arithmetic in the development of non–collinear electronic structure. We choose the basis of the Pauli matrices (Eq. (1.32)), for which it may be shown that i.e. $\{\boldsymbol{\sigma}_K \mid K \in \{0, 1, 2, 3\}\}$ forms a basis of $\mathrm{GL}(\mathbb{C}, 2)$. Because the Pauli matrices form a basis for $\mathrm{GL}(\mathbb{C}, 2)$, there must exist $\{X(2)^0, X(2)^1, X(2)^2, X(2)^3\}$ such that

$$X(2) = \sum_{K=0}^{3} X(2)^K \otimes \boldsymbol{\sigma}_K \quad . \tag{A.3}$$

From the definitions in Eq. (1.32), we may define linear transformations ($\mathscr{T}$ and $\mathscr{T}^{-1}$)

between the two bases and their components (the other being that of Eq. (A.2)),

$$\begin{bmatrix} \boldsymbol{\sigma}_0 \\ \boldsymbol{\sigma}_3 \\ \boldsymbol{\sigma}_2 \\ \boldsymbol{\sigma}_1 \end{bmatrix} = \mathscr{T} \begin{bmatrix} \boldsymbol{e}_\alpha \otimes \boldsymbol{e}_\alpha \\ \boldsymbol{e}_\alpha \otimes \boldsymbol{e}_\beta \\ \boldsymbol{e}_\beta \otimes \boldsymbol{e}_\alpha \\ \boldsymbol{e}_\beta \otimes \boldsymbol{e}_\beta \end{bmatrix} \qquad \mathscr{T} = \begin{bmatrix} 1 & 0 & 0 & 1 \\ 1 & 0 & 0 & -1 \\ 0 & -i & i & 0 \\ 0 & 1 & 1 & 0 \end{bmatrix} \quad , \tag{A.4a}$$

$$\begin{bmatrix} X(2)^0 \\ X(2)^3 \\ X(2)^2 \\ X(2)^1 \end{bmatrix} = \mathscr{T}^{-T} \begin{bmatrix} X(2)^{\alpha\alpha} \\ X(2)^{\alpha\beta} \\ X(2)^{\beta\alpha} \\ X(2)^{\beta\beta} \end{bmatrix} \qquad \mathscr{T}^{-1} = \frac{1}{2}\mathscr{T}^\dagger \quad . \tag{A.4b}$$

By resolving the identity with $\mathscr{T}$ in Eq. (A.2), we arrive at Eq. (A.3).

As a consequence of Eqs. (A.3), (A.4a) and (A.4b), a number of properties are immediately evident. Firstly, suppose there is another rank-2 spinor $Y(2)$ described as in Eq. (A.3), the product of $X(2)$ and $Y(2)$ takes on a component form

$$\begin{aligned} XY(2) = &\left(\sum_{K=0}^{3} X(2)^K Y(2)^K \right) \otimes \boldsymbol{\sigma}_0 \\ &+ \sum_{k=1}^{3} \left(X(2)^0 Y(2)^k + X(2)^k Y(2)^0 + \sum_{j,l=1}^{3} i\epsilon_{kjl} X(2)^j Y(2)^l \right) \otimes \boldsymbol{\sigma}_k \quad . \end{aligned} \tag{A.5}$$

This form is convenient for a number of reasons, however in the context of electronic structure, Eq. (A.5) exhibits particular utility in the context of operator traces, i.e. property evaluation. Using the product ansatz of Eq. (A.5), we may write the trace of $X(2)$ and $Y(2)$ (denoted $\mathrm{Tr}[X(2)Y(2)]$) simply as

$$\mathrm{Tr}[XY(2)] = 2 \sum_{K=0}^{3} \mathrm{Tr}\left[X(2)^K Y(2)^K \right] \tag{A.6}$$

This simplicity of this expression is due to the fact that the trace operation over the Kronecker product is given by

$$\mathrm{Tr}[\boldsymbol{A} \otimes \boldsymbol{B}] = \mathrm{Tr}[\boldsymbol{A}]\mathrm{Tr}[\boldsymbol{B}] \tag{A.7}$$

and that the Pauli matrices are traceless with the exception of $\boldsymbol{\sigma}_0$ which has a trace of 2.

This notion of Pauli representation may be extended to any arbitrary even–ranked spinor such that

$$X(2N) = \sum_{\sigma_1\sigma_1'\cdots\sigma_N\sigma_N'} X(2N)^{\sigma_1\sigma_1'\cdots\sigma_N\sigma_N'} \otimes \bigotimes_{i=1}^{N} \boldsymbol{e}_{\sigma_i} \otimes \boldsymbol{e}_{\sigma_i'}. \tag{A.8}$$

By resolving the $\mathscr{T}$ identity N times, we obtain

$$X(2N) = \sum_{K_1\cdots K_N} X(2N)^{K_1\cdots K_N} \otimes \bigotimes_{i=1}^{N} \boldsymbol{\sigma}_{K_i}, \tag{A.9}$$

where

$$X(2N)^{K_1\cdots K_N} = \frac{1}{2N} \sum_{\sigma_1\sigma_1'\cdots\sigma_N\sigma_N'} \mathscr{T}^*_{\sigma_1\sigma_1'} \cdots \mathscr{T}^*_{\sigma_N\sigma_N'} X(2N)^{\sigma_1\sigma_1'\cdots\sigma_N\sigma_N'} \tag{A.10}$$

Appendix B

PROOF OF ZERO TORQUE THEOREM USING GENERALIZED DENSITY VARIABLES

In this appendix, we validate that the zero torque theorem for the xc magnetic field is satisfied in the generalized gradient approximation given the transformation rules of Eq. (2.39). The local torque does not need to vanish identically at every point in space and this local contribution is required to obtain accurate spin dynamics and a proper time-evolution of the magnetization [88, 104, 105, 107–109]. The local torque of the xc magnetic field is the tensor field defined by [104]

$$\mathscr{T}_i(\boldsymbol{r}) = \sum_{j,k=1}^{3} \varepsilon_{ijk}\rho^j(\boldsymbol{r})B^k_{GGA}(\boldsymbol{r}), \quad i \in \{1,2,3\}, \tag{B.1}$$

where ε_{ijk} is the rank-3 Levi-Civita tensor and the xc magnetic field is given by

$$B^k_{GGA}(\boldsymbol{r}) = \frac{\delta E^{GGA}[\rho, \nabla\rho]}{\delta\rho^k(\boldsymbol{r})}. \tag{B.2}$$

From Eq. (B.1), we may define the global torque of the xc magnetic field as

$$\mathscr{T}_i^{global} = \int \mathrm{d}^3\boldsymbol{r}\ \mathscr{T}_i(\boldsymbol{r}). \tag{B.3}$$

Remark that the set of U variables in Eq. (2.39) is partitioned by those variables which depend on $\mathbf{m}(\boldsymbol{r})$ and those which depend on $\nabla\mathbf{m}(\boldsymbol{r})$. Recognizing that our choice of U variables are local functions and applying the Euler–Lagrange formula for functional derivatives to Eq. (B.2), we obtain

$$B^k_{GGA}(\boldsymbol{r}) = \frac{\partial f}{\partial\rho^k(\boldsymbol{r})} - \nabla\cdot\frac{\partial f}{\partial\nabla\rho^k(\boldsymbol{r})} = B^{(\rho),k}_{GGA}(\boldsymbol{r}) - B^{(\nabla),k}_{GGA}(\boldsymbol{r}) \tag{B.4}$$

where

$$B_{GGA}^{(\rho),k}(\boldsymbol{r}) = \frac{\partial f}{\partial n^{+}(\boldsymbol{r})}\frac{\partial n^{+}(\boldsymbol{r})}{\partial \rho^{k}(\boldsymbol{r})} + \frac{\partial f}{\partial n^{-}(\boldsymbol{r})}\frac{\partial n^{-}(\boldsymbol{r})}{\partial \rho^{k}(\boldsymbol{r})}, \tag{B.5}$$

$$B_{GGA}^{(\nabla),k}(\boldsymbol{r}) = \nabla\cdot\left(\frac{\partial f}{\partial \varphi^{++}(\boldsymbol{r})}\frac{\partial \varphi^{++}(\boldsymbol{r})}{\partial \nabla\rho^{k}(\boldsymbol{r})} + \frac{\partial f}{\partial \varphi^{+-}(\boldsymbol{r})}\frac{\partial \varphi^{+-}(\boldsymbol{r})}{\partial \nabla\rho^{k}(\boldsymbol{r})} + \frac{\partial f}{\partial \varphi^{--}(\boldsymbol{r})}\frac{\partial \varphi^{--}(\boldsymbol{r})}{\partial \nabla\rho^{k}(\boldsymbol{r})}\right). \tag{B.6}$$

We refer the reader to the Appendix of Ref. [88] for explicit expressions for the partial derivatives of $\{U^{NC}(\boldsymbol{r})\}$ given by Eq. (2.34). Thus, the local and global torque expressions may also be similarly as they are linear in $\mathbf{B}_{GGA}(\boldsymbol{r})$,

$$\mathscr{T}_i(\boldsymbol{r}) = \mathscr{T}_i^{\rho}(\boldsymbol{r}) + \mathscr{T}_i^{\nabla}(\boldsymbol{r}), \tag{B.7}$$

$$\mathscr{T}_i^{\rho}(\boldsymbol{r}) = \sum_{j,k=1}^{3}\varepsilon_{ijk}\rho^{j}(\boldsymbol{r})B_{GGA}^{(\rho),k}(\boldsymbol{r}), \qquad \mathscr{T}_i^{(\rho),global} = \int \mathrm{d}^3\boldsymbol{r}\ \mathscr{T}_i^{\rho}(\boldsymbol{r}), \tag{B.8}$$

$$\mathscr{T}_i^{\nabla}(\boldsymbol{r}) = \sum_{j,k=1}^{3}\varepsilon_{ijk}\rho^{j}(\boldsymbol{r})B_{GGA}^{(\nabla),k}(\boldsymbol{r}), \qquad \mathscr{T}_i^{(\nabla),global} = \int \mathrm{d}^3\boldsymbol{r}\ \mathscr{T}_i^{\nabla}(\boldsymbol{r}). \tag{B.9}$$

To identify the local and global torque contributions from Eq. (B.5), we may consolidate it with the magnetization components of Eq. (2.49),

$$B_{GGA}^{(\rho),k}(\boldsymbol{r}) = \mathscr{Z}_{\rho}^{k}(\boldsymbol{r}) = \frac{1}{2}\left(\frac{\partial f}{\partial n^{+}(\boldsymbol{r})} - \frac{\partial f}{\partial n^{-}(\boldsymbol{r})}\right)\frac{\rho^{k}(\boldsymbol{r})}{|\mathbf{m}(\boldsymbol{r})|}. \tag{B.10}$$

Substituting into Eq. (B.8), we obtain,

$$\mathscr{T}_i^{\rho}(\boldsymbol{r}) = \frac{1}{2}\left(\frac{\partial f}{\partial n^{+}(\boldsymbol{r})} - \frac{\partial f}{\partial n^{-}(\boldsymbol{r})}\right)\sum_{j,k=1}^{3}\frac{\varepsilon_{ijk}\rho^{j}(\boldsymbol{r})\rho^{k}(\boldsymbol{r})}{|\mathbf{m}(\boldsymbol{r})|} = 0, \quad \Longrightarrow \quad \mathscr{T}_i^{(\rho),global} = 0 \tag{B.11}$$

where we have utilized the fact that $\sum_{j,k=1}^{3}\varepsilon_{ijk}\rho^{j}(\boldsymbol{r})\rho^{k}(\boldsymbol{r}) = 0$. Thus the local torque contribution of this term is zero in all space, implying that its global torque contribution is zero as well.

Similarly, we may identify Eq. (B.6) with the magnetization components of Eq. (2.50),

$$B_{GGA}^{(\rho),k}(\boldsymbol{r}) = \sum_{\xi\in\{x,y,z\}}\nabla_{\xi}\mathscr{Z}_{\nabla,\xi}^{k}(\boldsymbol{r}). \tag{B.12}$$

However, unlike Eq. (B.11), the torque arising from Eq. (B.12) is *not* zero in all space. We must them examine its global torque contribution,

$$\begin{aligned}\mathscr{T}_i^{(\nabla),global} &= \sum_{j,k=1}^{3} \sum_{\xi\in\{x,y,z\}} \varepsilon_{ijk} \int \mathrm{d}^3\boldsymbol{r}\ \rho^j(\boldsymbol{r})\ \nabla_\xi \mathcal{Z}^k_{\nabla,\xi}(\boldsymbol{r}) \\ &= -\sum_{j,k=1}^{3} \sum_{\xi\in\{x,y,z\}} \varepsilon_{ijk} \int \mathrm{d}^3\boldsymbol{r}\ \mathcal{Z}^k_{\nabla,\xi}(\boldsymbol{r}) \left(\nabla_\xi \rho^j(\boldsymbol{r})\right). \end{aligned} \tag{B.13}$$

Here, we have integrated the first line by parts and utilized the fact that the density and its derivatives disappear at the boundary by definition. Substituting in the expressions from Eq. (2.50),

$$\begin{aligned}\mathscr{T}_i^{(\nabla),global} = -\frac{1}{2}\sum_{j,k=1}^{3} \sum_{\xi\in\{x,y,z\}} \varepsilon_{ijk} \int \mathrm{d}^3\boldsymbol{r}\ \nabla_\xi \rho^j(\boldsymbol{r}) \Bigg(\nabla_\xi \rho^S(\boldsymbol{r}) \mathfrak{H}^k(\boldsymbol{r}) \left(\frac{\partial f}{\partial \varphi^{++}(\boldsymbol{r})} - \frac{\partial f}{\partial \varphi^{--}(\boldsymbol{r})} \right) + \\ \nabla_\xi \rho^k(\boldsymbol{r}) \left(\frac{\partial f}{\partial \varphi^{++}(\boldsymbol{r})} - \frac{\partial f}{\partial \varphi^{+-}(\boldsymbol{r})} + \frac{\partial f}{\partial \varphi^{--}(\boldsymbol{r})} \right) \Bigg) \\ = 0, \end{aligned} \tag{B.14}$$

where we have used the following relations

$$\nabla\rho^S(\boldsymbol{r}) \cdot \nabla\rho^j(\boldsymbol{r}) \mathfrak{H}^k(\boldsymbol{r}) = \nabla\rho^S(\boldsymbol{r}) \cdot \nabla\rho^k(\boldsymbol{r}) H^j(\boldsymbol{r}) \quad \Longrightarrow \quad \sum_{jk} \varepsilon_{ijk} \nabla\rho^S(\boldsymbol{r}) \cdot \nabla\rho^j(\boldsymbol{r}) \mathfrak{H}^k(\boldsymbol{r}) = 0, \tag{B.15}$$

$$\sum_{jk} \varepsilon_{ijk} \nabla\rho^j(\boldsymbol{r}) \cdot \nabla\rho^k(\boldsymbol{r}) = 0. \tag{B.16}$$